



UNIVERSITÀ
DEGLI STUDI
DI PADOVA

UNIVERSITÀ DEGLI STUDI DI PADOVA

Dipartimento di Ingegneria Industriale DII

Corso di Laurea Magistrale in Ingegneria Aerospaziale

**HDR imaging techniques applied to a Schlieren set-up for
aerodynamics studies**

Relatore: Prof. Ernesto Benini

Correlatore: Dr. Mark Quinn

Studente:

Giammarco Boscaro

1179058

Anno Accademico 2019 – 2020

ESTRATTO

La fotografia schlieren è una tecnica di visualizzazione ottica che rivela le variazioni di densità in un fluido. È spesso necessario incrementare molto la sensibilità del sistema per poter distinguere chiaramente i più piccoli dettagli presenti nel flusso. Questa operazione può però portare a saturazione le zone dell'immagine in cui sono presenti i fenomeni più intensi. Queste regioni diventano completamente bianche o nere, e le informazioni contenute al loro interno vengono perse. L'obiettivo di questo studio è constatare se è possibile recuperare questi dettagli espandendo la gamma dinamica delle immagini tramite la tecnica fotografica dell'HDR, rendendo quindi possibile visualizzare in un'unica foto gli elementi del flusso più intensi e quelli più deboli contemporaneamente.

Lo studio è stato effettuato su flussi stazionari e non stazionari, subsonici e supersonici. La tecnica HDR ha permesso di espandere la gamma dinamica e di ripristinare con successo le aree sovraesposte delle immagini quando la sensibilità del sistema era abbastanza elevata da saturare il sensore della fotocamera. Tuttavia, le immagini ottenute, una volta processate per la visualizzazione in un classico schermo con gamma dinamica limitata, sono risultate di qualità inferiore e meno dettagliate rispetto alle tradizionali immagini schlieren. La ricerca ha dimostrato che i sensori montati nelle fotocamere moderne sono in grado di catturare, in una singola foto, tutte le variazioni di intensità luminosa prodotte dall'apparato schlieren quando questo è impostato a sensibilità medio-basse. In situazioni più estreme la tecnica HDR preserva la propria efficacia, ma i problemi introdotti dall'elevata sensibilità (fenomeni di diffrazione, intervallo di misura ridotto e asimmetrico) portano ad avere immagini inadeguate per un accurato studio del flusso.

In futuro, ulteriori esperimenti potrebbero essere condotti in diversi impianti, in particolare gallerie del vento transoniche e supersoniche operanti a pressioni atmosferiche. Essendo i gradienti di densità prodotti da queste strutture molto più intensi che nel tunnel utilizzato nello studio, il sensore potrebbe saturarsi a sensibilità molto minori. In queste condizioni le criticità precedentemente descritte non si presentano e i risultati potrebbero quindi essere più soddisfacenti.

ABSTRACT

The schlieren imaging technique makes it possible to visualize changes of density in a fluid by rendering a grayscale image, but it is often necessary to rise the sensitivity of the system to discern weaker details of the flow. This process is likely to saturate the regions of the scene where stronger flow features are present, losing important information within them. The purpose of this investigation is to determine if, by making use of various HDR imaging techniques, the dynamic range of the schlieren images can be expanded to recover these lost details and reproduce both strong and weak flow features in a single picture. These techniques have been applied to steady as well as unsteady aerodynamics flows, both subsonic and supersonic. The HDR approach successfully allowed to expand the images dynamic range in every experiment performed, restoring their over ranged regions when the apparatus was sensitive enough to saturate the sensor. However, the resulting pictures, processed to be presented on a standard display, did not outperform traditional schlieren images captured at lower sensitivities, having an inferior image quality and rendering fewer flow features. The investigation has shown that the modern camera sensors are capable of capturing all the luminance variations produced by a schlieren facility when low to moderate sensitivity is used. In more extreme situations, the HDRI techniques become effective but the issues introduced by such high cut-off rates (like diffraction phenomena, reduced and asymmetrical measurement range or the apparatus) generate images inadequate for accurate aerodynamic studies. In future works, more experiments might be performed in different facilities, in particular transonic and supersonic atmospheric wind tunnels. There, the much stronger density gradients could saturate the sensor already at low knife-edges, when the issues cited above do not occur, possibly producing more satisfactory results.

TABLE OF CONTENTS

| | |
|--|-----------|
| NOMENCLATURE | 9 |
| INTRODUCTION | 11 |
| 1. SCHLIEREN IMAGING TECHNIQUE | 15 |
| 1.1. INTRODUCTION | 15 |
| 1.2. THEORY | 17 |
| 1.3. LIMITATIONS | 19 |
| 2. HDR IMAGING | 21 |
| 2.1. THE DYNAMIC RANGE | 21 |
| 2.2. HIGH DYNAMIC RANGE IMAGING | 22 |
| 2.3. EXPOSURE BLENDING ALGORITHMS | 24 |
| 3. EXPERIMENTAL APPARATUS | 27 |
| 3.1. SCHLIEREN APPARATUS | 27 |
| 3.2. HIGH SUPERSONIC WIND TUNNEL | 28 |
| 3.3. POST-PROCESSING SOFTWARE | 29 |
| 4. HDRI APPLIED TO SCHLIEREN | 31 |
| 4.1. THEORY | 31 |
| 4.2. EXPERIMENTAL SETUP AND PROCEDURE | 32 |
| 4.3. RESULTS | 36 |
| 4.4. CONCLUSIONS | 41 |
| 5. HDR SCHLIEREN WITH STEADY FLOWS | 43 |
| 5.1. EXPERIMENTAL SETUP AND PROCEDURE | 43 |
| 5.2. RESULTS | 45 |
| 5.3. CONCLUSIONS | 53 |

| | | |
|-------------|---|------------|
| 6. | TONEMAPPING AND IQ ASSESSMENT | 55 |
| 6.1. | TONE MAPPING OPERATORS..... | 55 |
| 6.2. | IQ ASSESSMENT | 57 |
| 6.3. | RESULTS..... | 58 |
| 6.4. | CONCLUSIONS..... | 63 |
| 7. | POST-PROCESSING..... | 65 |
| 7.1. | POST-PROCESSING TECHNIQUES..... | 65 |
| 7.2. | RESULTS..... | 66 |
| 7.3. | CONCLUSIONS..... | 71 |
| 8. | HDR SCHLIEREN WITH UNSTEADY FLOWS..... | 73 |
| 8.1. | INTRODUCTION..... | 73 |
| 8.2. | DUAL ISO | 74 |
| 8.3. | EXPERIMENTAL SETUP AND PROCEDURE | 75 |
| 8.4. | RESULTS..... | 79 |
| 8.5. | CONCLUSIONS..... | 84 |
| 9. | FINAL CONCLUSIONS..... | 87 |
| 10. | FUTURE WORK | 89 |
| | REFERENCES | 91 |
| A. | APPENDIX - SCRIPTS..... | 95 |
| A.1 | SHUTTER SPEEDS ESTIMATION | 95 |
| A.2 | HDR BLENDING | 96 |
| A.3 | TMO OPTIMIZATION | 105 |
| A.4 | TMO IQ ASSESSMENT..... | 106 |
| A.5 | TONE MAPPING OPERATORS..... | 108 |
| A.6 | POST-PROCESSING | 110 |
| A.7 | TONE CURVE PROCESSING..... | 111 |
| A.8 | HDR BLENDING WITH VIRTUAL BRACKETING | 113 |
| A.9 | TOOLS..... | 115 |

NOMENCLATURE

| Symbol | Equations | Description | Units |
|---------------------------------|------------------------------------|----------------------------------|------------------------------|
| <i>a</i> | 1.4, 1.6 – 1.8, 4.2 | knife-edge slit height | <i>m</i> |
| Δa | 1.5 | displacement | <i>m</i> |
| <i>B</i> | 1.3 – 1.5 | light source luminance | <i>cd/m²</i> |
| <i>b</i> | 1.3 – 1.5 | source slit width | <i>m</i> |
| <i>C</i> | 1.6, 1.7 | contrast | |
| <i>DR</i> | 2.1, 2.2, 4.5, 6.1 | dynamic range | <i>EV</i> |
| <i>E</i> | 1.4, 1.6, 1.8, 1.9, 2.3 – 2.5, 2.8 | background illuminance | <i>cd · sr/m²</i> |
| <i>E₀</i> | 1.3 | first mirror illuminance | <i>cd · sr/m²</i> |
| ΔE | 1.5, 1.6, 1.8, 1.9, 4.2 | differential illuminance | <i>cd · sr/m²</i> |
| ε | 1.2, 1.6 – 1.9 | angle of deflection | <i>rad</i> |
| <i>F</i> | 4.1 | f-number | |
| <i>f_i</i> | 1.3 – 1.9 | focal lengths | <i>m</i> |
| <i>f</i> | 2.4, 4.3 | camera response function | |
| <i>g</i> | 2.5, 2.6, 4.5 | inverse camera response function | |
| <i>h</i> | 1.3, 1.9, 4.2 | source slit height | <i>m</i> |
| <i>I</i> | 4.4 | image matrix | |
| <i>K</i> | 1.1 | Gladstone-Dale constant | |
| <i>k</i> | | heat capacity ratio | |

| | | | |
|-------------|--------------------------|-------------------------|------------------|
| λ | 2.5 | smoothing factor | |
| M | | Mach number | |
| m | 1.3 – 1.5 | magnification factor | |
| N | 2.7, 4.4 | number of pixels | |
| n | 1.1, 1.2 | refractive index | |
| P | 2.7, 2.8 | number of photos | |
| P | | pressure | Pa |
| P_0 | | total pressure | Pa |
| R | | individual gas constant | $J/(kg \cdot K)$ |
| ρ | 1.1 | density | kg/m^3 |
| ρ_0 | | total density | kg/m^3 |
| S | 1.7 | sensitivity | |
| T | | temperature | K |
| T_0 | | total temperature | K |
| Δt | 2.3 – 2.5, 2.8, 4.1, 4.3 | exposure time | s |
| ϑ | 2.5 | objective function | |
| w | 2.5, 2.8 | weight function | |
| X | 2.3, 4.3 | exposure | J/m^2 |
| y | 2.1, 2.2 | pixel luminance value | |
| Z | 2.4 – 2.8, 4.3 | pixel value | |

INTRODUCTION

The schlieren¹ technique allows to visualize density fluctuation in any thermal or aerodynamic flow by producing a monochrome image. A shift in density is represented on the picture as a change in brightness intensity. Distinct density regions in the flow refract the light rays in different ways. By placing a knife-edge between the observed object and the image plane, some of them will be blocked while others will be let through. It is this principle that makes possible to create schlieren images (*Chapter 1*).

The schlieren effect has been known since the 17th century, when the first observations of a thermal air disturbance were made by Robert Hooke. In his method, there was no external knife-edge. It was the pupil that was partially blocking the light rays, in fact acting as the knife-edge. It was only in the 19th century when an explicit cut-off was introduced in the apparatus by J.B. Leon Foucault. At this time, the technique was mostly used for testing telescopes mirrors and optical inhomogeneities in a glass. The use of the schlieren technique as a scientific instrument was pioneered by Toepler between 1859 and 1864. He was the first to propose a practical apparatus with mirrors, adjustable knife-edge and light source, and to describe a strategy to set it up quickly and accurately. At that time no cameras were available so the observed phenomena had to be hand-drawn [1].

In the modern era, the schlieren technique was employed in wind tunnels to visualize flows around aerodynamic bodies, shockwaves and expansion fans, heat transfer processes etc. The schlieren method has been extremely important for the development of ballistics and high-speed aerodynamics. Moreover, with the advent of photo cameras it was possible to capture the actual schlieren figure, making the process easier and more accurate.

In recent years, the technique has been improved with rainbow/colour schlieren, that allows to retain more data than classic black and white schlieren (for example, it can visualize the direction of the gradients) or calibrated schlieren, with which it is possible to actually measure the density variations in the field [2, 3]. Furthermore, the improvement in optics quality and the diffusion of digital photography have made possible to capture large, sharp, high quality pictures and even high-speed videos in a more practical way than the old and clumsy film. Even more important,

¹ The term *schlieren* means “streaks” or “striae”.

this digitalization process has enabled the development of advanced routines for post-processing and image enhancement, real time velocimetry, shockwave tracking and many more, and led to the creation of a completely new schlieren technique named Background-Oriented Schlieren (BOS), that heavily relies on the processing power of the modern computers [4].

During the experimentations with the schlieren apparatus, it is really common to find phenomena that consist in both weak and strong flow features. Visualizing these small and faint details requires to setup the facility to be extremely sensitive. A similar configuration has the disadvantage of amplifying all the features, included the strong ones that could easily become so intense that they exceed the limits of the dynamic range of the camera sensor and the schlieren apparatus. When this happens, the saturated regions appear as completely black or white (*figure 2.1*), and within them no details can be discerned.

This problem is well-known in photography, where capturing scenes with extreme variations of illuminance can saturate the film or the sensor producing, for example, burned skies, deep black shadows or in general unappealing images as a whole. A solution for this issue has been proposed two decades ago when the first high dynamic range imaging algorithms have been developed [5–8]. The vast majority of the HDRI techniques combine multiple differently exposed photos into one single picture that contains the whole range of illuminance present in the real scene. The highlights will be captured correctly by the under-exposed images, while the shadows will be rendered correctly by the over-exposed ones. Blending all the images will produce one picture where all the features of the real-world scene are visible (*Chapter 2*).

The purpose of this study is investigating if and how the HDR blending techniques can be applied to schlieren images to portray weak as well as strong features in one single photo by using a high-sensitivity setup and recovering the lost information during the post-processing. This workflow could simplify the acquisition process of the schlieren images as there would not be the need to run the experiment several times with different knife-edges anymore. Moreover, since HDR images consist of floating-point irradiance values they could be utilized to accurately recover the density values in the scene and improve the calibrated schlieren method.

The study will begin with a feasibility evaluation where it will be proven that the HDR techniques can recover the lost data and extend the dynamic range of over ranged schlieren images (*Chapter 4*). Afterwards, HDR images of a steady hypersonic flow around an aerodynamic body will be captured and analysed to understand if the pictures produced effectively contain more information and if they can better reproduce the phenomenon compared to the classic schlieren

photos (*Chapter 5*). Various tone mapping operators (needed to correctly display the HDR images in a low dynamic range device) will be implemented and compared, and the image quality will be assessed (*Chapter 6*). Moreover, different post-processing techniques will be proposed to improve even more the pictures (*Chapter 7*).

Ultimately, a different HDRI technique, known as Dual ISO, will be employed to capture extended dynamic range photos of an unsteady turbulent flow, and again the results will be compared with the traditional schlieren images (*Chapter 8*).

1. SCHLIEREN IMAGING TECHNIQUE

1.1. INTRODUCTION

The schlieren technique is a method to visualize a flow or a heat transfer process in any medium. It is based on the change of refractive index of the medium caused by a variation of density. The change in the refractive index deflects the light in different ways and makes possible to visualize images of the fluid field. For a gaseous medium, these quantities are related by:

$$n - 1 = K\rho \quad (1.1)$$

where K is the *Gladstone-Dale constant*. It is easily understood that if the intention is to visualize an aerodynamic flow, this must be compressible.

The schlieren method, as many other density-based techniques, reproduces the flow features in an imaging plane, where different light intensity means different density.

The functioning of a schlieren system is easier to understand when its light source is a point [1]. The light from the source is collimated by a lens and then focussed again by another one, while the object that needs to be observed is placed in them. This results in a real inverted image on the screen. However, to visualize the flow features, one more component is necessary.

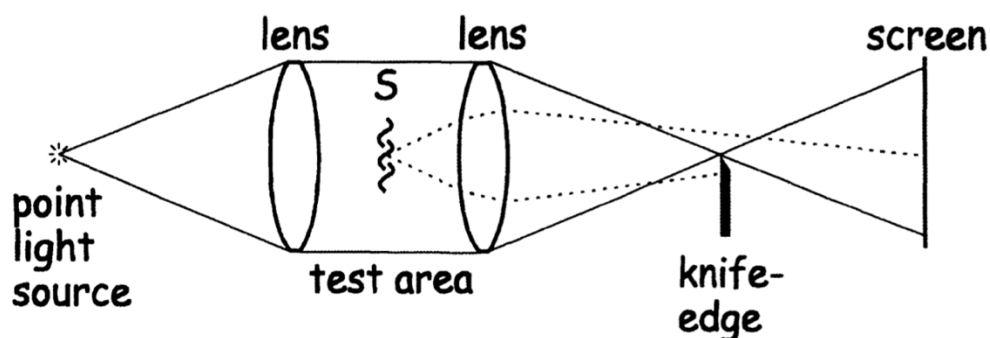


Figure 1.1 – Point light source schlieren system [1]

This component is the knife-edge, that is usually a razor blade. When placed at the focus point, the knife-edge is able to block some of the light rays refracted by the flow around the object. The blocked rays will not reach the screen, so they will appear as dark spots in a bright screen.

Given a point source, as in this example, the image revealed on the screen will be a binary image. This means that every point on the screen will be either completely dark or completely white, with no in between.

To produce an actual grayscale image, an extended light source is needed. In this way, the image will have a gradient of light intensity from black to white, and many more flow features will be visualized. The extended light source can be imagined as an array of many point sources. Now, not a single ray but a bundle of rays will be deflected by the density field. This bundle of refracted rays is partially blocked by the knife-edge (*figure 1.2*) and it will cause the corresponding point on the screen to be darker or brighter than the background.

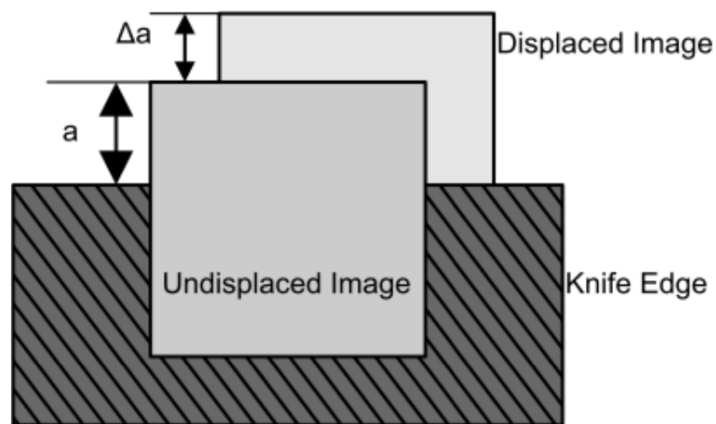


Figure 1.2 – Displaced image in the knife-edge [9]

The final image is a superimposition of all these “elemental” images created by the refracted group of rays [1]. As seen in *figure 1.3*, this schlieren system needs an additional focusing lens.

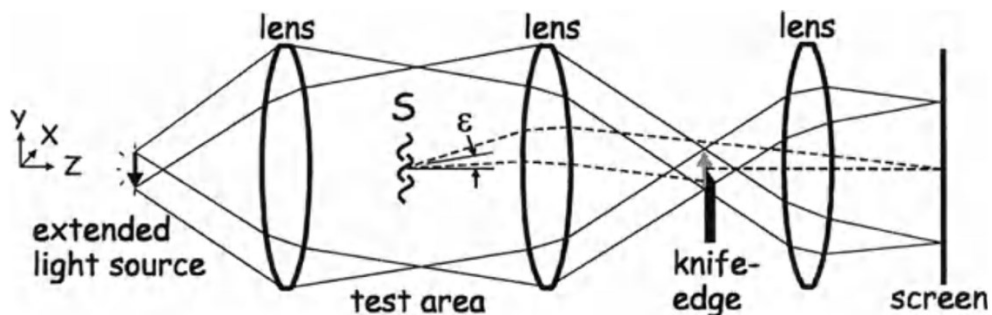


Figure 1.3 – Extended source schlieren system [1]

All these systems need high quality lenses in order to have an image as sharp as possible and minimize the chromatic aberration. These types of lenses can be quite expensive, especially for large ones. An alternative arrangement for a schlieren system employs mirrors instead of lenses. These are cheaper and need less maintenance. Furthermore, mirror systems do not suffer from chromatic aberration, although they do have problems with coma and astigmatism. Coma can be eliminated by tilting the two identical mirrors by the same angle and astigmatism can be minimized by keeping that angle small and using mirror with a long focal length [1]. The downsides of having a mirror based schlieren system is that it is more difficult to align, it is more sensitive to vibrations and can occupy more space than an in-line system.

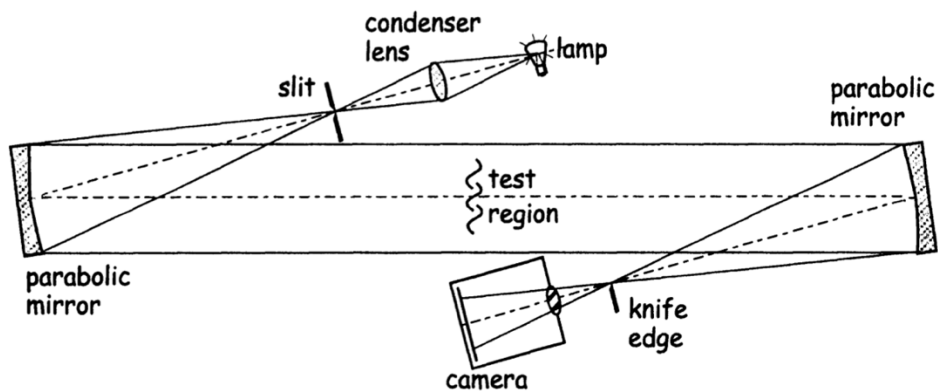


Figure 1.4 – Mirror based schlieren system with Z-layout [1]

It can be noted, from *figure 1.4*, that real schlieren setups have a few more elements other than the ones described before. These are the condenser lens and the slit. The condenser lens, as the name suggest, focus the light from the source into a point, where the slit is placed. The slit is necessary to define an “effective source” with known width, height and luminance. This new light source will have uniform brightness and a regular shape.

1.2. THEORY

A schlieren system is sensitive to the deflection angle ε . The larger is the refraction of the rays, the darker or brighter will be the spot on the image. The deflection angle is proportional to the gradient of the refractive index n , therefore also to the gradient of the density ρ , as shown in [1, 9, 10]:

$$\varepsilon_x = \frac{1}{n} \int \frac{\partial n}{\partial x} dz \quad \varepsilon_y = \frac{1}{n} \int \frac{\partial n}{\partial y} dz \quad (1.2)$$

The system responds only at one deflection direction at a time, based on the orientation of the knife-edge. If it is horizontal, only the gradient in the y direction will be visible in the final image. To show both gradients at the same time, an opaque mask with a circular hole can be used instead of a knife-edge [1].

If the luminance of the light source is B , and supposing a rectangular $b \times h$ slit, the illuminance that reach the image plane is [1, 9]:

$$E_0 = \frac{Bbh}{m^2 f_1^2} \quad (1.3)$$

When the knife-edge is added, the actual illuminance becomes (noticing that $h = \frac{af_1}{f_2}$):

$$E = \frac{Bba}{m^2 f_1 f_2} \quad (1.4)$$

where a is called cut-off height or unobstructed image height. If the schlieren object deflect a ray by an angle ε_y , the displacement once it reaches the knife-edge will be $\Delta a = \varepsilon_y f_2$ and the change of illuminance will be:

$$\Delta E = \frac{Bb\Delta a}{m^2 f_1 f_2} = \frac{Bb\varepsilon_y}{m^2 f_1} \quad (1.5)$$

Assuming a horizontal knife-edge blocking the bottom half of the image, a ray refracted upward by ε_y will increase the brightness of in a specific point of the image by ΔE . However, if a ray is deflected downward by the same angle ε_y , the brightness will decrease by ΔE .

The contrast and the sensitivity of the schlieren system can be defined as:

$$C = \frac{\Delta E}{E} = \frac{f_2 \varepsilon_y}{a} \quad (1.6)$$

$$S = \frac{dC}{d\varepsilon} = \frac{f_2}{a} \quad (1.7)$$

The equations state that the sensitivity depends only on the second mirror focal length and the cut-off height. Since f_2 cannot be changed without modifying the entire setup, the sensibility

can be adjusted only by moving the razor edge. The more light is cut off by the knife-edge, the higher the sensitivity will be (but there is a limit, and that is when the slit is so small that diffraction effects become important). Increasing the cut-off decrease the background brightness of the image, so a more powerful light source may be needed. If changing light source is not possible, increasing the exposure time of the camera leads to the same result, but a too slow shutter speed can cause motion blur [9].

1.3. LIMITATIONS

As seen in the previous section, the sensitivity of a schlieren apparatus is limited by the diffraction effects when the unobstructed image height is too small. However, this is not the only limitation. Also, the measuring range of a schlieren is limited and it is directly related to the maximum detectable deflection. If a displaced image is shifted in a way that is completely inside or outside the knife-edge, any deflection larger than that will not cause any change of illuminance in the image plane. The maximum observable deflection is [1]:

$$\varepsilon_{max} = \frac{\Delta E}{E} \frac{a}{f_2} \quad (1.8)$$

and it is proportional to the inverse of the sensibility, meaning that trying to extend the measurement range will necessarily decrease the sensibility.

Assuming a 50% cut-off, the equation becomes:

$$\varepsilon_{max} = \varepsilon_{min} = \frac{\Delta E}{E} \frac{h}{2f_2} \quad (1.9)$$

Setting a 50% cut-off means having a symmetrical measurement range, but often this is not possible because a higher sensitivity is needed. Increasing the cut-off causes the measuring range to become asymmetrical, widening the range of the brightening of the image but decreasing the range of the darkening [1, 9]. The measuring range and sensitivity required can be calculated for some simple cases by estimating the maximum expected deflection [1].

Other limitations of a schlieren set-up can be, as seen before, the quality of the lenses and mirrors, optical phenomena like coma, astigmatism and chromatic aberration. Also, if the medium is rarefied, many details could be hardly detectable. Ultimately, the limited dynamic range of the camera sensor can influence the visible flow features [1, 9].

2. HDR IMAGING

2.1. THE DYNAMIC RANGE

The dynamic range is the ratio between the largest and smallest value of a certain quantity. It could be a voltage, pressure, radiance value etc. In photography, the dynamic range is the ratio between the darkest and brightest tone.

The dynamic range is usually measured in stops or dB, and is calculated with these formulas:

$$DR = \log_2(y_{max}) - \log_2(y_{min}) \quad [stops] \quad (2.1)$$

$$DR = 20 \log_{10} \frac{y_{max}}{y_{min}} \quad [dB] \quad (2.2)$$

A real-world scene can have more than 20 stops of dynamic range, but a camera sensor has much narrower range (usually 9 to 11 stops, but modern cameras can reach 15 stops). This limitation means that it is not possible to perfectly represent a scene in a picture, because the dynamic range will need to be compressed. Furthermore, the digitalization process, that converts the sensor data to an image file will compress even more the range (an 8-bit file will have 8 stops of dynamic range). Ultimately, the display device will have its own dynamic range, based on the maximum and minimum pixel brightness that is capable of [11].

Since the dynamic range of the media² is smaller than the actual one, some details will be lost. The spots that are too bright or too dark will be “clipped” in the final image, that will then be referred as over ranged. The dynamic range is also restricted colour-wise, so many tones cannot be reproduced in the pictures. Looking at *figure 2.1*, one may observe many completely white or black areas. All the flow features inside these spots are lost because of the limited dynamic range of the sensor and/or file format.

² This could be a digital image, but also a film picture or a movie.



Figure 2.1 – Over ranged image [1]

2.2. HIGH DYNAMIC RANGE IMAGING

To improve the dynamic range of an image and reproduce more details, it is indispensable to employ a high dynamic range imaging technique (HDRI). An HDR picture contains more information than standard image and has a much wider dynamic range.

There are different techniques to obtain an HDR picture, but the most popular and straight forward is the exposure bracketing technique. Exposure bracketing means shooting few photos of the same scene (usually three or more), but with different exposures. It is usually done by attaching the camera to a tripod and shoot some photos with a different shutter speed. Pictures taken with a longer exposure time will reveal the details in the dark areas of the scene, but the highlights will be clipped. On the other hand, images with shorter exposure time will display more features in the brightest points of the scene, but the shadows will be completely black.

The photo sequence will then be blended together to produce the HDR image. The blending algorithm will use the correctly exposed pixels in every photo and discard the over ranged ones. The final result is a picture where all the regions of the scene are correctly exposed (*figure 2.2*). This file is called radiance map. A radiance map contains pixel values that are linearly related to the relative luminance of the scene. Since the eyes do not respond linearly to a difference in luminance and they react differently to distinct colours, an HDR map it is usually not satisfying to look at. Moreover, the radiance map contains a wide range of luminance data that is not possible to display in a standard monitor.

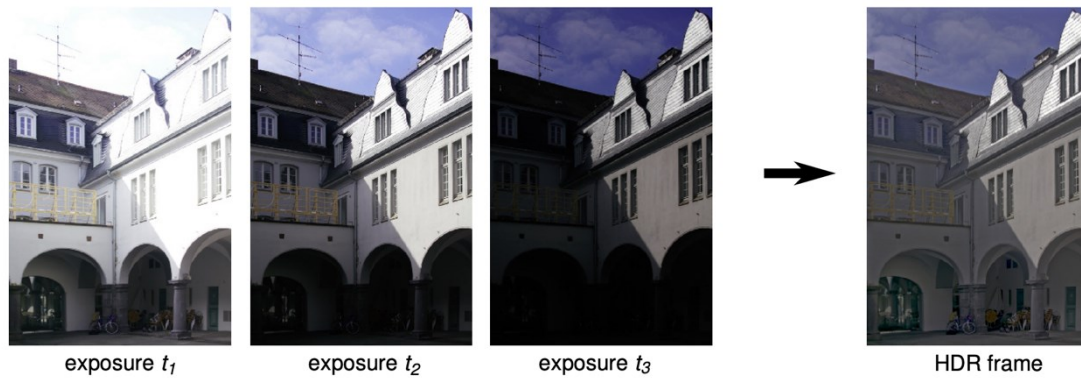


Figure 2.2 – Bracketing and HDR blending example [11]

This raw radiance map needs to be tone mapped to fit the limited dynamic range of the display and to improve the appearance of the picture. [11, 12] Tone mapping compresses the dynamic range again while trying to preserve as much information as possible. An example of tone mapping can be seen in *figure 2.3*.

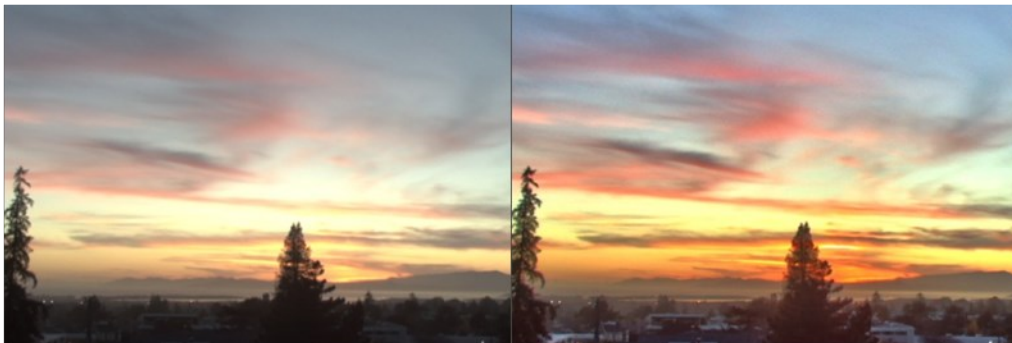


Figure 2.3 – Difference between a linear radiance map (left) and a tone mapped image (right) [13]

As stated before, every pixel in a radiance map is directly related to the relative luminance of the corresponding spot on the real-world scene, meaning that this kind of image can be used also to retrieve the actual luminance of the scene. At least one measurement with a luminance meter is necessary to find the scale factor and therefore the absolute luminance of the pixels. This method of retrieving the luminance has already been investigated with good results (errors of 10% at most) [5, 14]. The inaccuracies are mostly caused by the sensor RGB filter, which cannot capture the full visible light luminance but only the RGB radiance.

The HDR algorithm used in this investigation will be introduced in detail in the next section. This procedure will be used to generate HDR images by blending some bracketed images. It is easy to understand that this method can only be applied to steady subjects, since all the acquired

images need to be perfectly aligned to obtain an accurate result. When the phenomenon is not stable, other techniques can be employed to capture a picture with an extended dynamic range. One of these methods is the so-called Dual ISO. Here, the differently exposed pictures are obtained in a single frame by having, in the camera sensor, pixels with different sensitivities. Its functioning will be discussed in detail in *Chapter 8*.

2.3. EXPOSURE BLENDING ALGORITHMS

This section will present one of the many exposures blending algorithm. This particular process was developed in 1997 by Paul Debevec [5]. The basic idea is to retrieve the relative luminance of all the pixels in a picture and build a radiance map with it.

Considering a greyscale image, this is described by a 2D matrix of pixel values. Three differently exposed images will have three different pixel values for every specific spot of the scene. But that point, in the real-world, never changed his luminance. By exploiting this behaviour, the *camera response function* (CRF) can be recovered. The camera response function relates the scene luminance to the pixel values and so it incorporates all the non-linearities of the imaging pipeline. Once the camera response function is known, it can be used to create to find the pixels luminance and build the radiance map.

If E is the irradiance and Δt is the exposure time, then the exposure X is:

$$X = E\Delta t \tag{2.3}$$

This relation is called *reciprocity*. The algorithm to retrieve the response function is based on this relation and the assumption that only $E\Delta t$ matters. If E is doubled and Δt is halved, the result is the same.

The pixel value will be proportional to an unknown E_i (where i is the pixel index) and Δt_j (where j is the image number):

$$Z_{ij} = f(E_i\Delta t_j) \tag{2.4}$$

The function f is the camera response and is assumed monotonic and invertible. It can be recovered minimizing this following function:

$$\vartheta = \sum_{i=1}^N \sum_{j=1}^P \{w(Z_{ij})[g(Z_{ij}) - \ln(E_i) - \ln(\Delta t_j)]\}^2 - \lambda \sum_{z=Z_{min}+1}^{Z_{max}-1} \{w(Z_{ij})g''(z)\}^2 \quad (2.5)$$

where

$$g''(z) = g(z-1) - 2g(z) + g(z+1) \quad (2.6)$$

This way, $g(Z_{ij}) = \ln f^{-1}(Z_{ij})$ is calculated and, since it is invertible, the actual camera response function is known too. The weighting function can be a simple hat function [5] but also a Gaussian-like function [8]. *Figure 2.4* shows an example of a camera response function recovered with the algorithm.

It is not necessary and rather not recommended to use all the pixels to compute the curve, because the matrix can easily become too large to be inverted in practical time and without overflowing the computer memory. Just a few pixels are enough, and they can be either sampled manually or automatically. The minimum pixel number to sample is given by [5]:

$$N(P-1) > (Z_{max} - Z_{min}) \quad (2.7)$$

Using more pixels than the minimum can reduce the noise.

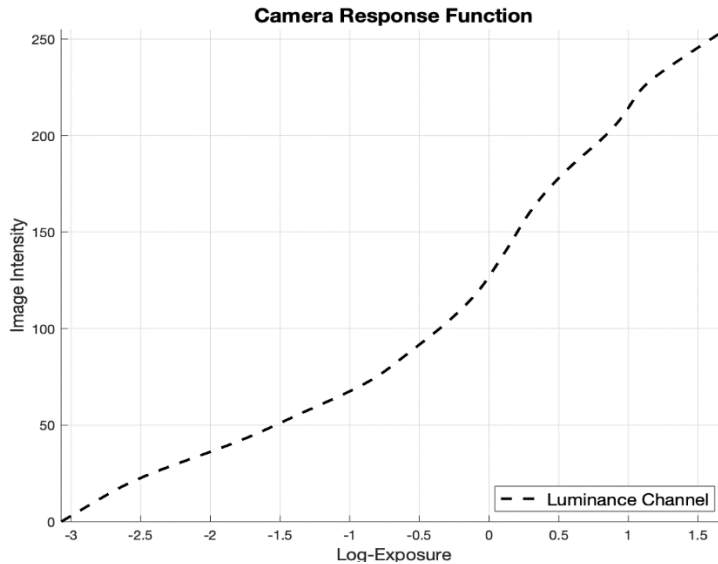


Figure 2.4 – Example of a camera response function for a grayscale image

If the images are coloured it will be necessary to recover three response functions, one for every channel. Usually these three curves will be slightly different.

Knowing the response curve, the irradiance value of a pixel is calculated with a simple weighted average, that discards the over ranged pixel values:

$$\ln(E_i) = \frac{\sum_{j=1}^P w(Z_{ij})(g(Z_{ij}) - \ln\Delta t_j)}{\sum_{j=1}^P w(Z_{ij})} \quad (2.8)$$

The result will be a matrix where every cell represents an irradiance value of a point in the scene. This matrix can be saved in a file as a radiance map. These files can be quite large, because every pixel value is usually computed as a 32-bits or 64-bits floating point number. To save some storage space, it is advised to use the RGe file format (also known as RADIANCE), that requires just one third more storage space than a standard low dynamic range image [5].

This is not the only existing algorithm to retrieve the camera response function and create an HDR image. For example, the polynomial approximation of the function can be derived (Mitsunaga and Nayar [12]), or an empiric model can be used to shape the curve (Grossberg and Nayar [15]). Alternatively, a tone mapped HDR picture can be created without computing neither the CRF nor the radiance map. This strategy is employed, for example, by the Exposure Fusion technique [16], that involves a weighted blending of the images based on contrast, exposure and saturation.

In this investigation the Debevec algorithm will be used to recover every response function and radiance map, as it is easy to implement, fast and as accurate as the others [17]. In addition, the Exposure Fusion technique will be evaluated, and the resulting pictures will be compared with the ones obtained with classic HDR techniques.

3. EXPERIMENTAL APPARATUS

All the experiments in this study have been performed using the University of Manchester High Supersonic Wind Tunnel (HSST) and schlieren apparatus [18]. In the following section the two systems will be described.

3.1. SCHLIEREN APPARATUS

The schlieren apparatus used for this study is a Töepler's Z-type schlieren system. The system is powered by a 450W Xenon arc lamp. The light is focused into a slit thanks to a plano-convex lens and generates the point light source. The light rays are then collimated by a 30.5 cm diameter f/7.9 parabolic mirror and pass through the test section. This element is comprised of two 300 x 210 mm rectangular quartz windows, a floor-mounted rail and an arc balance sting to fix the test object inside the chamber. After the test section, the rays are focused to a point by an identical mirror as the one described before. At the focal point, the vertical knife-edge is placed. After that, a focusing lens focus the light directly into the camera sensor without the use of any other lens. The camera used is the commercially available Nikon D5200, that it is fitted with a 24-megapixel APS-C sensor. Knife-edge, focusing lens and camera are all mounted in a rail so they can be moved to calibrate the system and to change the field of view of the camera (*figure 3.1*). The camera is connected via USB to a workstation to let the user remotely control it and avoid involuntary changes in the configuration. The software used to do so is digiCamControl [19]. This software lets the user change most of the camera settings, shoot photos or videos remotely and directly save them in the PC hard drive. It also features a very useful live view mode with real time histogram.

To capture pictures of the unsteady flow in *Chapter 8*, a Canon EOS 500D equipped with Magic Lantern [20] has been used.

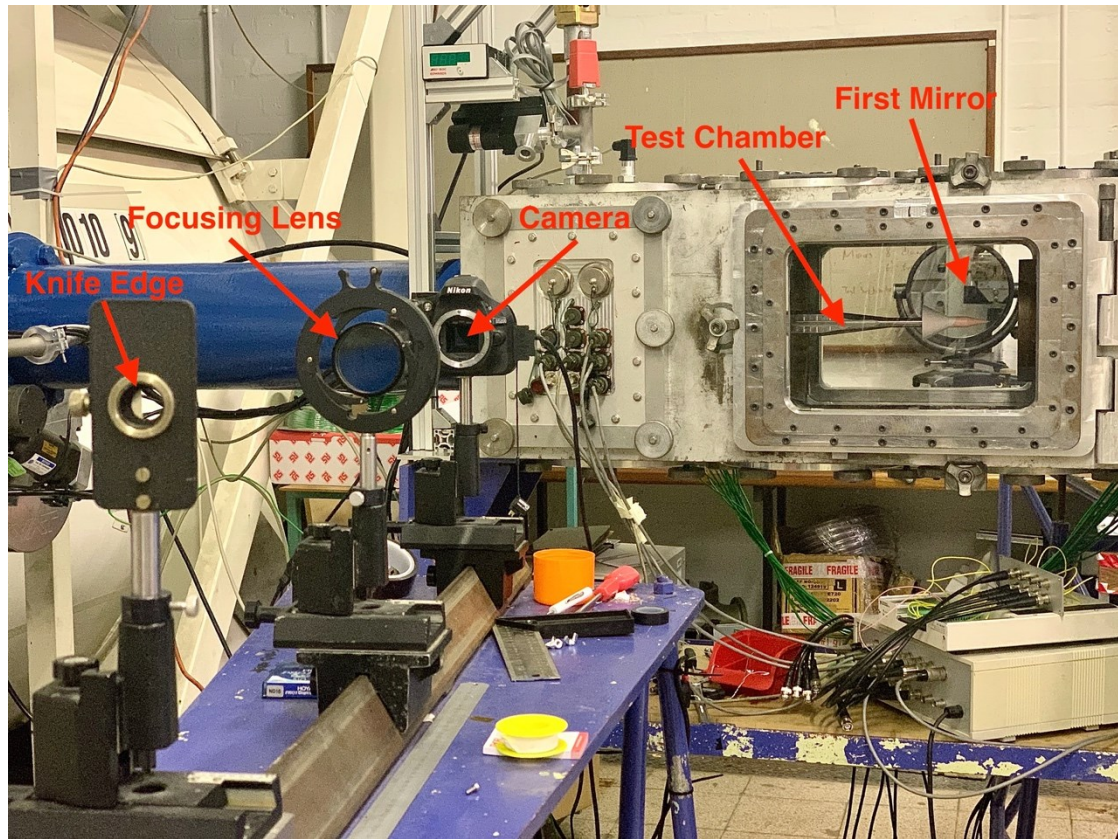


Figure 3.1 – University of Manchester Z-type schlieren system

3.2. HIGH SUPERSONIC WIND TUNNEL

The schlieren apparatus is used to visualize a supersonic flow around some test objects. The flow is generated by the University of Manchester High Supersonic Wind Tunnel (HSST). The HSST is capable of Mach numbers from 4 to 6 (based on which nozzle is mounted), with a total temperature T_0 ranging from 300 K to 950 K and a maximum total pressure P_0 of 850 kPa. The supersonic flow can last, in stable conditions, for about 7.5 seconds. A convergent-divergent nozzle with an exit diameter of 152 mm accelerates the flow to Mach 5 before entering the test section, where the aerodynamic body to test is placed [18]. The fluid can be heated with a 15 kW heater. The pictures are then captured using the schlieren apparatus described before. A schematic of the facility is presented in *figure 3.2*.

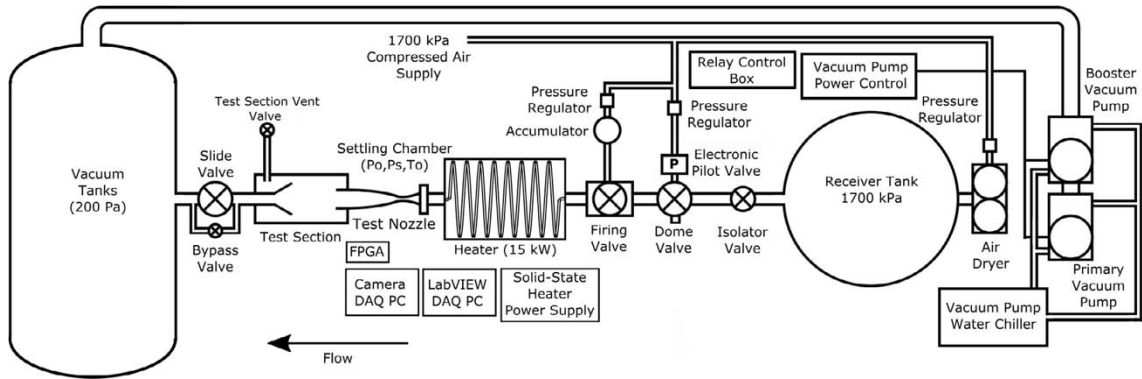


Figure 3.2 – HSST facility schematics [18]

3.3. POST-PROCESSING SOFTWARE

The main software used for post-processing and data analysis has been MATLAB. All the scripts developed during the investigation are available in *Appendix A*. In addition, some features offered by HDR Toolbox [17] have been used. ImageJ [21] has been employed to improve the pictures by removing dust particles, dark spots or other unwanted artefacts induced by lenses and glass imperfections, and for measuring the shockwave angles in *Chapter 5*. Darktable [22], a free post-processing software, has been used to edit the Dual ISO images in *Chapter 8*.

4. HDRI APPLIED TO SCHLIEREN

As seen in *Section 1.3*, in real world schlieren applications is often necessary to set a high cut-off to increase the sensitivity of the imaging system. This situation leads to over-ranged images like the one in *figure 2.1*, where details in the shadows and bright areas are lost. In the following chapter the first experiment will be presented. The purpose of this investigation is to determine if, by making use of the HDR image technique, the dynamic range of the captured images can be expanded to recover these details.

4.1. THEORY

Increasing the amount of light that is cut-off by the knife-edge raise the sensitivity of the schlieren system, as shown in *equation (1.7)*. In addition, the measurement range narrows, and the span of observable density changes decreases [1]. Greater density changes than the maximum one will not intensify the brightness of the related point in the screen, as seen in *Chapter 1*. In this case the measurement range is limited by the system itself and nothing can be done without changing the setup.

However, high sensitivity also means that a little change in density causes a great shift in brightness. This situation can produce too bright and too dark spots in the schlieren image that can exceed the dynamic range of the camera sensor and lead to over-ranged pixels in the captured pictures. In this case the limiting factor is the device used to acquire the photos, suggesting that the lost information can be recovered by taking advantage of the exposure bracketing technique seen in *Chapter 2*. Capturing under and over-exposed images allows the camera to retain useful information in the areas that were over-ranged on the initial picture. Blending the different exposures results in an image that contains more useful data and that can reproduce more details. The experiment aim is revealing if it is effectively possible to take advantage of HDRI techniques to improve the images captured with a schlieren apparatus. If the outcome is positive, the cut-off values where HDR become effective will be determined, and the expansion of the dynamic range will be quantified.

4.2. EXPERIMENTAL SETUP AND PROCEDURE

An ideal test body for the experiment must not change in time and must provide a brightness gradient from deep dark to very bright, stretching over the dynamic range limits of the apparatus. This object could be an extremely weak plano-convex lens, as the one used for calibrated schlieren techniques [3]. Since a similar lens was not available, a candle was used instead. A candle, confined inside the test area without any disturbance, produce a very stable flame and the changes in density caused by its thermal flux are clearly visible through the schlieren system. These density variations are enough to generate over-ranged pictures at high cut-offs. It is important to keep the flow steady, so the blending process do not create any ghosting artefact in the final radiance map.

For every cut-off value, five bracketed images have been captured varying only the shutter speed: one correctly exposed (the reference picture), two under-exposed by one and two stops, and two over-exposed by one and two stops³. The test matrix of the experiment is shown in *table 4.1*. It can be noticed that at the highest cut-off rates it became necessary to capture more than two under exposed pictures. The reasons will be explained in the next section.

Table 4.1 – Test matrix of the experiment

| <i>Cut-Off</i> | <i>Bracketing stops</i> | <i>Reference shutter speed [s]</i> |
|----------------|-------------------------|------------------------------------|
| 50% | 0, ± 1, ± 2 | 1/1600 |
| 75% | 0, ± 1, ± 2 | 1/800 |
| 85% | 0, ± 1, ± 2 | 1/500 |
| 90% | 0, ± 1, ± 2, (-3) | 1/320 |
| 95% | 0, ± 1, ± 2, (-3, -4) | 1/160 |

To correctly compare the images, the background of every reference picture must have the same average pixel value. A value of 127 have been chosen so the background would be rendered as middle grey by the camera. A uniform middle grey background is suggested to capture good quality schlieren images [1]. Since the lamp used in the schlieren apparatus is very bright, to obtain the desired background value at low cut-off rates it would be necessary to use the fastest shutter speed available for the camera, thus meaning that the under-exposed pictures could not possibly be captured in these conditions. To solve the issue, a 3 stops neutral density filter (ND8)

³ A variation of one stop doubles or halves the amount of light that reach the camera sensor.

has been used. This filter uniformly darkens the image hence forcing the camera to use longer exposure times. The effect of the filter on the image quality is negligible.

The actual cut-off height cannot be easily measured, so a strategy to estimate it has been employed. With the cut-off fully open, and nothing inside the test chamber, the shutter speed has been selected so that the background was middle grey. This condition can be achieved with a reasonable accuracy by looking at the live histogram in digiCamControl while varying the shutter speed until most of the pixels have a value of 127. It is now easy to calculate all the shutter speeds needed to achieve the desired cut-offs while maintaining the background at the same brightness level. Neglecting the ISO level (that is fixed at ISO 100) the exposure value is given by:

$$EV = \log_2 \frac{F^2}{\Delta t} \quad (4.1)$$

where also F , the *f-number*⁴, is constant since neither the focal length nor the aperture change during the process. Because no lens is attached to the camera body the F value is unknown but, since only relative exposure values are needed, its value can be chosen freely. The exposure value for no knife-edge can now be calculated using the shutter speed obtained previously. Since a 50% cut-off would block half of the incoming light, the difference of EV from no cut-off to 50% cut-off is one stop. At 75% there would be one stop difference from the 50% knife-edge and two stops from the no cut-off. Following this logic, the stops variation from the reference case of the knife-edge fully open can be calculated with:

$$\Delta EV = \text{stops} = \log_2 \left(1 - \frac{a}{h} \right) \quad (4.2)$$

where a/h is the cut-off rate. Adding ΔEV to $EV_{0\%}$ and inverting *equation (4.1)* allows to calculate the shutter speed needed to have the desired cut-off, while keeping a middle grey background. This procedure can be repeated to find the exposure times for every single cut-off required.

Since the camera only allows to change the shutter speed by discrete increments (usually 1/2 or 1/3 of a stop), it can sometimes happen that some calculated values will not be feasible. In this case, the closest settable exposure time should be used. The actual cut-off value achieved with this new shutter speed can be then estimated. Evaluating *equation (4.1)* with this new exposure time will reveal the real EV of the picture. Subtracting this value to the reference $EV_{0\%}$ will

⁴ $F = f/D$ where f is the focal length and D is the aperture of the diaphragm

result in the real stops difference between the two knife-edges. The actual cut-off rate is then obtained by inverting *equation (4.2)*. The MATLAB script used for the estimation of the shutter speeds is presented in *Appendix A.1*. During the experiment, the shutter speed has been selected based on the desired cut-off, and the knife-edge has been moved until the background pixels were centred around the value 127. When this happens, it means that the wanted cut-off value has been achieved.

It is essential to remember that before the beginning of any experiment, the schlieren apparatus need to be set up properly. The best way to do so is to put a tiny object inside the test chamber, zoom into it and move the focusing lens until the image is as sharp as possible. In addition, the knife-edge must be positioned at the focal point of the second mirror. This requires the knife-edge to be moved to or away from the second mirror until, while adjusting the cut-off, the image darkens or brightens uniformly [9].

During the actual experiment, inside the test chamber a lit candle is present, and the background around it becomes perturbed. To correctly set the background to middle grey, a small area of interest far away from the candle flame has been considered, instead of the whole schlieren image.

The output from the camera are 14-bits NEF files⁵. These have been converted to 8-bits TIFF files using *macOS Preview* (or *dcrw* [23] on Windows systems) for the post-processing. A MATLAB script using the Debevec algorithm saw in *Section 2.3* has been implemented to blend the images and create the radiance map. The complete code can be seen in *Appendix A.2*. All the images have been converted to grayscale to make the process faster, since colours do not carry any useful information. This way, only one camera response function is recovered instead of three. As discussed in *Section 2.3*, to compute the response curve not all the pixels are needed. In this case, having five photos, 64 pixels are enough to solve the problem. However, attention must be paid when selecting them. If a spot on the schlieren image is extremely bright or dark, it could appear over-ranged on more than one picture. At different exposure times, that pixel would maintain the same value. Such event could make the resulting CRF less accurate. To avoid this issue, the MATLAB code let the user select a region of interest (ROI) where the pixels can be sampled. As shown in *figure 4.1*, the flame of the candle is represented extremely bright in the picture, so the area of interest used does not include these pixels.

After acquiring all the pictures, the correctly exposed low dynamic range images (LDR) have been compared to highlight the changes of pixel values at different cut-off rates. These would be the

⁵ *Nikon Electronic Format. RAW image file exclusive to Nikon cameras.*

images obtained from the schlieren system if no HDR technique was used. Since is not possible to compare every single pixel of a picture, a line of pixels from the lower bottom of every image is extracted and superimposed to the others (*figure 4.2*).

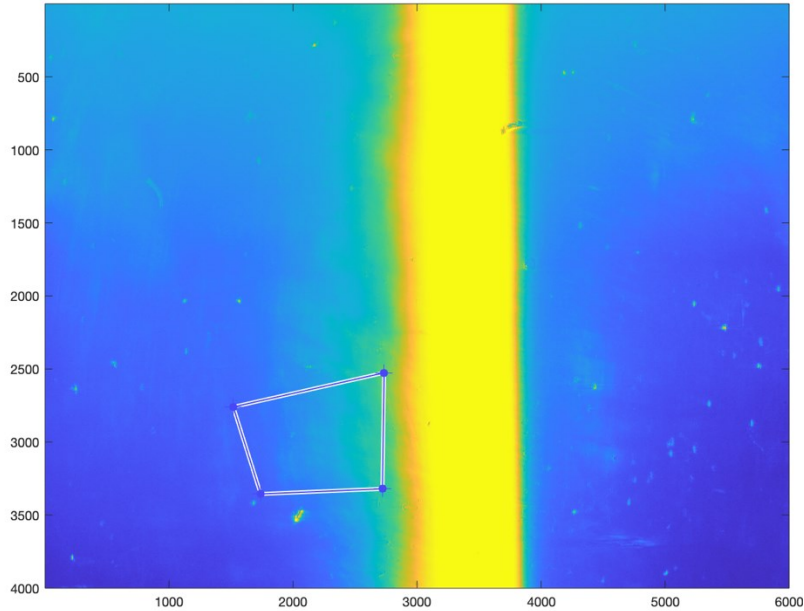


Figure 4.1 – ROI selection for pixel sampling

The accuracy of the recovered CRF needs to be estimated. To do so, a virtual image is created from the resulting radiance map as suggested in [5]. Since the HDR pixels contain radiance values, after choosing a virtual shutter speed equal to the one used to capture the original image, an exposure map can be created. Evaluating this matrix with the CRF return the virtual image, as shown in *equation (4.3)* where f is the response curve.

$$Z = f(\ln(X)) = f(\ln(E) + \ln(\Delta t)) \quad (4.3)$$

If the response function has been perfectly recovered, every single pixel of the virtual image should be identical to the original one. Subtracting one image to the other and computing the root mean square of the difference matrix provide a quality index for the recovered CRF.

$$RMS = \sqrt{\frac{1}{N} \sum_{x,y}^N (I_{original} - I_{virtual})^2} \quad (4.4)$$

The dynamic range expansion cannot be evaluated directly with *equation (2.1)* since the original image is a matrix of 8-bits integers, representing the pixel values, while the HDR radiance map is described by 32-bits floating point numbers representing the relative irradiance values as explained in *Section 2.3*. Nevertheless, since the CRF associates the pixel values to the scene radiance, it is simple to retrieve the maximum and minimum irradiance value of the original image:

$$DR_{original} = \log_2 \left(\frac{g(\max(original))}{g(\min(original))} \right) \quad (4.5)$$

where $g = f^{-1}$ is the inverse CRF recovered by the Debevec algorithm.

Since the HDR image already contains the irradiance values, its dynamic range can be directly obtained from *equation (2.1)*. The two values can now be correctly compared.

The radiance map cannot be visualized as it is and needs to be tone mapped to fit the dynamic range of the display, as described in *Section 2.2*. All the HDR images have been tone mapped using the MATLAB *localtonemap* function, that uses a Laplacian filter tone mapping technique [24]. There are many more tone mapping operator available that will be compared thoroughly in *Chapter 6*. The resulting image can be saved as an 8-bits JPEG or PNG without compression.

4.3. RESULTS

In *figure 4.2* the evolution of the pixel values at different cut-offs is shown. It can be noticed how the bright pixel of the picture are far away from their maximum value⁶ when the knife-edge is at 50% and 75%. At 85% some pixels are considerably close to the upper boundary. At 90% and 95% cut-off most of the bright pixels corresponding to the candle flame are saturated. It is particularly appreciable looking at the 95% curve, where around 700 pixels have a value of 255 and create a flat spot in the centre of it. It is expected that in these two cases the HDR technique will yield the best results.

⁶ 255 for the 8-bits images

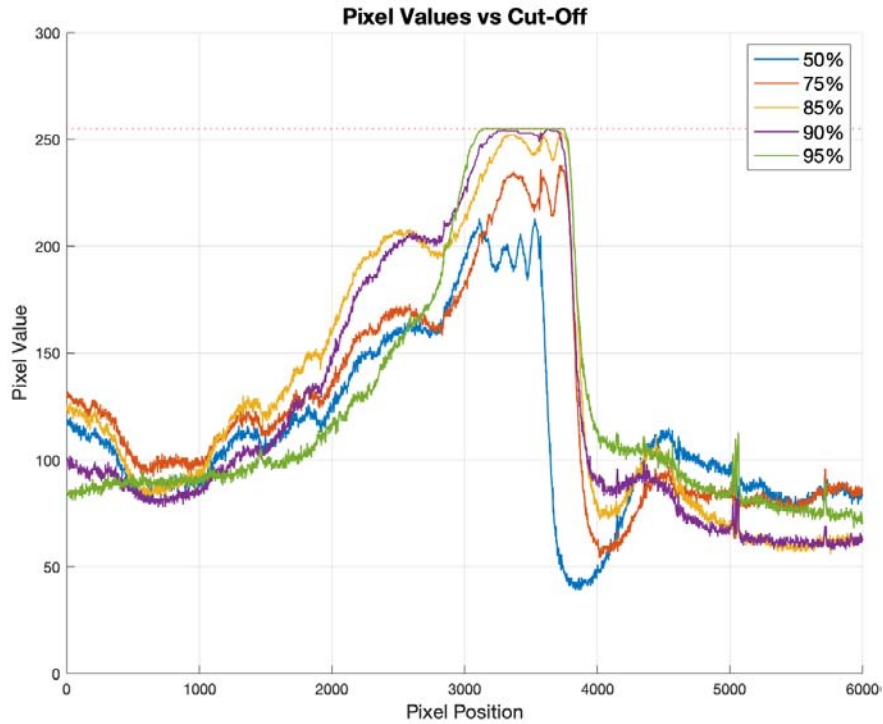


Figure 4.2 – Pixel values evolution with increasing cut-off value

The HDR radiance map is then computed and the results compared with the original correctly exposed LDR image. The resulting CRF percentage errors are reported in *table 4.2*. All of them are fairly low with the exception of the 85% cut-off, possibly a result of a blending of non-perfectly aligned images likely caused by a destabilization of the candle flame. In the same table, the average background pixel values are shown. It can be noticed how all of them are reasonably close to the target middle grey value, also meaning that the cut-off is close to the desired value. *Table 4.2* show also the dynamic range expansion computed with *equation (2.1)* and *equation (4.3)*.

Table 4.2 – Results from the first experiment

| Cut-Off [%] | Background Pixel Value | Error [%] | Original DR [EV] | Extended DR [EV] | CRF Error [%] |
|-------------|------------------------|-----------|------------------|------------------|---------------|
| 50% | 119 | 3.1 % | 5.1 | 5.1 | 0.7 % |
| 75% | 120 | 2.7 % | 5.6 | 5.8 | 0.3 % |
| 85% | 131 | 1.6 % | 5.1 | 6.3 | 7.2 % |
| 90% | 110 | 6.7 % | 4.5 | 5.8 (6.0) | 3.8 % |
| 95% | 131 | 1.6 % | 4.3 | 6.0 (6.9) | 2.5 % |

For lower cut-offs, where the pictures are not over-ranged, the dynamic range is not increased by much. Indeed, for 50% cut-off there is no difference in dynamic range from the original image to the radiance map. From 85% on, where pixels start to saturate, the dynamic range expansion is much more noticeable, spanning from 1.2 stops to 1.7 stops. The higher the cut-off, the broader the radiance map dynamic range becomes. This behaviour is visualized in *figures 4.3 and 4.4*.

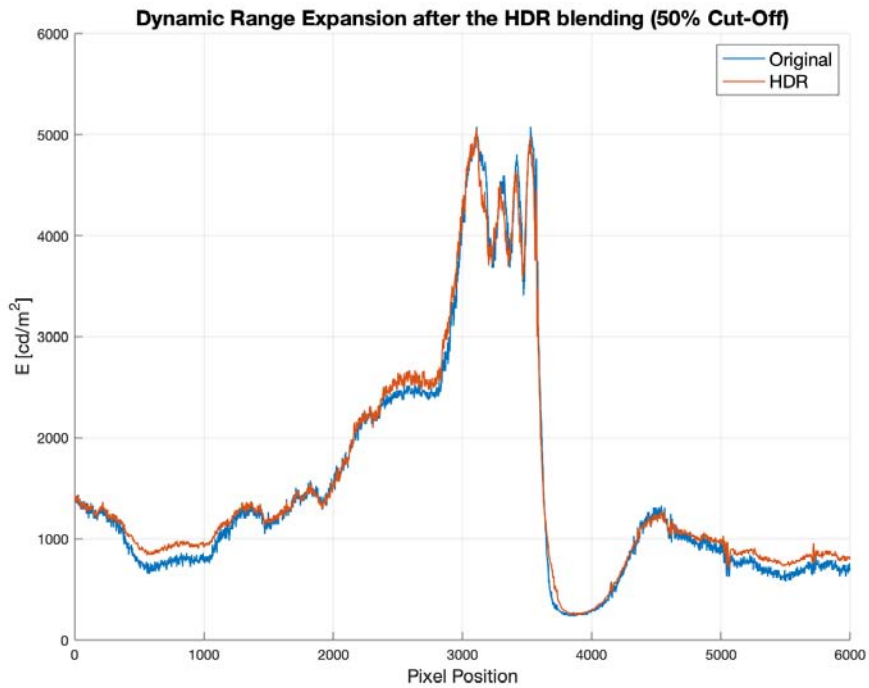


Figure 4.3 – The HDR blending process does not increase the DR for lower cut-off values

Since at high cut-offs the picture that was under-exposed by 2 stops looked still extremely bright near the candle flame, additional under-exposed images were captured, as shown in *table 4.1*. Doing so allowed for an even greater dynamic range expansion, quantified as 1.5 stops for 90% cut-off and 2.6 stops for 95% cut-off.

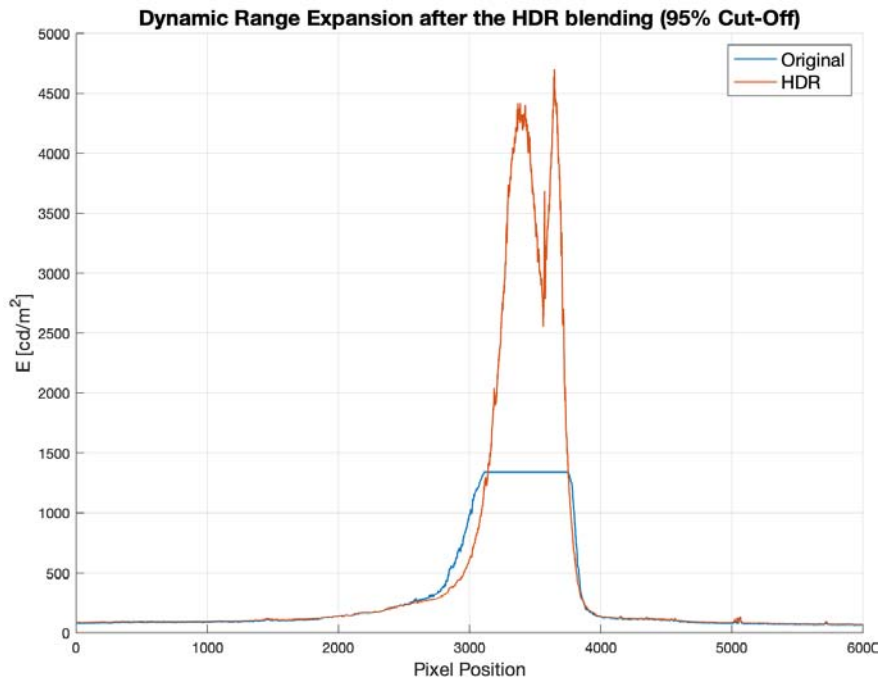


Figure 4.4 – The DR expansion is extremely noticeable for high cut-off values

A comparison between the initial single correctly exposed picture and the final tone mapped HDR image is shown in *figure 4.5*. The enhancement of the details is clearly visible. While on the original picture the candle flame was completely white and no elements could be distinguished in and around it, in the final image the flow characteristic are visible, and many more details can be discerned.

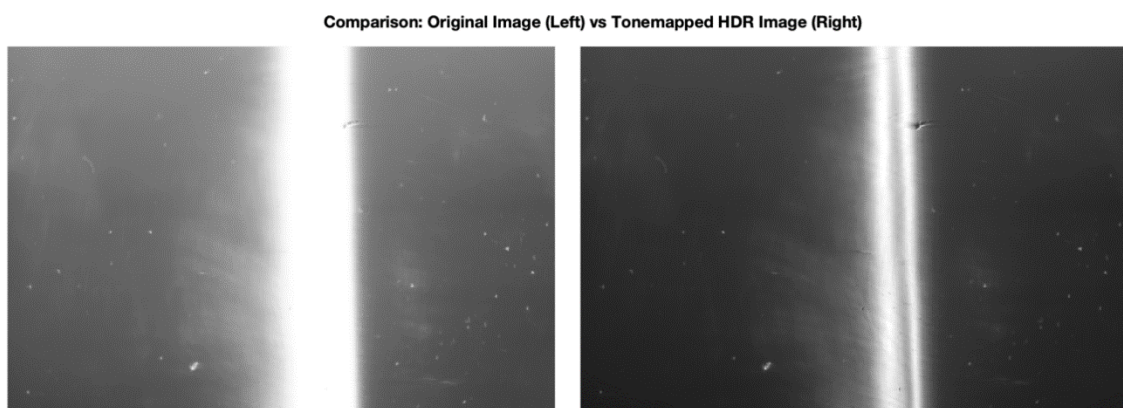


Figure 4.5 – Comparison between the original LDR image and the tone mapped HDR image (95% cut-off)

Comparing the original pixel values to the tone mapped ones (*figure 4.6*) demonstrate how the tone mapping process can squeeze the extended dynamic range of the radiance map to the

limited range of 8-bits images without over-ranging any pixel. Also, the figure undoubtedly shows how the dynamic range of the final image pixels have been extended.

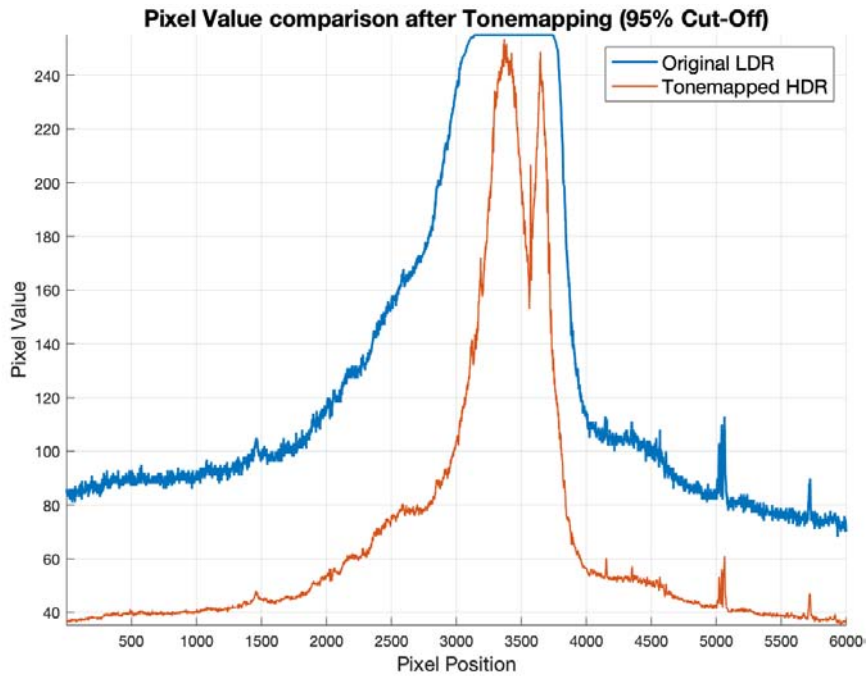


Figure 4.6 – Pixel values in the original image and in the final tone mapped image (95% cut-off)

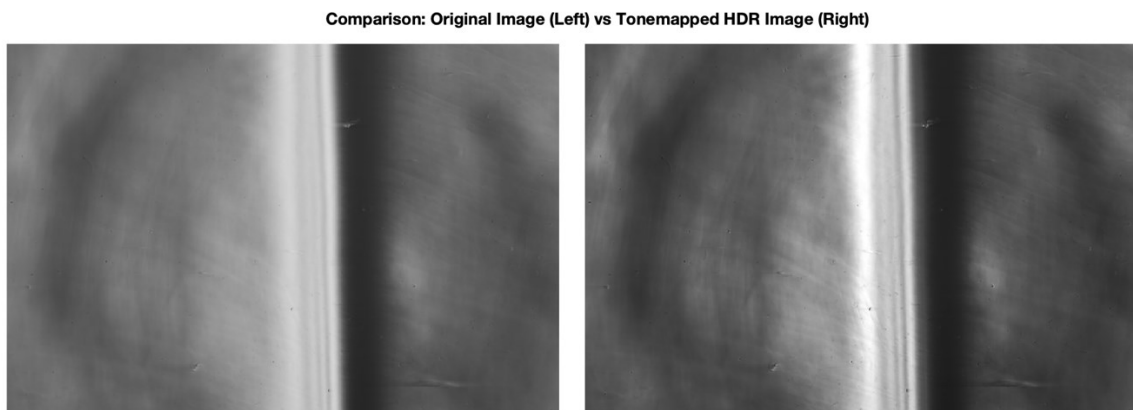


Figure 4.7 – Comparison between the original LDR image and the tone mapped HDR image (50% cut-off)

Even if at lower cut-offs the dynamic range cannot be extended by much, as discussed previously, the tone mapping process can still improve the captured schlieren images. *Figure 4.7* shows the comparison between the two images for a 50% cut-off. In the original image all of the details inside the flame are already detectable, but the tone mapping operator distributes the pixel values over all the available range, enhancing the contrast and making the details more

easily distinguishable. The transformation of the pixel values before and after the tone mapping are visible in *figure 4.8*.

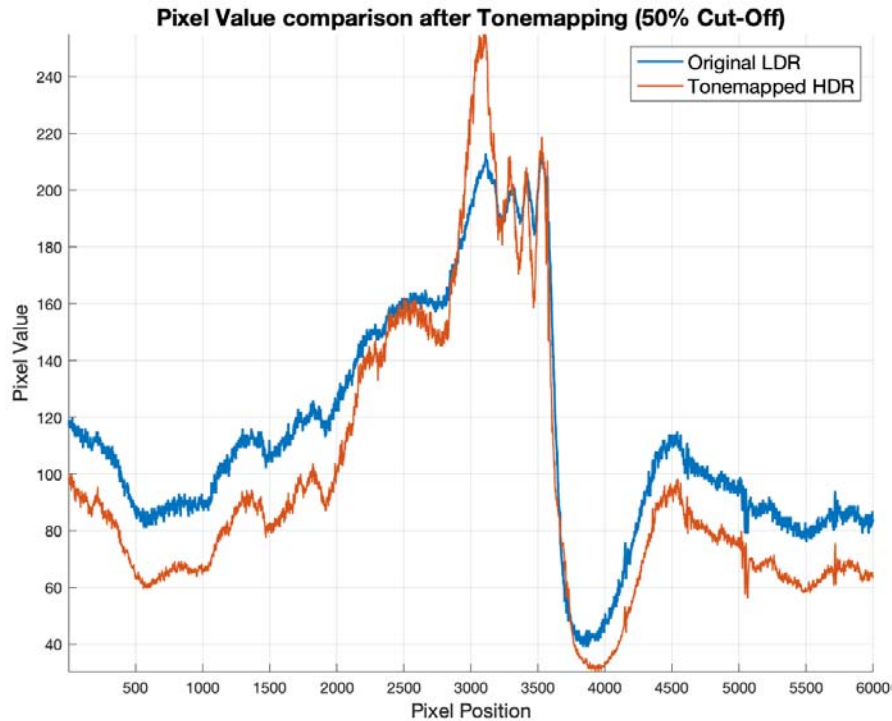


Figure 4.8 – Pixel values in the original image and in the final tone mapped image (50% cut-off)

4.4. CONCLUSIONS

This chapter has introduced the procedures used to properly set up the experiment, capture and blend the images, and estimate the dynamic range improvements.

The HDRI technique has been proven to be effective for recovering data within the over ranged regions of the schlieren image when these are present at higher cut-off rates. The resulting radiance map has been tone mapped successfully to produce a picture without any over ranged pixel. The tone mapping process has been proven to be useful also when applied to traditional schlieren images, where it could enhance faint details and improve their contrast.

5. HDR SCHLIEREN WITH STEADY FLOWS

One of the main issues of the schlieren technique is capturing both strong and weak flow features in a single image. Visualizing weak features requires a high cut-off value, but this way the strong features will become over ranged. In this chapter, the HDR technique described previously will be applied to visualize a steady hypersonic flow around an aerodynamic body. The aim of this investigation is to determine if the technique can produce a picture with more details than the classic schlieren images, recovering the over ranged strong features while at the same time maintaining the weak features.

5.1. EXPERIMENTAL SETUP AND PROCEDURE

The aerodynamic body used for the experiment is a flared cone, shown in *figure 5.1*, at zero angle of attack. This body will generate a complex flow around itself, including an attached conical shock, flow expansions, shear layers and a strong shock interaction that will stress the limits of the schlieren apparatus [18] (*figure 5.2*).

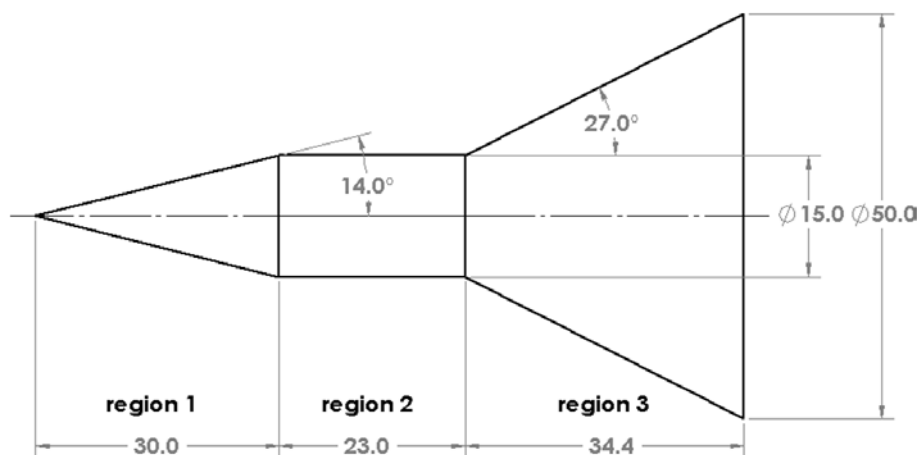


Figure 5.1 – Flared cone geometry [mm] [18]

The tests have been run in the HSST tunnel at $M = 5$, with a total pressure $P_0 = 800 \text{ kPa}$ and a total temperature $T_0 = 300 \text{ K}$. Since the gas is dry air, $k = 1.4$ and $R = 287$, that leads to a

total density $\rho_0 = 9.29 \text{ kg/m}^3$ and a static density $\rho = 0.105 \text{ kg/m}^3$. The knife-edge has been maintained vertical throughout the entire experiment.

Three regions of interest have been selected to compare the original image with the HDR one, for the same reasons stated in *Chapter 4*. Region A include the first (weaker) shock, the first expansion and the first shear layer. Region B include the second (stronger) shock and expansion. Region C include the weak shear layer behind the body. It can be seen in *figure 5.2* how the latter is extremely faint and hardly noticeable, while the second shockwave is so strong that appears as completely black.

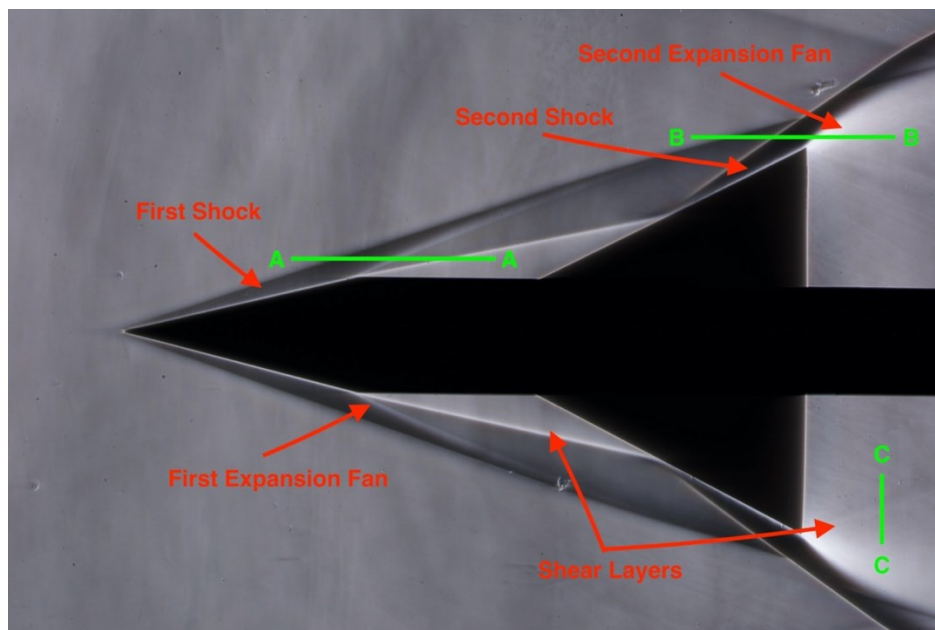


Figure 5.2 – Flow features and regions of interest

As in *Chapter 4*, the tests have been repeated for different cut-off rates (see *Table 5.1*). For every one of them, a series of five bracketed images have been captured at $0, \pm 1, \pm 2$ stops. Again, at higher cut-off rates two additional pictures have been taken, at -3 and -4 . For every cut-off value, the background has been maintained at middle grey with the same technique described in *Section 4.2*. Like in the first experiment, it has been necessary to use an ND8 filter to be able to capture the under-exposed pictures when the cut-off rate is low.

The HDR radiance map has been recovered with the Debevec algorithm and the before and after radiance values along the regions of interest have been compared. Only pixels outside the flared cone body have been taken into account in the post-processing of the images since it is rendered

as nearly black at every shutter speed and could undermine the correct estimation of the dynamic range. This has been accomplished by applying to every image a black mask shaped like the conical body that indicates which pixels not to consider for the calculations. The mask can be seen over the body in *figures 5.3* and *5.4*.

Table 5.1 – Test matrix of the experiment

| <i>Cut-Off</i> | <i>Bracketing stops</i> | <i>Reference shutter speed [s]</i> |
|----------------|-------------------------|------------------------------------|
| 35% | 0, ± 1, ± 2 | 1/400 |
| 50% | 0, ± 1, ± 2 | 1/320 |
| 75% | 0, ± 1, ± 2 | 1/160 |
| 85% | 0, ± 1, ± 2, (-3, -4) | 1/100 |
| 90% | 0, ± 1, ± 2, (-3, -4) | 1/60 |

Since to capture all the photos it has been necessary to run the tunnel several time, the mean and standard deviation of P_0 and T_0 have been calculated to confirm that all the pictures have been shot under the same boundary conditions.

As seen in *Section 4.1*, sometimes the shutter speed needed to achieve a certain cut-off value is not available in the camera settings, and the closest shutter speed available will be selected. Consequently, the actual cut-off values obtained when the background value is 127 will be slightly different than the theoretical ones. For this reason, the estimated actual cut-off values will be reported in the results.

Ultimately, the results obtained from 8-bit images and 16-bit images have been compared.

5.2. RESULTS

The real total pressure and temperature, obtained from the HSST sensors, are $P_0 = 807.64 \text{ kPa}$ and $T_0 = 304.4 \text{ K}$, with an error at 3σ respectively of 0.19 % and 0.36 %. These results certify that the boundary conditions have been maintained virtually constant throughout the experiment. In *figure 5.3* the empirical shockwave angles have been calculated and visualized with ImageJ. Using the $\theta - \beta - M$ charts or equations [25] it is possible to estimate the theoretical angles and compare them to the empirical ones. The first compression generates a wave angle of 18.95° , that differs 0.15° from the one obtained by the compressible flow theory.

After the first shock, the Mach number drops to $M \approx 3.93$. The second flare has a deflection angle of 27° that should produce an oblique shock inclined by 33.86° . This differs only 0.22° from the actual angle obtained by the experiments. The theoretical results are compatible with the empirical ones and they show again that the desired boundary conditions have been obtained. Moreover, they show how accurate the compressible flow theory is, even at high supersonic speed.

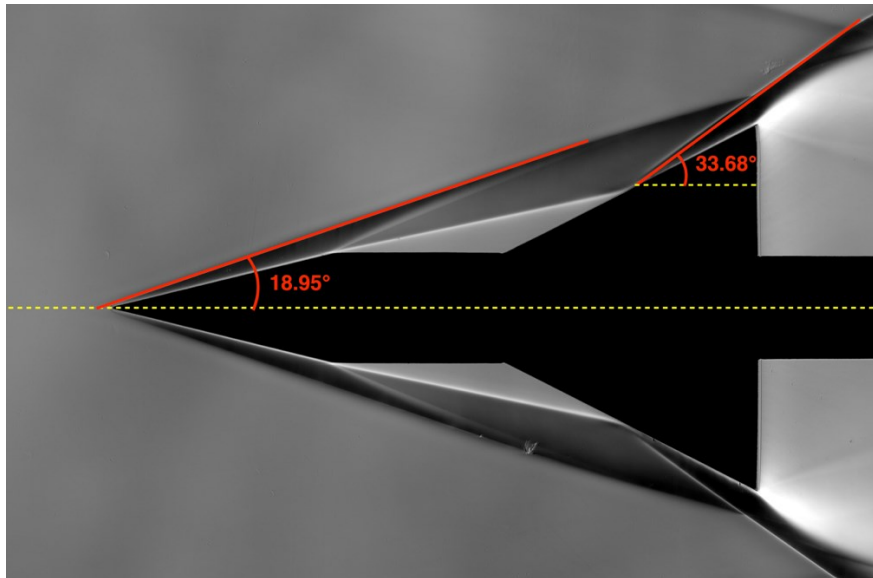


Figure 5.3 – Shockwave angles obtained from the schlieren image

Figure 5.4 compares the pixel values from the original correctly exposed image at 35% and 90% cut-off. It can be noticed how the brightest pixels are located in the rear of the cone, where the strongest expansion occurs. At low cut-off rates, only a few burned⁷ pixels are present, while at higher cut-off a considerable region in the aft of the body becomes over ranged. It is expected that this will be the area where the most information can be recovered. On the other hand, the only black pixels found in the image are the ones representing the body, where no useful data is stored. In the 90% cut-off image also the first expansion fan and shear layer seem nearly over ranged, suggesting that some data can be recovered in that location too. Ultimately, some over ranged pixels are found on the edge of the body and on the edge of the second shock. These are not flow features, but diffraction artefacts caused by the high cut-off rates. No useful information can be found at these locations.

⁷ In photography, burned pixels are the bright white over ranged pixels.

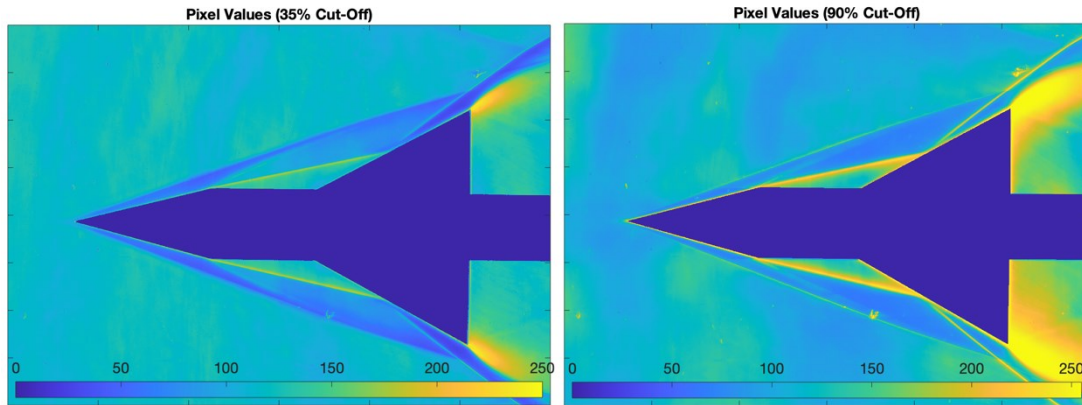


Figure 5.4 – Pixel values comparison between 35% (left) and 90% cut-off rate (right)

The pixels values of the original low dynamic range image have been compared for every cut-off value. As anticipated, only three regions of interest have been used for the analysis. *Figure 5.5* shows the changes in values in the region of the first compression (the weaker shockwave, region A—A). It can be seen how no pixel is over ranged, even at 90% cut-off rate.

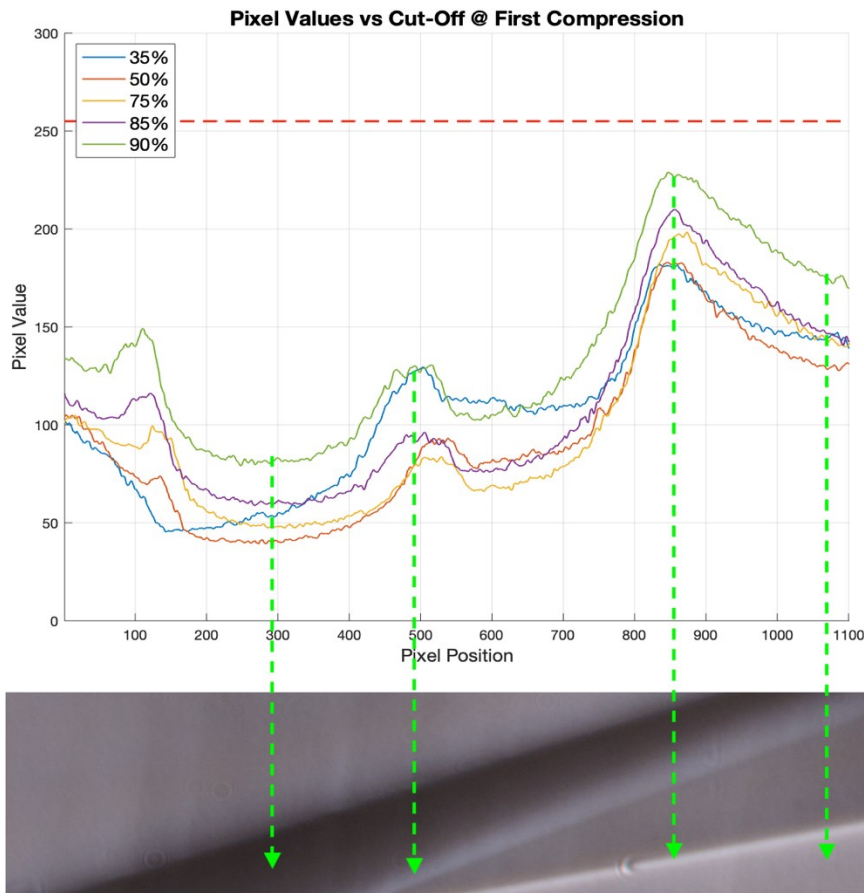


Figure 5.5 – Pixel values comparison at section A—A (First shockwave)

Instead, in correspondence of the second shockwave (the strongest one, region B—B) pixels reach the upper limit of 255 already at 75% cut-off, showing how this flow produce much stronger density gradients than the candle seen in the first experiment. As anticipated, these burned pixels are found adjacent to the rear expansion fan (*figure 5.6*).

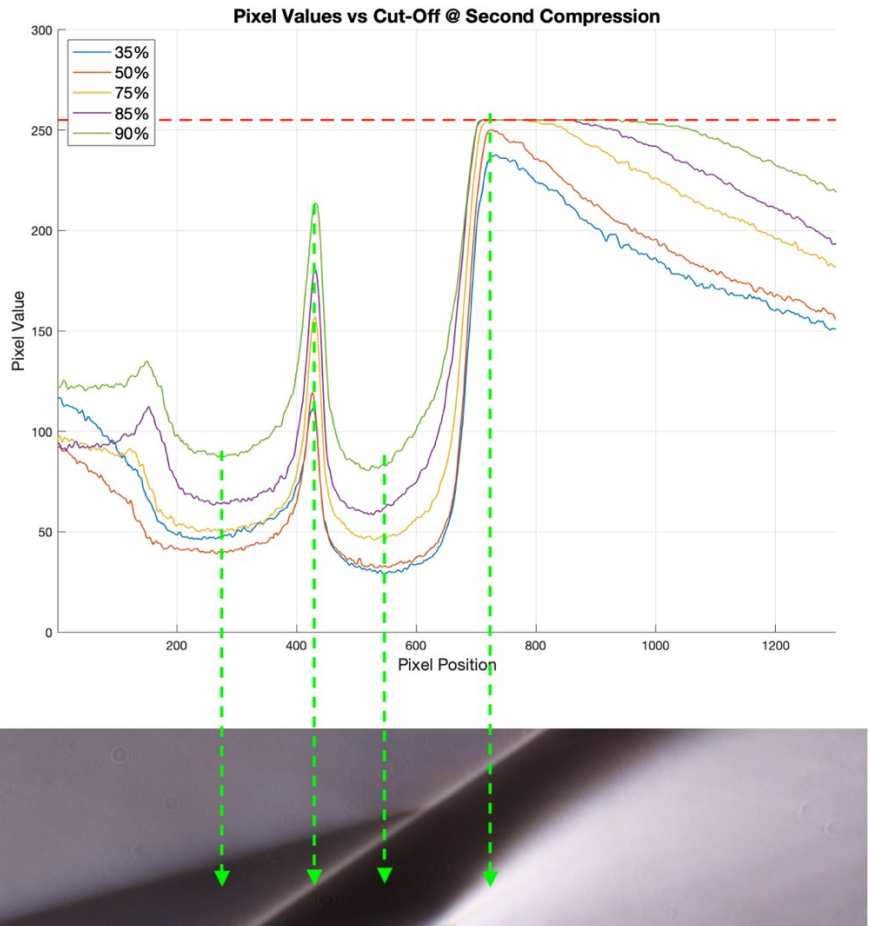


Figure 5.6 – Pixel values comparison at section B—B (Second shockwave)

Finally, in *figure 5.7* the pixel values at the rear shear layer (region of interest C—C) are compared. Again, not a single pixel is over ranged in this area. It is also really noticeable how little the pixel values change along the line meaning that the contrast is very low, and it is the reason why the shear layer in the line C—C is barely noticeable in the schlieren image. Always looking at *figure 5.7*, it can be observed that the highest contrast is obtained at 85% cut-off, since the values vary the most in this case. It can be assumed that this will be the cut-off value were this flow feature will be rendered the best, even if only slightly better than the other cases.

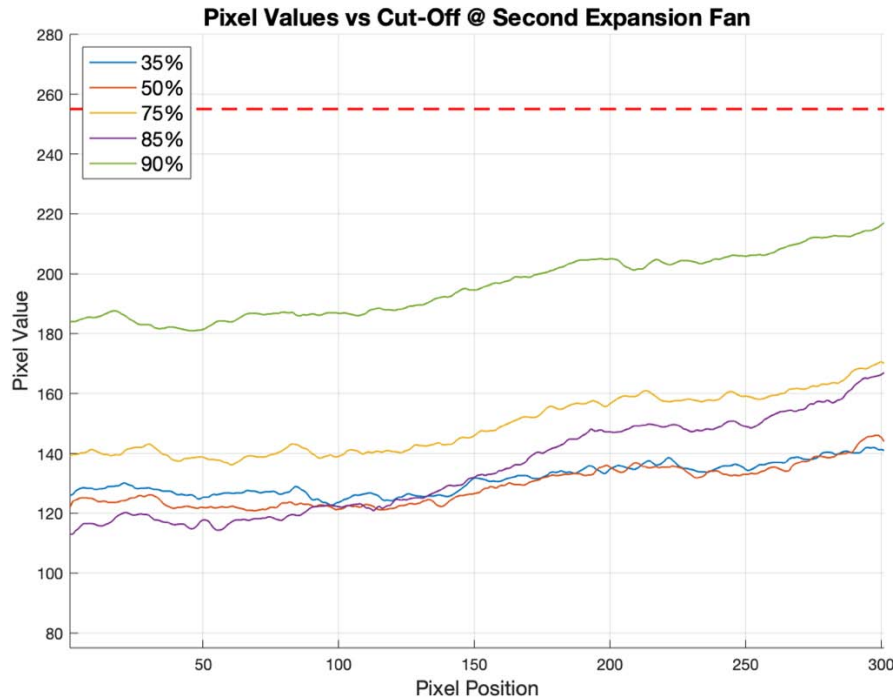


Figure 5.7 – Pixel values comparison at section C—C (Rear expansion fan)

The HDR radiance map has then been computed, and the irradiance values have been compared with the original low dynamic range image. As in *Chapter 4*, only black and white images have been used, so only the luminance channel CRF is estimated.

In all the test cases the background grey level has been successfully maintained close to 127 and the estimated errors for the recovered CRF are fairly low (*Table 5.2*). As expected, at lower cut-offs values there is no dynamic range expansion since no pixels were initially over ranged. However, unlike the candle experiment, starting from 50% cut-off rate some details can be already recovered and the dynamic range can be extended. The reason, as stated before, is that density gradients are much stronger in this flow than in the previous one and can over range the camera sensor and the schlieren apparatus at much lower cut-off values.

At 35% cut-off there is not difference between the original and the HDR image in terms of dynamic range. At 50% the dynamic range increase is hardly noticeable, with a difference of 0.2 EVs between the two pictures, whereas at 75% cut-off the dynamic range has been extended by 1.0 stop, and at 85% and 90% by 1.1 and 1.3 stops. These values are comparable to the results seen in the previous experiment. Another 0.2 to 0.4 stop can be recovered by using two additional under-exposed images at higher cut-offs.

Table 5.2 – Results from the second experiment

| Cut-Off [%] | Background Pixel Value | Error [%] | Actual Cut-Off [%] | Original DR [EV] | Extended DR [EV] | CRF Error [%] |
|-------------|------------------------|-----------|--------------------|------------------|------------------|---------------|
| 35% | 124 | 1.2 % | 37.5 % | 6.2 | 6.2 | 0.5 % |
| 50% | 120 | 2.7 % | 50 % | 6.4 | 6.6 | 1.0 % |
| 75% | 123 | 1.6 % | 75 % | 6.1 | 7.1 | 0.9 % |
| 85% | 113 | 5.5 % | 84.4 % | 6.0 | 7.1 (7.3) | 0.6 % |
| 90% | 118 | 3.5 % | 90.6 % | 5.9 | 7.2 (7.6) | 3.6 % |

Most of the details are recovered nearby the bright expansion at the rear of the body (figure 5.9). The dynamic range has also been slightly extended around the region of the first expansion (figure 5.8). For really high cut-offs (85% and 90%) a minor increase in dynamic range is obtained also at the second shear layer (figure 5.10).

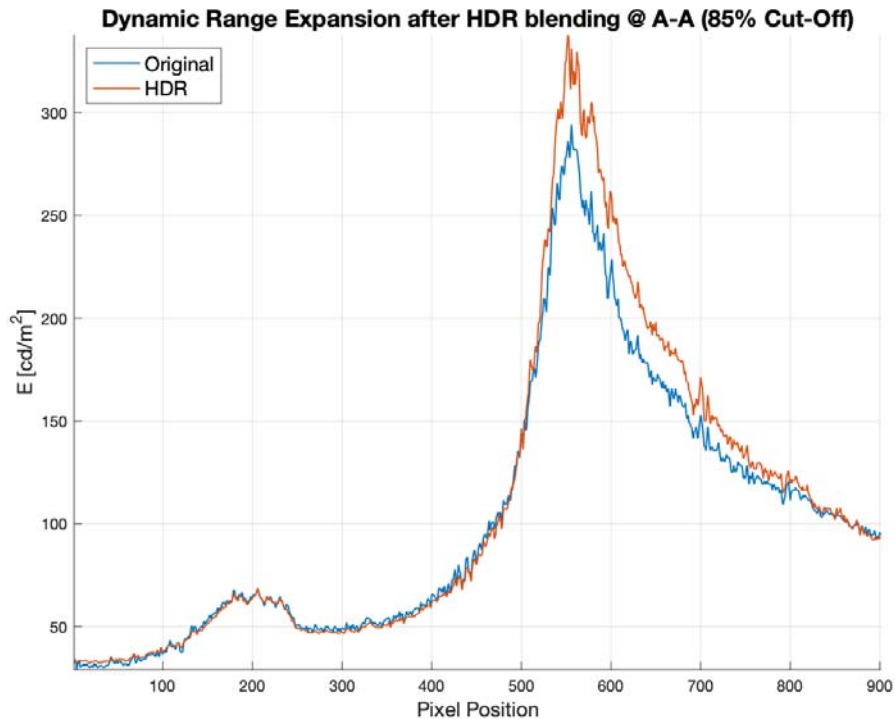


Figure 5.8 – DR expansion nearby the first shockwave (5 images blend)

When the two additional under-exposed images are used, the CRF error increases. Moreover, looking at the tone mapped images, more artefacts are present. This condition can be due the extreme brightness changes present in the bracketed images. In the -4 and -3 stops pictures,

most of the pixels become completely black, while only the rear expansion fan renders some details. Having pixels that do not change values at different shutter speeds can affect the recovery of the camera response function. This is the same reason why sampling pixels outside over-ranged regions is suggested and can improve the resulting response curve (see *Section 4.2*).

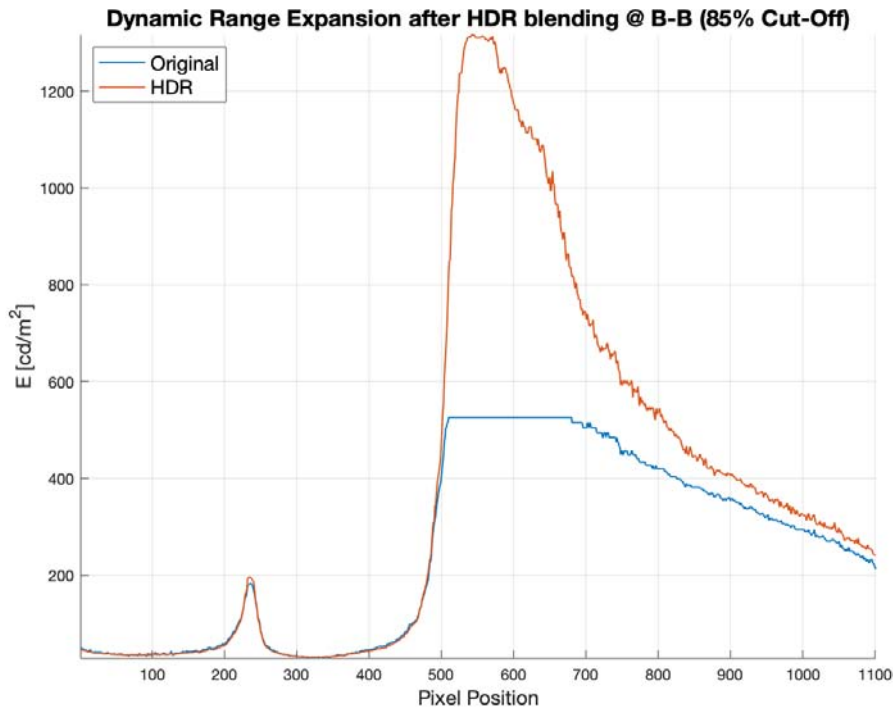


Figure 5.9 – DR expansion nearby the second shockwave (5 images blend)

It is not advised to capture photos too under or over-exposed because, even if the calculated dynamic range expansion can be wider in terms of radiance, the resulting images may have a lower quality compared to the pictures obtained with just ± 2 stops bracketing.

Finally, results from 8-bits and 16-bits TIFFs have been compared. The CRF errors obtained in the two cases are virtually the same. In *figure 5.11* a detail of the radiance maps obtained from 8-bits and 16-bits images has been compared. It can be noticed how the 16-bits pictures helped recover the radiance values more accurately in the centre of the expansion fan, where the strongest expansion happens. The same area is rendered as completely yellow in the false colour image of the radiance map obtained with 8-bits images. This occurrence could be a consequence of the conversion from RAW to 8-bits TIFF.

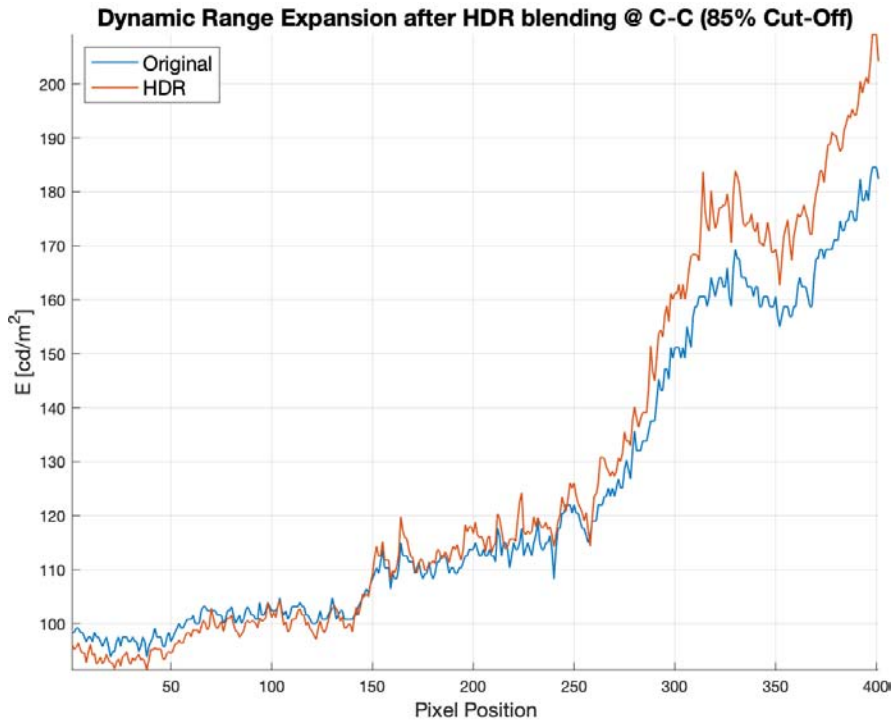


Figure 5.10 – DR expansion at the rear shear layer (5 images blend)

The original output from the camera sensor is a 14-bits image, that can be then converted as either an 8-bits or 16-bits TIFF. Since the shades available in the former format are many fewer, inevitably some pixel that are really bright but not over ranged in the original file will get converted to a value of 255, extending the clipped (*figure 5.12*). Taking the 8-bits images and multiplying them by 256 creates pictures that are encoded as 16-bits, but virtually the same as the original 8-bits one.

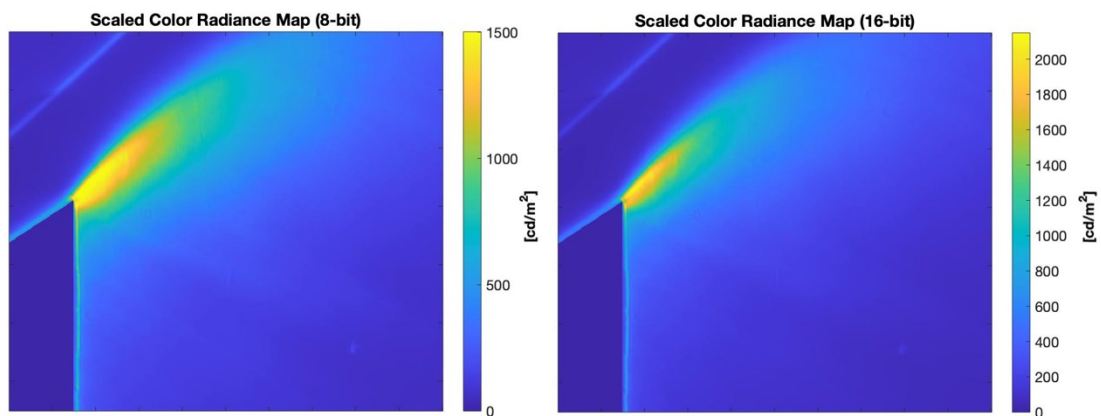


Figure 5.11 – Comparison between radiance maps obtained with 8-bits (left) and 16-bits (right) images

The dynamic range expansion after blending these pictures is the same retrieved with the latter, and lower than the one obtained from true 16-bits ones, furtherly proving the point. It can be concluded that pictures encoded with 16-bits could possibly help recover a more accurate radiance around almost over ranged areas.

Since the retrieved maximum radiance is higher for the 16-bits images, mathematically the dynamic range expansion appears wider. This behaviour is more appreciable for images captured at high cut-off rates (85% and 90%), where the dynamic range expansion was 0.6 EVs higher than the one obtained with the same images but encoded with only 8-bits. At lower knife-edges the difference was close to none.

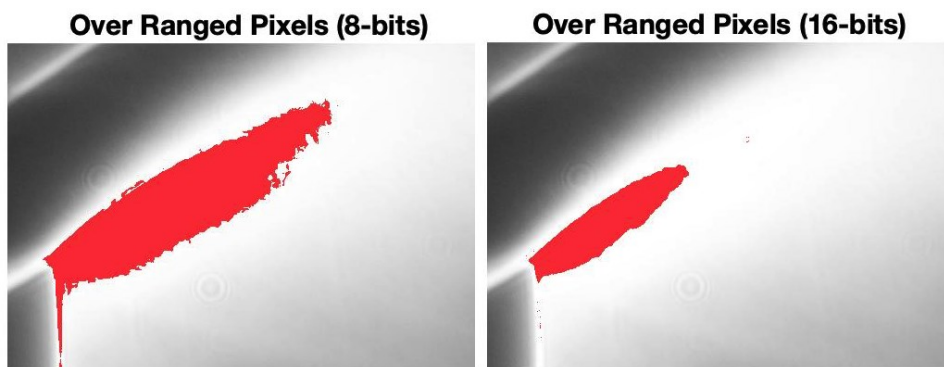


Figure 5.12 – Clipped pixels in 8-bits (left) and 16-bits images (right)

In reality, the 16-bits images do not show an appreciable visual improvement of the HDR image. Classic 8-bits images, as suggested in [1], contain enough data for the purpose of qualitative schlieren imaging. The additional shades of grey rendered by images with a deeper bit depth are nearly invisible to the eyes but could be useful for accurate density measurements with calibrated schlieren. However, sometimes a noticeable improvement in image quality can be gained by saving the tone mapped image with a bit depth of 16 instead of 8 (*Chapter 6*).

5.3. CONCLUSIONS

The HSST has been successfully run several times without any significant change in the boundary conditions, meaning that all the pictures have been captured at the same density, temperature and Mach number. All the computed background values were close to middle grey,

suggesting that the desired knife-edges have been achieved throughout the experiment. Moreover, the estimated CRF errors were fairly low, showing that the recovery of the radiance map was completed successfully and with a reasonable accuracy.

Since the density gradient produced by the HSST were much greater than in the previous experiment (*Chapter 4*), the sensor began to saturate already at 75% cut-off rate. As expected, the HDRI was able to recover information on the over ranged regions of the scene, mostly within the rear expansion fan. In the next chapter, the radiance map will be tone mapped to evaluate its advantages over a classic schlieren image.

When processing the images it is also worth to consider their bit depth, thus a comparison between 8-bits and 16-bits encoding has been performed. The test has shown how 8-bits images can lose information during the conversion from the 14-bits RAW files to TIFF (or any other format), while 16-bits images can generate a more detailed radiance map. Even if visually the differences are hardly noticeable, using 16-bits images could be useful to deliver more accurate results with techniques that measure the density changes like calibrated schlieren.

6. TONEMAPPING AND IQ ASSESSMENT

The previous chapter has shown the improvement obtained with the HDR image in terms of dynamic range expansion and recovery of data in the over ranged regions. However, to study the flow around the body it is necessary to visualize the image by fitting the extended dynamic range into the limited dynamic range of a display. This process is done by tone mapping operators (TMOs). In this chapter different TMOs will be compared, and the best ones will be selected with the help of some image quality assessment indexes. Ultimately, the final tone mapped image will be compared with the original low dynamic range image to determine if the HDR blending technique has actually improved the general image quality and usefulness.

6.1. TONE MAPPING OPERATORS

Tone mapping operators try to fit the wide dynamic range of a radiance map into the limited range of a display or printer in the best way possible, meaning with as little artefacts and noise as possible while maintaining all the details and visual fidelity. TMOs can be divided in global, local, segmentation and frequency operators. Global operators apply the same function to all pixels, while with local operators the mapping depends on nearby pixels. Segmentation operators divide the image in various regions where different functions are applied. Finally, frequency operators, also known as gradient operators, separate the image in different frequency-based layers that will be mapped in different ways [17]. In addition, some TMOs try to simulate the response of the human visual system (HSV) to the illuminance of the scene rendered by the radiance map.

It can be quite hard to find the perfect tone mapping operator for an image. An operator that works really good in one situation can lead to disappointing results in other circumstances. Moreover, each TMO has some parameters to set (in many cases more than one) that add complexity in the process.

Ten TMOs has been selected to tone map the HDR schlieren pictures (*Table 6.1*). These include all types of mapping functions (global, local, segmentation and frequency). None of them simulate the HSV since it is not meaningful for the investigation.

Table 6.1 – List of tone mapping operators used in the investigation

| TMO | Script Source | Reference | TMO Type | n. Param. |
|--|---------------|-----------|--------------|-----------|
| <i>Adaptive Histogram Equalization</i> | MATLAB | [26] | Segmentation | 4 |
| <i>Local Laplacian Filter</i> | MATLAB | [24] | Local | 2 |
| <i>Multi-scale Decomposition</i> | MATLAB | [27] | Frequency | 5 |
| <i>Reinhard</i> | Custom Script | [28] | Global | 1 |
| <i>Linear</i> | Custom Script | [17] | Global | 0 |
| <i>Kim Kautz</i> | HDR Toolbox | [29] | Global | 2 |
| <i>Adaptive Logarithmic Map</i> | HDR Toolbox | [30] | Global | 1 |
| <i>Ashikhmin</i> | HDR Toolbox | [31] | Local | 2 |
| <i>Exponential</i> | HDR Toolbox | [17] | Global | 1 |
| <i>Fast Bilateral Filter</i> | HDR Toolbox | [32] | Segmentation | 1 |

At first, appropriate parameters for each of the TMOs have been found with a basic optimization algorithm using the image quality metrics (IQ metrics) that will be shown in *Section 6.2*. The algorithm iterates over all the available parameters and then reports the combination that obtained the highest IQ score (the script can be seen in *Appendix A.3*). Successively, the tone mapped images have been subjectively and objectively compared, again with the help of IQ assessment metrics. Finally, the best operator has been chosen based not only on IQ but also on computing time and personal preference. In addition, the results from the Exposure Fusion technique [16], mentioned in *Section 2.3*, have been analysed and compared. The analyses have been performed for a knife-edge of 85%, but the process can be repeated with every cut-off value.

Tone mapping is not the only way to visualize an HDR picture. An alternative way to display it is by rendering just a portion of the extended dynamic range at a time without any tone mapping. The regions that cannot fit into the dynamic range of the display will be clipped. It is possible to interactively shift the dynamic range window that is visualized with a slider or by pointing at the region that needs to be correctly exposed, as done by HDR Toolbox [17] (*figure 6.1*).

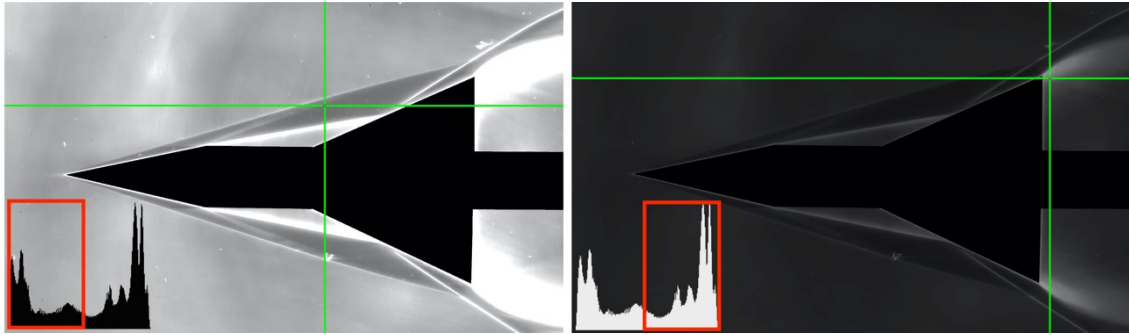


Figure 6.1 – Interactive exposure visualization (histogram for illustration purposes only)

6.2. IQ ASSESSMENT

Image quality can be evaluated empirically or with the help of objective metrics. The former requires many human participants to subjectively evaluate the pictures and it is time consuming, so plenty objective metrics have been developed during the years to avoid arranging experimental investigations. These works by either comparing a test image to a reference image (referenced metrics) or by just analysing the picture by itself (no reference) [33]. Some metrics can also predict the regions where an individual could notice differences between the two images, mimicking in some way an experimental evaluation (like HDR-VDP-2 [34]).

Most of the IQ metrics are made for classic low dynamic range images, even if recently some of them have been expanded to work on HDR images [17]. The majority of them, as expected, yield scores that are the higher the more similar the test images are to the reference ones (RMSE, PSNR, SSIM [35]). This work properly when comparing, for example, a compressed or a noisy image to the uncompressed or clean original one. In this research, however, it is necessary to compare the original photo with the final tone mapped one. These two images will inherently have differences, since the final one is expected to contain more details and possibly have more contrast. Since none of the metrics available at the moment comply with these requirements, a simple non-referenced visual quality index has then been developed to assess the quality of the tone mapping operators by taking into account these four parameters:

- Number of over ranged pixels: a tone mapped image should have little or no over ranged pixels.

- Number of noisy pixels: the processing of tone mapping can produce noisy pixel, easily more than the original image. A good tone mapping operator should not present too many of them.
- Number of noticeable artefacts: tone mapping can generate visible artefacts (visual anomalies caused by the processing) in the picture that would disrupt the image quality. It is important for a TMO to not deliver an image with noticeable artefacts.
- Dynamic range: a tone mapping operator should be able to make use of all the available dynamic range in an 8-bits or 16-bits image, so the final image should have a dynamic range (in terms of pixel values) as wide as possible.

The visual score can be computed as a weighted average of these four parameters:

$$score = 100 * \frac{w_1(1 - \sum o.r. pix.) + w_2(1 - \sum noisy pix.) + w_3(1 - \sum artefacts) + w_4 \frac{DR}{bit}}{width * height * \sum_{i=1}^4 w_i} \quad (6.1)$$

where *pix.* stands for pixels, *DR* stands for dynamic range and *o.r.* stands for over ranged. Since a high-quality tone mapped picture is expected to have fewer over ranged regions, noisy pixels and artefacts but a wider dynamic range than the original picture, given *equation (6.1)* a higher score means a better TMO. The maximum score yielded by *equation (6.1)* is always 100, while the minimum is 0. The artefacts and noise maps have been determined using the MATLAB *piqe* function that implements the Perception-based Image Quality Evaluator [36]. This metric is not only useful for schlieren pictures but may be used with every kind of image to assess its quality. Alternatively, the IQ can be evaluated using the Tone Mapping Quality Index (TMQI) [36], that compares images with different dynamic range (the HDR radiance map and the tone mapped image) and outputs a score based on the structural fidelity and naturalness. As suggested in [18], this metric can be used for the TMOs parameters optimization along with *Equation (6.1)*. It is important to recognize that these metrics cannot completely substitute a subjective judgment, but they can help identify which operators are worth focusing the attention to.

6.3. RESULTS

Optimal parameters for every TMOs have been found with the help of the code discussed previously. As expected, some manual adjustments were needed. The IQ index using

equation (6.1) performed better than the TMQI during the optimization process, meaning that the parameters found by it produced images subjectively more appropriate.

All the TMOs listed in *Table 6.1* were then compared, again using both metrics. For *equation (6.1)* different weights have been tested. All the tone mapped images obtained are shown in *figure 6.2*. *Table 6.2* presents the four best tone mapping function computed by the IQ indexes. The Adaptive Histogram Equalization operator appear to be the best ones in most cases. The Bilateral Filter results the best when w_4 is set to zero, meaning that the dynamic range is not taken into account. Further, Ashikhmin, Kim Kautz and Exponential emerge as few of the best TMOs between the ten tested.

Table 6.2 – Best TMOs found by the IQ metrics

| TMQI | Equation (6.1) Weights | | | |
|--------------------|------------------------|--------------------|---------------|--------------------|
| | 1 - 1 - 1 - 1 | 1 - 0 - 0 - 1 | 1 - 1 - 1 - 0 | 3 - 0.5 - 2 - 1 |
| Adaptive Hist. Eq. | Adaptive Hist. Eq. | Adaptive Hist. Eq. | Bilat. Filter | Adaptive Hist. Eq. |
| Kim Kautz | Ashikhmin | Ashikhmin | Reinhard | Ashikhmin |
| Exponential | Kim Kautz | Kim Kautz | Exponential | Bilat. Filter |
| Ashikhmin | Exponential | Exponential | M. S. D. | Exponential |

Table 6.3 shows other parameters to help verify the quality and usefulness of the TMOs. The table presents the contrast, computed simply as maximum pixel value divided by minimum pixel value, along the regions of interest selected in *Section 5.1*. This information can reveal if in these areas the contrast has increased or not between the original image and the tone mapped one, letting weak and small details be more visible. It is particularly important for region C—C (rear shear layer). Additionally, *Table 6.3* shows the computational time⁸ needed to map the HDR image, the percent of over ranged pixels, noisy pixels and artefacts, as well as the dynamic range (in terms of 8-bits pixel values).

⁸ Running on an Intel i5 5257U (Dual Core, 2.7 GHz)

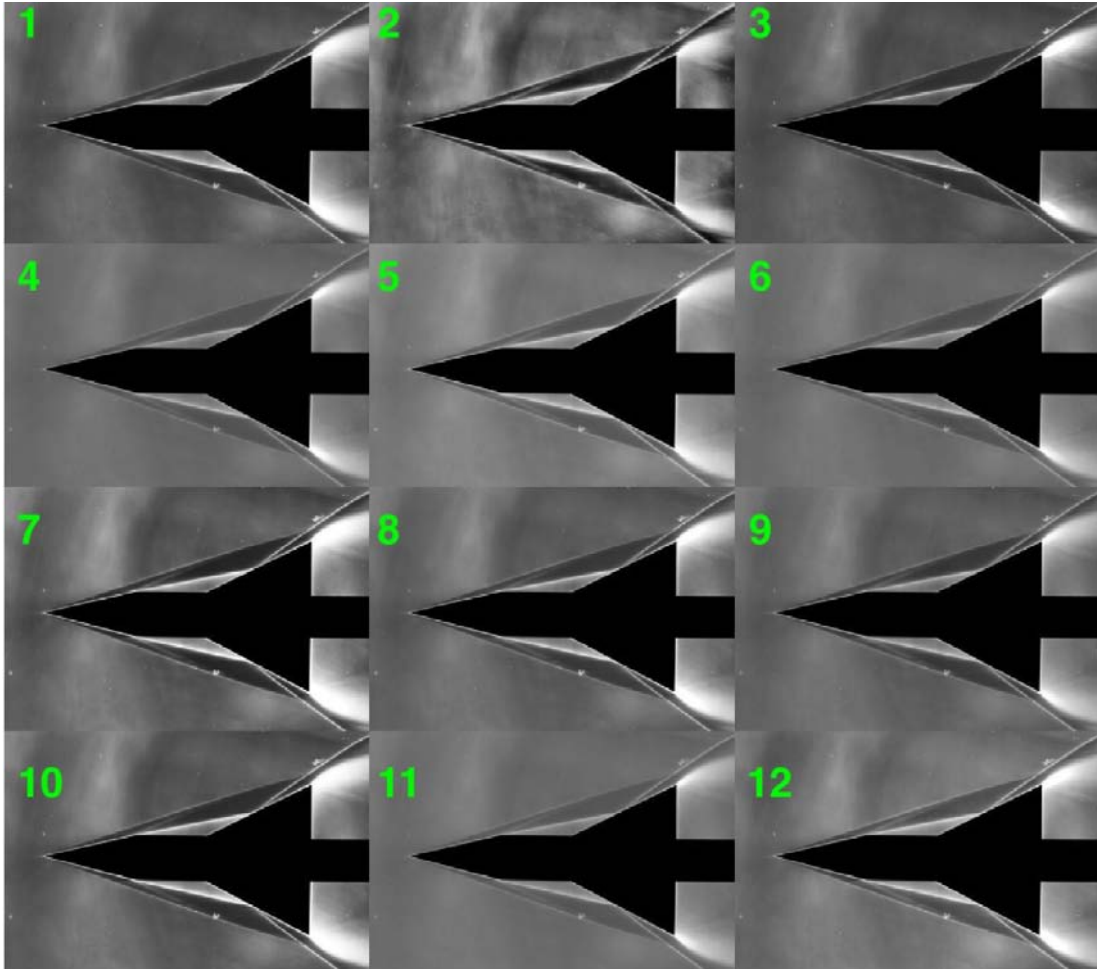


Figure 6.2 – Final tone mapped images (1) Original (2) Adaptive Hist. Eq. (3) Lap. Filter (4) Multi-scale decomp. (5) Reinhard (6) Linear (7) Kim Kautz (8) Adaptive Log. (9) Ashikhmin (10) Exponential (11) Bilat. Filter (12) Exp. Fusion

It can be noticed how the Adaptive Histogram Equalization yields the highest contrast for sections A—A and B—B but lose contrast in the rear region compared to the original photo. On the other hand, Exponential, Kim Kautz and Ashikhmin slightly increase the contrast on that region. The Adaptive Histogram Equalization generates a picture with fewer over ranged pixels than all the other operators, but also with many noisy pixels and artefacts.

The Bilateral Filter has a lower dynamic range than the original picture, along with the Reinhard TMO, resulting in a low contrast image as seen in *figure 6.2*. Moreover, the Bilateral Filter it is one of the slowest TMOs evaluated. The images have remarkably low noise and artefacts, and very few over ranged pixels.

Visually, Exponential and Kim Kautz TMOs are fairly similar and both produce a high contrast image. On the other hand, they exhibit more over ranged pixels than the original picture, making the use of the HDR counterproductive.

Ultimately, Ashikhmin TMO produces a picture with only a few over ranged pixels and artefacts, and fairly low noise. Even if the computational time is long this TMO produces the best tone mapped image (by subjective evaluation) without the need of post processing. The Bilateral Filter and Reinhard operator produce a better-quality image, as revealed by the IQ indexes, but since the contrast is so low that details are not easily discerned, some processing might be necessary (*Chapter 7*).

Table 6.3 – Contrast, computing time and various IQ parameters of some TMOs

| TMO | Contrast | | | Computing Time [s] | Over Range [%] | Noise [%] | Artefacts [%] | DR [EVs] |
|------------------|----------|-----|-----|-----------------------|-------------------|--------------|------------------|-------------|
| | A–A | B–B | C–C | | | | | |
| Original (35%) | 4.2 | 8.5 | 1.2 | / | 0.0 | 0.04 | 9.80 | 7.9 |
| Original (85%) | 3.7 | 4.5 | 1.4 | / | 0.2 | 0.04 | 11.10 | 8.0 |
| Adapt. Hist. Eq. | 5.5 | 8.2 | 1.3 | 2.6 | 0.02 | 1.65 | 19.8 | 8.0 |
| Kim Kautz | 4.8 | 5.4 | 1.5 | 3.3 | 1.02 | 0.04 | 11.2 | 8.0 |
| Ashikhmin | 3 | 3.9 | 1.4 | 66.4 | 0.08 | 0.25 | 8.44 | 8.0 |
| Exponential | 4.2 | 4.7 | 1.5 | 0.9 | 0.31 | 0.03 | 15.0 | 4.0 |
| Bilateral Filter | 1.9 | 2.8 | 1.2 | 7.0 | 0.02 | 0.02 | 1.65 | 2.0 |
| Reinhard | 2.1 | 2.7 | 1.3 | 2.4 | 0.02 | 0.02 | 15.2 | 2.3 |
| Exp. Fusion | 3.1 | 2.7 | 1.3 | 64.0 | 0.47 | 0.02 | 13.6 | 8.0 |

Additionally, the pictures obtained from the Exposure Fusion technique have been analysed. The results are similar to the other TMOs studied (*figure 6.2*). The picture shows low noise and the dynamic range is the maximum available in 8-bits. There are more over ranged pixels than the average, while the artefacts presence matches the other mapping techniques. The computing time is one of the longest, because it also includes all the processing to fuse the bracketed images. If the computing time to retrieve the CRF and create the radiance map is taken into account for all the others TMOs, the Exposure Fusion becomes the fastest technique.

As anticipated in *Chapter 5*, tone mapped images encoded with 8-bits and 16-bits have been compared. Unsurprisingly, a 16-bits encoding helps reducing the artefacts introduced by the TMOs by having more shades available to smooth the grey gradients in the picture. As shown in *figure 6.3*, the differences can be quite noticeable. Therefore, it is suggested to save the tone mapped images as 16-bits if the TMO allows to select this option.

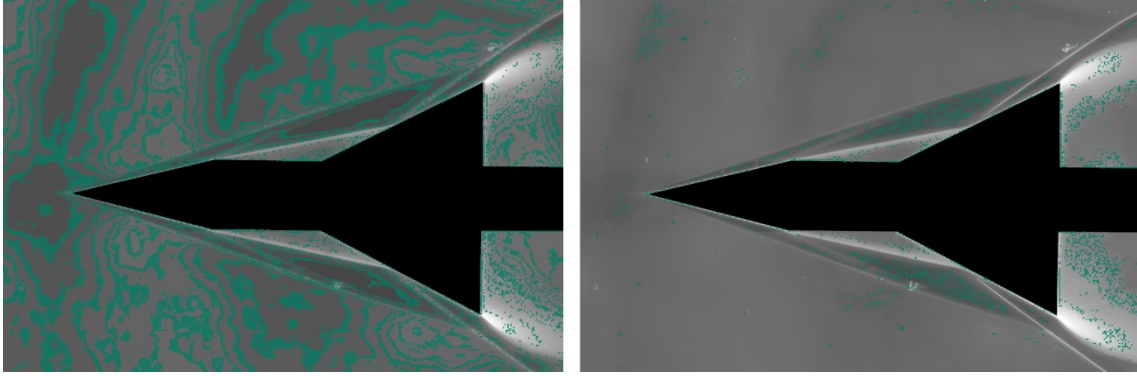


Figure 6.3 - 8-bits (left) and 16-bits (right) artefacts mask after a linear tone mapping

It is extremely important to observe *figure 6.4*. While it is true that some over ranged regions have been recovered with the HDR technique at high cut-offs, the final image does not appear to actually contain more details than a single picture captured with a knife-edge at 35%. Indeed, the latter clearly shows more features particularly around the first conical shockwave. While increasing the knife-edge raises the sensitivity of the system, it also narrows the measurement range. Moreover, it becomes strongly asymmetric, meaning that it takes a greater change in density to reach the upper limit of brightness than the lower one (*figure 6.5*). While this high sensitivity can improve the weak flow features and easily over range the camera sensor, making the HDR technique useful, it also reduces the shades visible in the darkest regions of the image. For this reason, the gradients inside the first shock are only visible with a 35% cut-off, while with the 85% they all appear as nearly uniform black. Indeed, as showed in *Table 6.3*, at high cut-offs lot of contrast and details are lost in the darkest regions, where the shockwaves are stronger. Furthermore, high cut-offs introduce diffraction effects that can degrade even more the image quality.

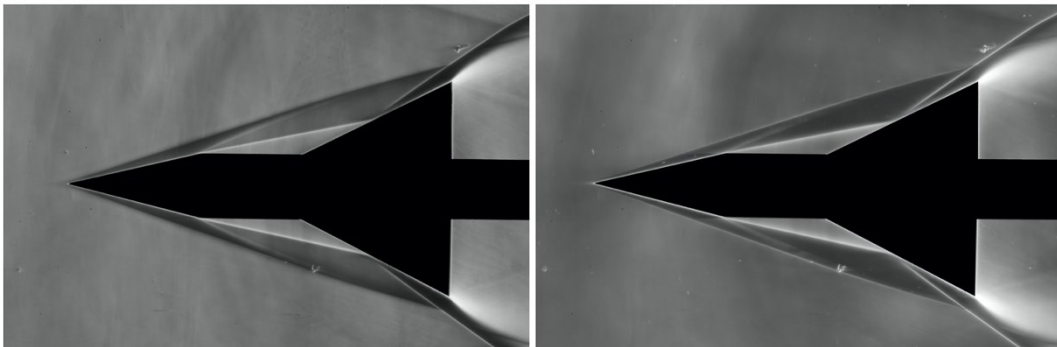


Figure 6.4 – Comparison between the picture taken at 35% knife-edge (left) and the HDR image at 85% (right)

Increasing the sensitivity should have at least improved the contrast on the weakest flow features. As seen in *Table 6.3*, this is exactly what happens in the region C—C, even if the gain is quite low. The knife-edge position, that was kept vertical for all the experiments, could be the reason why only a modest contrast change was achieved. A horizontal or even oblique knife-edge may be more appropriate to study this feature. Repeating all the experiments with various knife-edge arrangements could be quite time consuming and unpractical. Furthermore, depending on the facility in use, it could also be economically unsustainable. When the optimal knife-edge position is unknown or if with a single orientation is not enough to completely study the flow, the Background-Oriented Schlieren (BOS) could be a better approach to the problem, since it allows to create a synthetic knife-edge during the post-processing [4, 18]. With a single BOS image is possible to try many knife-edges positions without repeating the experiment.

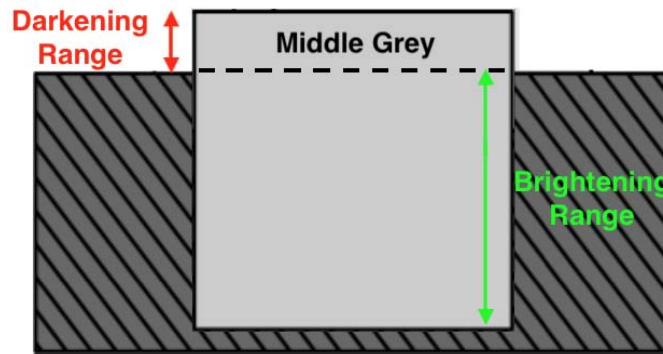


Figure 6.5 – Asymmetric measurement range at high cut-off rates

6.4. CONCLUSIONS

Two IQ assessment indexes have been employed to optimize the TMOs parameters and to reveal the best operators between the ten tested. The resulting images were analysed and compared, both subjectively and objectively by estimating the noise and artefact presence, the number of over ranged pixels and the contrast along the regions of interest. The best TMO overall has proved to be the Ashikhmin operator. Other operators, like the Bilateral Filter, produce good images but with low contrast. This flaw could be improved by applying some post-processing techniques as it will be investigated in *Chapter 7*.

It has been also verified that saving the tone mapped images with a 16-bits encoding, when this option is available, can deliver a better-quality image with noticeable less artefacts.

Ultimately, the final HDR image (obtained from pictures at 85% cut-off) has been compared with a traditional schlieren image taken at 35%. Unfortunately, the former picture shows less details than the latter, particularly within the first shockwave. The bracketing range was wide enough to contain the whole range of luminance of the scene: the under-exposed images had no white burned pixels and the over-exposed ones had no over ranged black pixels. The radiance map was effectively generated with all the information available. However, at high knife-edge rates the measuring range of the schlieren apparatus becomes greatly asymmetrical, decreasing the shades available to render the darkest regions of the image. Moreover, in these conditions even little deflections can exceed the “darkening side” of the measurement range of the system (*figure 6.4* clearly depict the issue). For these reasons, many features discernible in the low cut-off picture are visualized as nearly uniform dark grey and black in the HDR photo. This behaviour is a physical limitation of the schlieren apparatus thus no photographic technique can recover these details. Indeed, the problem appeared with every tone mapping operator, and even displaying the radiance map in an HDR monitor without any dynamic range compression would have shown the same issues. However, the high cut-off increases the sensitivity of the system, enhancing some weak details like the rear shear layer. The contrast gain is detectable but visually it is hardly noticeable. In conclusion, when compared side by side, the classic schlieren images captured at lower cut-off rates appear visually better overall, showing more flow features and density gradients than the tone mapped HDR pictures.

These results and conclusions are strongly related to the wind tunnel used. The University of Manchester HSST operates at a very low freestream density, thus the changes produced by the facility are generally small. As a consequence, it is necessary to use high cut-off values for the HDR to become effective, introducing all the issues cited previously, and even then, only small regions of the scene become over ranged. Nevertheless, the HDR technique could still be useful when applied to systems equipped with older cameras or atmospheric density transonic and supersonic facilities. These systems can produce much stronger density gradients that saturate the sensor at lower cut-off rates, where the measurement range is larger and symmetrical, possibly producing an image with larger over ranged regions both in the dark and bright side of the range (similar to *figure 2.1*). In this condition, the resulting HDR images could actually improve the visualization of the flow and be properly used for aerodynamics investigations.

7. POST-PROCESSING

In this chapter, basic post-processing techniques will be investigated with the purpose of improving the schlieren images, both classic and HDR.

7.1. POST-PROCESSING TECHNIQUES

The post-processing techniques are usually aimed at improving contrast, sharpen the edges and reducing the noise. To enhance the contrast, two procedures have been investigated: Linear Contrast Stretching (LCS) and Histogram Equalization (HE) [1]. The former is a mapping function that spreads all the intensity values in the image to cover the entire range of available. In the latter, the pixels values are modified to obtain a histogram that is as flat as possible.

To sharpen the picture, the Unsharp Masking (UM) technique has been employed, where a copy of the image is blurred and subtracted from the original to enhance the details [1]. To improve the result even more, a reference image (captured when the wind tunnel is not running) can be subtracted to the original one. This operation increases the sharpness and contrast and can help cleaning the picture by removing dust spots, glass imperfections and similar irregularities.

The operations of HDR blending, tone mapping and post-processing introduce noise in the picture, so a denoising operation could be necessary. An Adaptive Low-Pass Wiener Filter has been used with this purpose [37].

The post-processing has been performed with MATLAB (the code is shown in *Appendix A.6*). ImageJ [21] has been used for the reference image subtraction. All these techniques can be combined to improve even more the image quality.

The low contrast image obtained from the Bilateral Filter tone mapping has been processed and compared with the one resulting from the Ashikhmin operator, as anticipated in *Chapter 6*. In addition, the low dynamic range picture captured at 35% cut-off has been enhanced and analysed.

7.2. RESULTS

The results of various post-processing combinations are shown in *figure 7.1*. It can be immediately noticed how the Histogram Equalization does not produce a good image, substantially lowering the overall quality of it.

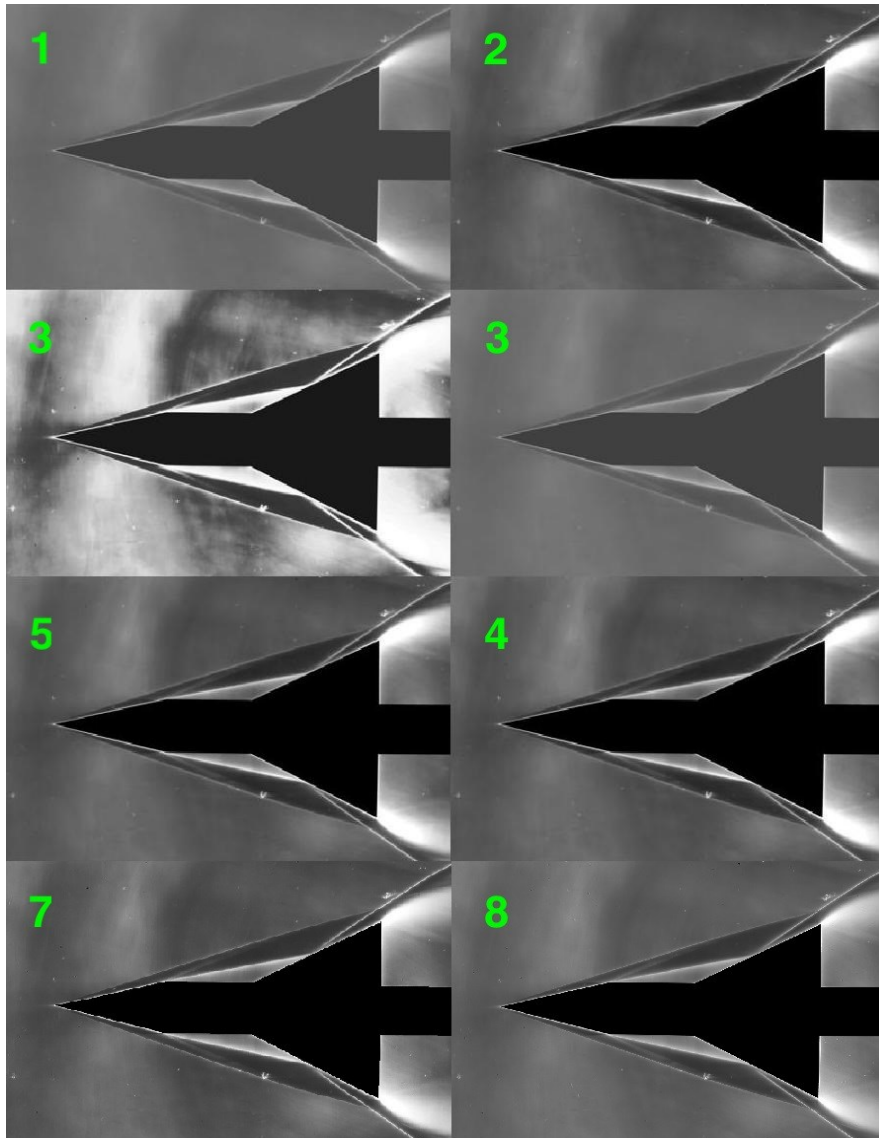


Figure 7.1 – Resulting images after the post-processing (Bilateral Filter TMO, 85% cut-off) (1) No processing (2) Linear Contrast Stretching (3) Histogram Equalization (4) Unsharp Masking (5) Unsharp Masking + Linear Contrast Stretch (6) Unsharp Masking + Linear Contrast Stretch + Denoise (7) Original LDR (8) Ashikhmin

The contrast is increased but many artefacts and over ranged pixels are introduced. Similar results have been obtained with every picture tested. The same figure shows the contrast enhancement obtained using the Linear Contrast Stretch. When applied to the Bilateral Filter tone

mapped image, the contrast clearly increases, matching and even surpassing the pictures generated by Ashikhmin TMO. On the other hand, the technique introduces more over ranged pixels and artefacts, some of them definitely evident. This behaviour can be seen also in *figure 7.2*.

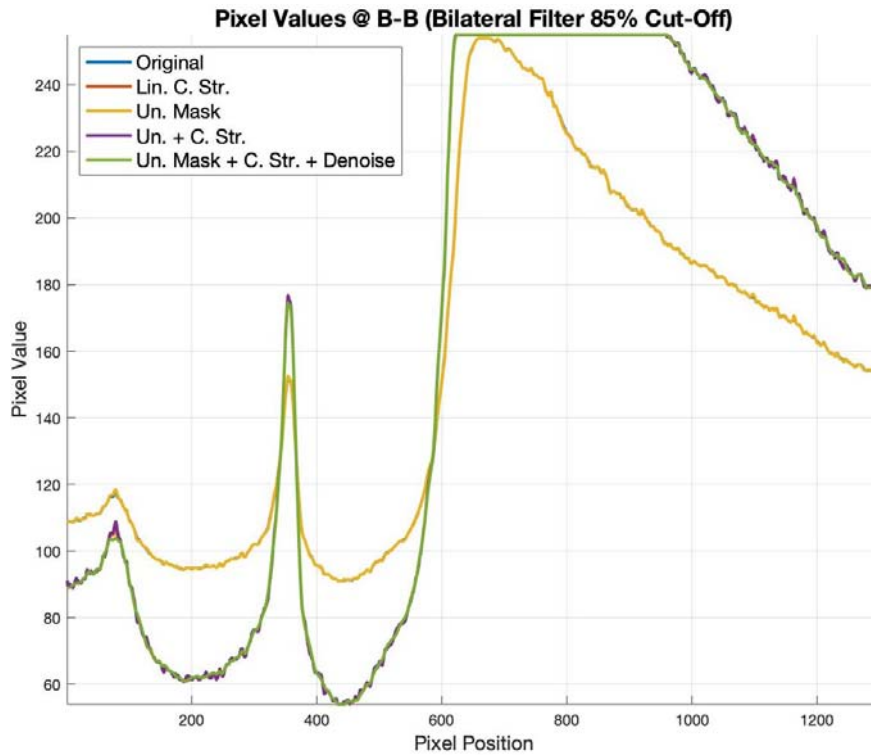


Figure 7.2 – Pixel values along the second shock after different post-processing techniques (the Original and UM curves are completely overlapped and cannot be distinguished)

The contrast can be boosted slightly more by applying an Unsharp Mask before the LCS. The UM alone does not visibly enhance the image. Denoising the image reduces the noise and also the visible artefacts but also decreases the contrast, although the loss is minimal and hardly noticeable. The final image, after all these techniques have been applied, has more contrast and less noise and artefacts than the Ashikhmin mapped image, but slightly more over ranged pixels. *Figure 7.3* shows the contrast gained within the rear shear layer (the weakest feature visible in the flow). In the same figure it can be observed how the denoising maintains the contrast while smoothing the pixel values. Numerical results are shown in *Table 7.1*.

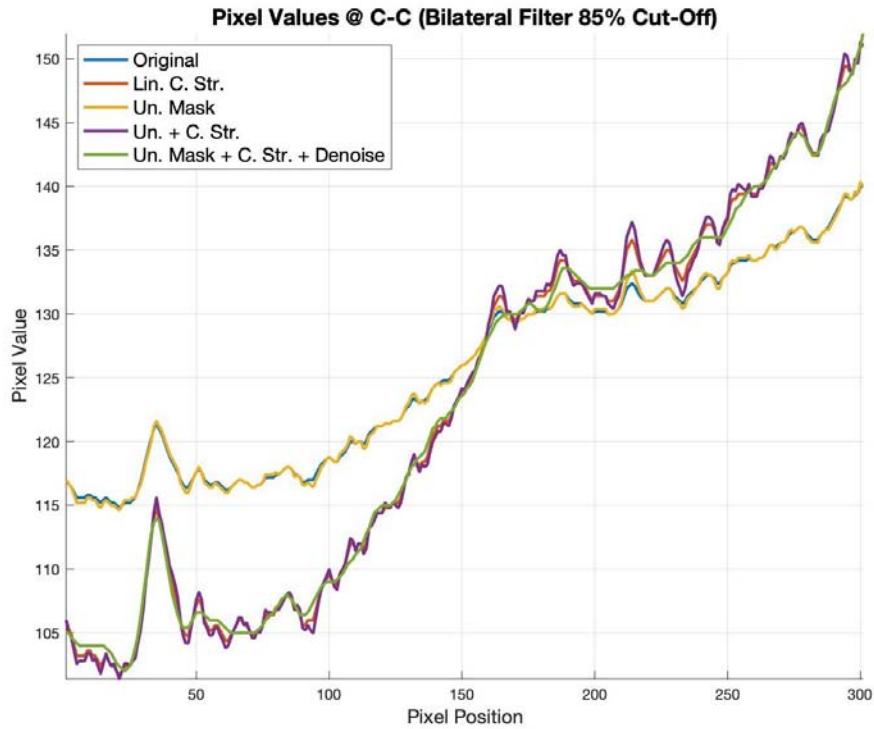


Figure 7.3 – Pixel values along the rear shear layer after different post-processing techniques

Table 7.1 – Contrast and other IQ indexes for Bilateral Filter after post-processing

| Post-Processing Technique | Contrast | | | Artefacts | Noise | Over Range |
|---------------------------|----------|-----|-----|-----------|-------|------------|
| | A—A | B—B | C—C | [%] | [%] | [%] |
| Original | 1.9 | 2.8 | 1.2 | 1.7 | 0.0 | 0.0 |
| LCS | 4.1 | 4.7 | 1.5 | 57.7 | 0.1 | 1.0 |
| HE | 4.4 | 4.5 | 1.3 | 48.7 | 16.1 | 1.6 |
| UM | 2.0 | 2.8 | 1.3 | 55.2 | 0.1 | 0.0 |
| UM+LCS | 4.4 | 4.8 | 1.6 | 53.0 | 1.2 | 1.0 |
| UM+LCS+DN | 3.9 | 4.7 | 1.5 | 0.7 | 0.0 | 1.0 |

It appears that the Ashikhmin operator already maximises the contrast. Editing the Ashikhmin picture does not improve the contrast but in fact it marginally lowers it while increasing noise and artefact. The denoise operation reduces the noise again but the contrast remains lower than the unedited photo (Table 7.2).

Table 7.2 – Contrast and other IQ indexes for Ashikhmin after post-processing

| Post-Processing Technique | Contrast | | | Artefacts | Noise | Over Range |
|---------------------------|----------|-----|-----|-----------|-------|------------|
| | A—A | B—B | C—C | [%] | [%] | [%] |
| Original | 3 | 3.9 | 1.4 | 8.4 | 0.3 | 0.1 |
| LCS | 2.9 | 3.2 | 1.4 | 10.1 | 0.6 | 1.0 |
| HE | 4.4 | 4.5 | 1.3 | 25.1 | 7.5 | 1.5 |
| UM | 4.8 | 5.4 | 1.7 | 16.2 | 0.8 | 1.2 |
| UM+LCS | 4.8 | 5.4 | 1.7 | 16.2 | 0.8 | 1.2 |
| UM+LCS+DN | 4.5 | 5.2 | 1.6 | 0.6 | 0.0 | 1.1 |

Considering now the classic schlieren image captured with a knife-edge at 35%, the Unsharp Masking was able to slightly increase the contrast, while the LCS could not. As expected, noise and artefacts increased after the processing but could be reduced by applying the Wiener Filter (Table 7.3).

Table 7.3 – Contrast and other IQ indexes for the single image at 35% cut-off (without reference subtraction) after post-processing

| Post-Processing Technique | Contrast | | | Artefacts | Noise | Over Range |
|---------------------------|----------|-----|-----|-----------|-------|------------|
| | A—A | B—B | C—C | [%] | [%] | [%] |
| Original | 4.2 | 8.5 | 1.2 | 9.8 | 0.0 | 0.0 |
| LCS | 4.1 | 6.5 | 1.2 | 11.8 | 0.2 | 1.0 |
| HE | 4.8 | 5.7 | 1.3 | 15.9 | 35.3 | 1.6 |
| UM | 4.4 | 8.8 | 1.2 | 16.0 | 0.8 | 0.0 |
| UM+LCS | 4.3 | 6.9 | 1.2 | 12.2 | 5.9 | 1.1 |
| UM+LCS+DN | 4.0 | 6.2 | 1.1 | 2.3 | 0.1 | 1.0 |

Much more relevant improvements have been obtained with the reference image subtraction technique (figure 7.4). The contrast increased substantially without increasing much the noise while decreasing the artefacts. This enhancement was located mostly around the two shock-waves and only marginally around the rear expansion fan. Furthermore, the subtraction cleaned

and smoothed the background of the picture, rendering a nearly uniform middle grey background. The LCS could improve again the picture, even more when combined with the UM. In this last case, the noise became extremely evident, making denoising necessary.

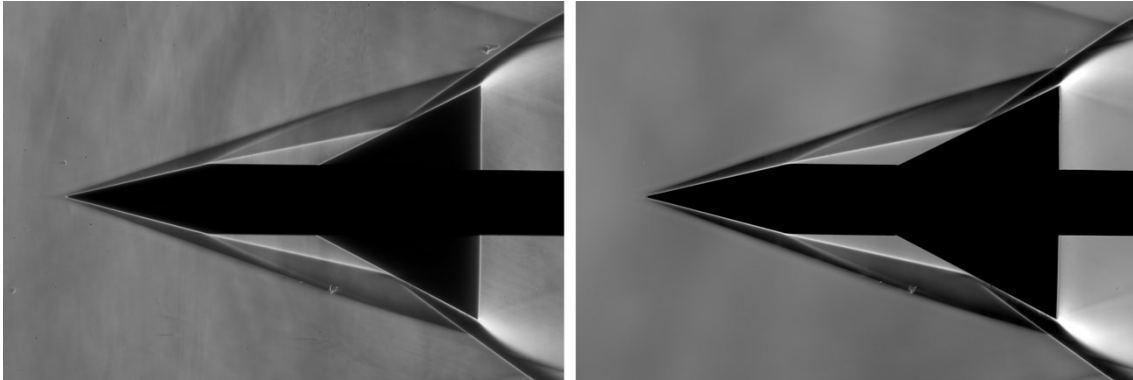


Figure 7.4 – Comparison between the unedited picture (left) and the clear one, obtained after subtraction (right)

However, applying the Wiener filter decreased the contrast more than expected. Ultimately, applying only the Linear Contrast Stretching to the cleaned image yielded a better image overall (Table 7.4). A summary of this workflow, that yielded the best results for the classic schlieren image, is shown as a diagram in figure 7.5.

The image subtraction has been tested also with the HDR images, with unsatisfactory results. The tone mapped image is too different from the reference image and the operation introduce quite noticeable artefacts without increasing contrast or smoothing the background.

Table 7.4 – Contrast and other IQ indexes for the single image at 35% cut-off (with reference subtraction) after post-processing

| Post-Processing Technique | Contrast | | | Artefacts | Noise | Over Range |
|---------------------------|----------|------|-----|-----------|-------|------------|
| | A—A | B—B | C—C | [%] | [%] | [%] |
| Original | 6.8 | 255 | 1.2 | 4.7 | 1.7 | 0.4 |
| LCS | 15.2 | 255 | 1.3 | 5.7 | 6.8 | 2.1 |
| HE | 63.8 | 63.8 | 1.1 | 29.2 | 56.8 | 3.2 |
| UM | 7.9 | 255 | 1.3 | 5.5 | 23.3 | 0.4 |
| UM+LCS | 22.5 | 255 | 1.3 | 5.6 | 45.1 | 2.2 |
| UM+LCS+DN | 12.7 | 255 | 1.2 | 16.3 | 0.4 | 1.7 |

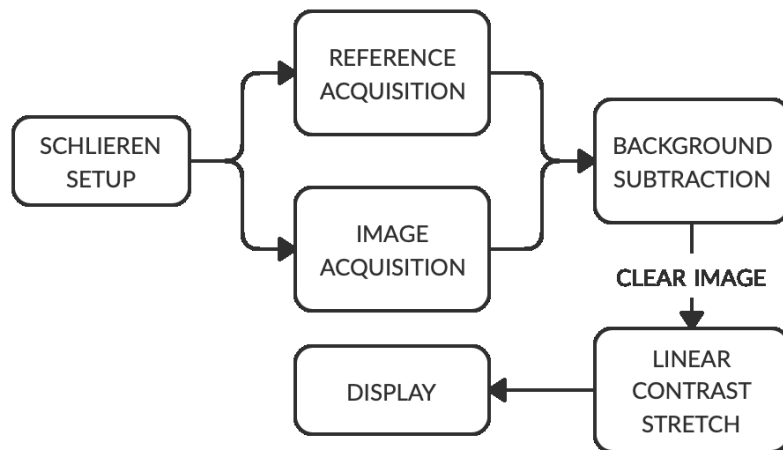


Figure 7.5 – Processing workflow for a traditional schlieren image

7.3. CONCLUSIONS

Confirming the conclusions of *Section 6.3*, a single image captured at 35% cut-off rate contains more detail and is preferred compared an HDR image tone mapped with any TMO, even more when the former is improved with a reference image subtraction and a contrast stretch. The post-processing could improve the Bilateral Filter image but, as expected, could not recover some details visible in the 35% image since these are lost at higher cut-offs due a physical limitation of the schlieren apparatus. Moreover, the processed image broadened the over ranged regions around the rear shear layer. While the Ashikhmin TMO has slightly more noise and artefacts, it appears the best TMO overall, especially because no post-processing is necessary after the tone mapping. The post-processing could also improve the traditional schlieren image by improving the contrast. The best results have been obtained by subtracting to the original image a reference image captured without any flow running in the tunnel.

8. HDR SCHLIEREN WITH UNSTEADY FLOWS

The HDR techniques investigated in the previous chapters cannot be applied to moving subjects since they can change shape and position during the capturing process. An HDR image of phenomena that evolve in time or space must be acquired with a single shutter actuation. The Dual ISO technique can be utilized for this purpose. In the following chapter this imaging method will be used to investigate the possible improvements in dynamic range and quality of schlieren pictures in conjunction with unsteady flows.

8.1. INTRODUCTION

A moving subject or an unstable phenomenon changes position and shape in space and time. In this situation, capturing few bracketed images and blending them with the techniques mentioned in *Section 2.3* will certainly yield unsatisfactory results. First of all, the dynamic environment will undermine the CRF recovery (*figure 8.1*). Moreover, after the blending ghosting artefacts, also known as motion artefacts, will appear (*figure 8.2*) [17]. These are the same artefacts that can be introduced by camera movements during the bracketing process.



Figure 8.1 – CRF computed from still pictures compared with a visibly wrong CRF obtained with a dynamic subject

In these cases, the extended dynamic range picture needs to be captured in a single frame, along with a fast-enough shutter speed to freeze all the movements. Various methods are available to accomplish this. Multiple cameras with different exposure times can be used to capture many photos at the same time. This strategy produces many optical and perspective effects that need to be handled. Better results can be obtained using a multi-sensor system, where a beam-splitter project the scene in two or more sensors, each one set up with a different shutter speed. This exposure time difference can still generate motion artefacts [17]. A spatially varying exposure, where various regions of the sensor are exposed differently, is another way to achieve the same result [6]. Ultimately, native HDR sensor can be employed, although these are usually expensive [17]. All of these techniques can be also applied to record HDR videos.

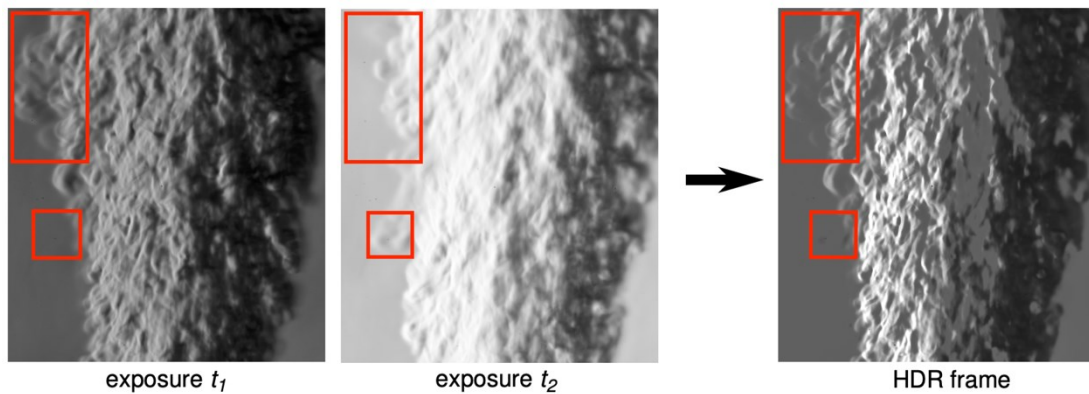


Figure 8.2 – Ghosting artefacts after blending pictures of a moving subject

8.2. DUAL ISO

In this investigation, the Dual ISO technique [38] will be used to capture schlieren pictures of an unsteady flow. The Dual ISO is a spatially varying exposure technique where the sensor captures two different exposures at the same time by alternating the ISO every two lines of pixels (*figure 8.3*). The ISO is an index used to quantify the electronic amplification, applied during the sensor read-off, that determines how sensitive the pixels are to the incoming light. Higher ISO values produce brighter images like a longer exposure would do, but since ISO is a gain applied after the light is collected by the sensor, it introduces some noise that is the stronger and the more noticeable the higher the sensitivity is set.

By having lines of pixels with different sensitivity, a single image will contain two different exposures. These need to be separated and then mixed together while interpolating the missing lines,

but this process halves the vertical resolution. Many advanced interpolation methods have been developed to recover the lost resolution while keeping as many details as possible with good results [38]. The processed image will contain more data than the original one, particularly in the shadows, and will resemble the HDR pictures seen earlier. Besides the loss of resolution, other disadvantages are the potential introduction of aliasing effects along sharp edges and moiré interference effects if patterns are present in the scene [38].



Figure 8.3 – Resulting interlaced image (left) and the alternated Bayer pattern (right) [38]

Dual ISO is included in Magic Lantern [20], a custom firmware only available for Canon cameras that adds many new functionalities to them. Magic Lantern needs to be installed in the SD card that the camera is using. The firmware will be automatically loaded at the start-up. This is a non-destructive process since the Magic Lantern code is loaded in addition to the original firmware and it does not modify it.

8.3. EXPERIMENTAL SETUP AND PROCEDURE

A Canon EOS 500D with Magic Lantern has been set up to capture Dual ISO pictures of a turbulent flow produced by a heat gun. The same cut-off values tested in Section 4.2 have been used and the background has been maintained middle grey with the same technique used in the previous experiments. Since the experiment did not require the HSST to run, the test chamber windows have been left open to have a cleaner and smoother background.

Table 8.1 reports the shutter speeds used to capture the photos. The reference photos, taken without the Dual ISO technique, have been captured with exposure times that render the background as middle grey.

Table 8.1 – Test matrix of the experiment

| Cut-Off | Reference shutter speed [s] | Dual ISO shutter speed [s] | | |
|---------|-----------------------------|----------------------------|---------|----------|
| | | 100/400 | 100/800 | 100/1600 |
| 50% | 1/1250 | 1/2500 | 1/4000 | 1/4000 |
| 75% | 1/640 | 1/1250 | 1/2000 | 1/2500 |
| 85% | 1/400 | 1/800 | 1/1250 | 1/1600 |
| 90% | 1/250 | 1/500 | 1/640 | 1/1000 |
| 95% | 1/125 | 1/250 | 1/320 | 1/500 |

Since the Dual ISO can only increase the sensitivity of the sensor, when it is turned on the additional exposure will be brighter than the default one. Knowing from the previous experiments that the highlights will be the first region to be over ranged at higher cut-offs, it is easy to understand that it is not a good strategy to capture the Dual ISO pictures using the reference shutter speed. Doing so would certainly yield an image that have both high gain and low gain lines over ranged, leading to unsatisfactory results. It has been chosen to under-expose the Dual ISO images so the lines at base ISO would correctly render the highlights while the more sensitive lines would correctly expose the shadows. For every knife-edge, three photos have been captured with different sensitivities. The base ISO has been always kept at 100, while the second exposure ISO was set at 400, 800 and 1600 (equivalent to +2, +3 and +4 EVs) with an estimated maximum dynamic range expansion of 1.6, 2.0 and 2.2 EVs respectively [38].

Table 8.1 shows the shutter speeds used with the Dual ISO technique. These have been chosen in such a way that the interlaced lines would under-expose and over-expose the image by the same number of stops. For example, since the combination 100/400 will expose the high ISO lines by +2 stops, the shutter speed to be used must expose the low sensitivity pixels by -1 stop and the high sensitivity pixels at +1 stop relatively to the reference image. Again, an ND8 filter has been included in the setup since at lower cut-off rates the lamp is so bright that there is no fast-enough shutter speed to expose the background correctly.

The RAW images produced by the camera appear as in figure 8.3, clearly showing the horizontal alternating lines. All the files need to be converted with the CR2HDR tool (supplied by Magic Lantern) that interpolates the lines and generates DNG files ready to be visualized and processed. Moreover, these files need to be converted to 16-bits TIFFs to be used with MATLAB.

The whole process can be time consuming when the number of images is considerable, or the files are large.

Like the HDR radiance maps, these files contain more information than a single low dynamic range image but, unlike the former, they do not need to be tone mapped. The pictures can be already visualized without any additional operation. The peculiar thing about these images is that the shadows can be lifted⁹ to show more details without a noticeable increase of noise [38]. The final result should resemble a tone mapped HDR image. Doing this operation with the original single exposure picture would lead to an extremely noisy and unsatisfactory image (*figure 8.4*).

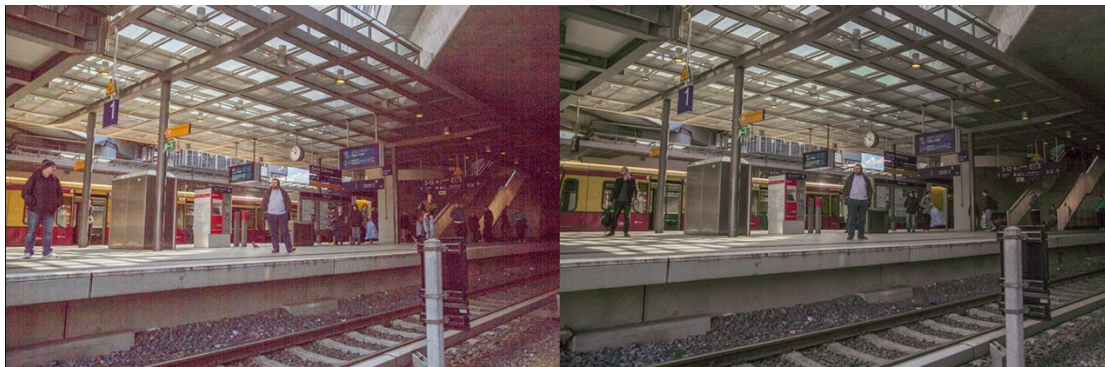


Figure 8.4 – Comparison between a classic (left) and a Dual ISO photo (right) after brightening the shadows [38]

One way to brighten the shadows is to re-map the pixel intensities by modifying the image tone curve. On the x-axis of a tone curve graph the greyscale pixel values are shown. This axis represents the tones of the image: the left side represents the darker tones (blacks and shadows) and the right the brighter ones (whites and highlights). On the y-axis, the re-mapped pixel values are reported. This axis describes how bright every tone is. The tone curve relates the original pixel intensities to their modified values. Shaping the tone curve will modify the appearance of the image by brightening or darkening its tones.

On an un-edited image, the tone curve is linear. If the left side of the curve is lifted, the pixels values belonging to the darker tones will be re-mapped to have a higher intensity, meaning that the shadows will become brighter. If the curve is dropped instead, the tones will darken. In contrast, if this process is performed on the right side, only the high intensity pixels (the brighter ones) will be affected.

⁹ “Lifting the shadows” in photography means brightening the dark areas of the image (without changing the overall exposure).

By arching the left side of the tone curve as shown in *figure 8.5*, the shadows in the Dual ISO pictures can be brightened to reveal the details contained in its darkest regions. The MATLAB script used to edit the curve is reported in *Appendix A.7*. The curve can be shaped by selecting some anchor points and shifting them up and down. The resulting tone curve is created with a cubic spline passing through these points. Additional points can be included to shape the curve more accurately.

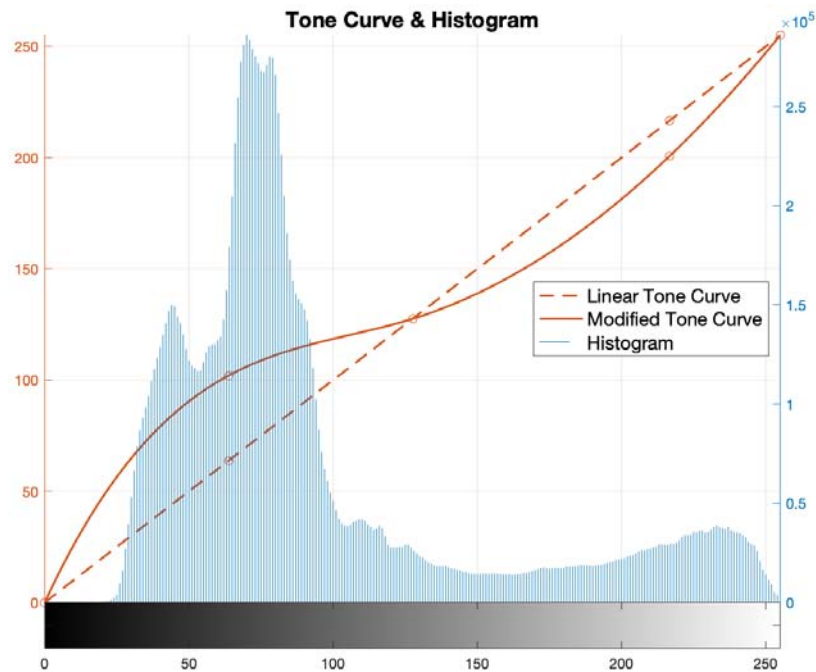


Figure 8.5 – Image histogram and modified tone curves

The shadows lifting process reduces the contrast, so some flow features can still be hardly discernible. Professional editing software address this problem with complex content-aware algorithms that, among other things, increase the local contrast. For this reason, the shadows lifting process will be performed also with Darktable [22], a free photo editing program, and the images resulting from the two different processing will be compared. The process is summarized by the diagram in *figure 8.6*.

Alternatively, the HDR picture can be generated with a blending algorithm (like Debevec or the Exposure Fusion) as seen in the previous experiments. However, in this case the bracketed images should be generated digitally by creating copies of the initial Dual ISO picture, each one with a different exposure [38]. Since a +1 stop difference means that double the light is captured by the sensor, a naïve solution to create an over-exposed image by 1 stop would be multiplying

all the pixel values by 2. However, this operation would only increase the brightness of the image and the result would be different from an actual picture taken by doubling the original exposure time. A more sophisticated solution is to estimate the radiance map of the scene by using only a single image. To accomplish this, the CRF of the camera must be known or estimated. By using the response function, the pixel values can be transformed in exposure values. Knowing the shutter speed at which the image was shot, the radiance map can be estimated with *Equation (2.3)*. Once the radiance map is known, the bracketed images can be created by recomputing the exposure map with the desired shutter speed, using again *Equation (2.3)*, and converting it to pixels values by employing the CRF. A script that perform this operation is available in *Appendix A.8*. Since the radiance map is computed from a single image, if over ranged regions are present in it some radiance values will not be recovered correctly.

This process needs to be performed also when the Exposure Fusion method is used since it requires at least two bracketed images that will need to be generated computationally, which makes one of the main advantages of the algorithm worthless.

The Dual ISO images will be processed with both shadows lifting technique and virtual HDR blending workflow, and results will be analysed. Ultimately, the Dual ISO images will be compared with a classic schlieren photo captured with a knife-edge at 50%.

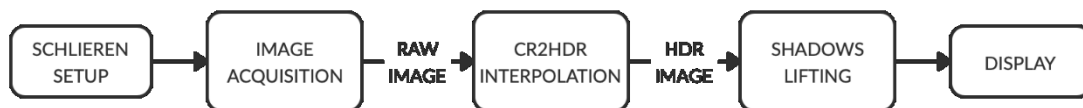


Figure 8.6 – Shadows lifting processing workflow for Dual ISO images

8.4. RESULTS

Table 8.2 shows the average background pixel value for every cut-off tested. This value is close to middle grey in every case, meaning that the knife-edge has been set up properly as seen in *Section 4.2*. The real cut-off rate has been estimated considering only the actual exposure time used compared to the theoretical one as previously done (*Section 5.1*).

Table 8.2 – Background values and real cut-off estimation

| Cut-Off [%] | Background Pixel Value | Error [%] | Theoretical Shutter Speed [s] | Actual Shutter Speed [s] | Actual Cut-Off [%] |
|-------------|------------------------|-----------|-------------------------------|--------------------------|--------------------|
| 50% | 120 | 2.7 % | 1/1250 | 1/1250 | 50.0 % |
| 75% | 127 | 0.0 % | 1/625 | 1/640 | 74.4 % |
| 85% | 123 | 1.6 % | 1/375 | 1/400 | 84.0 % |
| 90% | 128 | 0.4 % | 1/250 | 1/250 | 90.0 % |
| 95% | 138 | 4.3 % | 1/125 | 1/125 | 95.0 % |

As in the candle experiment (*Chapter 4*), since the changes in density are not particularly intense, over ranged regions appear only at really high cut-off rates. *Figure 8.7* shows how the saturated regions expands when increasing the cut-off. Very few sectors of the image reach the upper boundary of 255 at 90% cut-off, while at 95% the over ranged area becomes quite relevant. At lower cut-off rates no pixel exceed the dynamic range of the sensor.

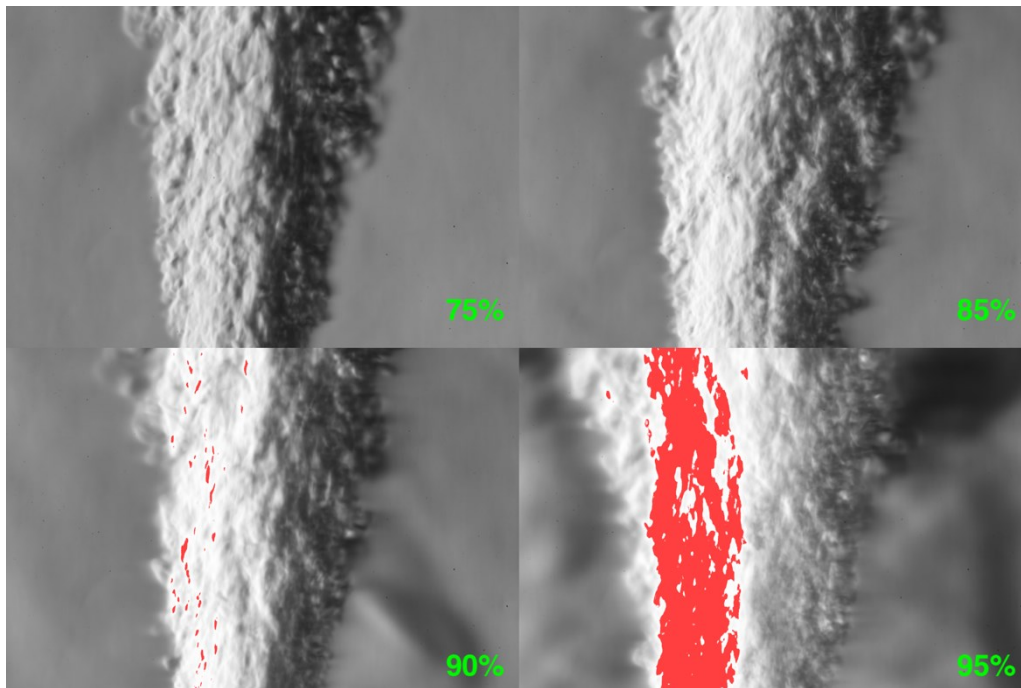


Figure 8.7 – Over ranged regions at different cut-off rates

Considering only the 90% and 95% knife-edges, which are the only two cases where the sensor is over ranged, the different ISO combinations have been compared. For the 90% cut-off, using the exposure technique explained in *Section 8.3*, a 100/400 Dual ISO setting already yields an

image with no clipped regions. For a 95% rate it is necessary to rise the ISO to the suggested maximum (100/1600) [38] to obtain a picture without any burned pixel (*figure 8.8*). The percent of over ranged pixels are reported in *Table 8.3*, where the noise and artefact presence are also given.

Table 8.3 – Quality indexes results at 90% and 95% cut-off rates for different ISO combinations

| ISO | Cut-Off 90% | | | Cut-Off 95% | | |
|-----------------|-------------|---------|--------------|-------------|---------|--------------|
| | % Artefacts | % Noise | % Over Range | % Artefacts | % Noise | % Over Range |
| 100 (Reference) | 9.5 % | 0.0 % | 0.4 % | 8.3 % | 0.0 % | 12.6 % |
| 100/400 | 8.5 % | 0.1 % | 0.0 % | 9.5 % | 0.0 % | 0.8 % |
| 100/800 | 9.9 % | 0.2 % | 0.0 % | 9.7 % | 0.1 % | 0.1 % |
| 100/1600 | 13.2 % | 0.2 % | 0.0 % | 11.3 % | 0.3 % | 0.0 % |

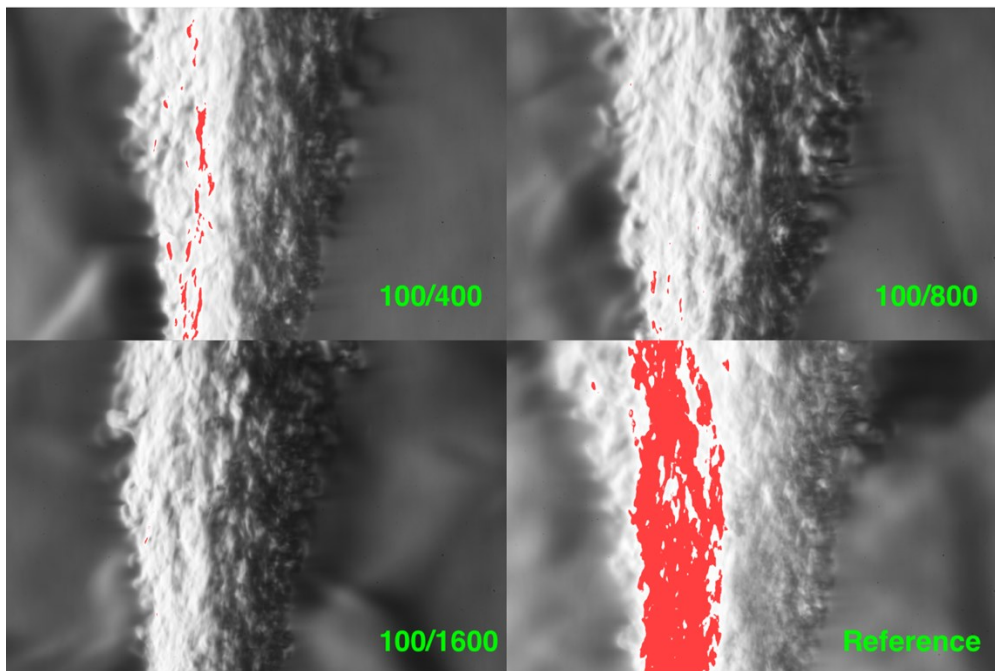


Figure 8.8 – Over ranged regions at different ISO combinations (95% cut-off)

As it might have been expected, the more extreme is the Dual ISO setting the more artefacts and noise are present. Nonetheless, the noise is virtually non-existent in every picture and the artefacts percent is just slightly larger than in the original image.

The Dual ISO pictures greatly reduce the number of over ranged pixels, especially at 95% cut-off, since the base ISO lines where under-exposing the image. The reference image in *figure 8.8*

clearly illustrates why using the same exposure time for a classic image and a Dual ISO one is not the optimal approach. In the former case, a large region of the picture is already clipped, therefore the higher sensitivity lines would just increase even more the number of over range pixels producing an unsatisfactory result. Correctly exposing the brightest part of a scene when the Dual ISO is active yields more desirable results.

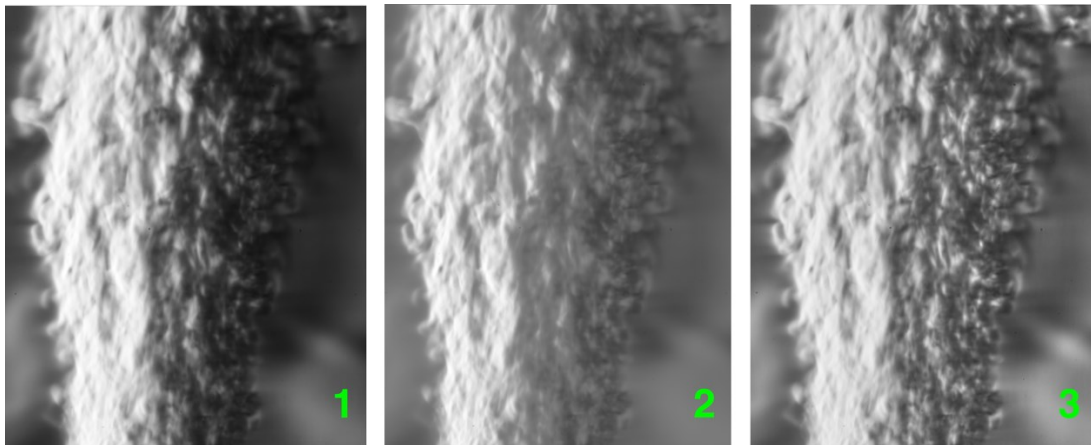


Figure 8.9 – Un-processed Dual ISO image (1), processed with tone curve shaping (2) and with Darktable (3)

Figure 8.9 shows a Dual ISO picture (taken at 95% cut-off) before and after the processing. The initial image is quite dark on the right side where not many details can be discerned. Brightening the shadows by shaping the tone curve reveals these details, but the contrast is severely reduced. Slightly reducing the highlights (with a tone curve shaped like in figure 8.5) also helps uncovering some features in the bright side of the picture but reduces the contrast once again. Even if more flow features are visible compared to the original image, these are not clearly distinguishable yet. The image can be improved by using Darktable. Instead of changing the tone curve, the shadows slider can be used to increase the exposure in the darker areas. By doing so, the content-aware algorithm is employed. As it can be noticed in figure 8.9, the resulting image has both brighter shadows and contrast added, and the flow features are much more evident than in the previous pictures.

Comparing a Dual ISO picture with a normal one (captured in the same conditions and affected by the same post-processing) shows, as expected, how the latter has more noticeable noise than the former. The noise is more obvious if the pictures are coloured, and when converted to grayscale it becomes less apparent. The higher quality of the Dual ISO image has been also acknowledged by the IQ index of Section 6.2.

The same Dual ISO picture has been processed with the Debevec algorithm and the Exposure Fusion technique using three artificial images with a ± 2 stops bracketing. The image generated by the Exposure Fusion method resulted the absolute best, having less noise, artefacts and saturated pixels than every other TMO used to map the HDR image obtained from the Debevec algorithm (*figure 8.10*). The picture is similar to the one obtained from Darktable but with less contrast and brightness on the right side.



Figure 8.10 – Image produced by the Exposure Fusion technique

Ultimately, the Dual ISO pictures have been compared with a classic schlieren picture acquired at 50% cut-off. The darker tones of the image can be enhanced using Darktable as seen previously. This operation introduces noise that however remains hardly noticeable, especially after the conversion to a grayscale image. The processed picture renders the flow features more clearly than any Dual ISO image, having also less diffraction effects and a wider measurement range, proving that processing a classic schlieren image is faster and yields better results than acquiring and processing a Dual ISO one (*figure 8.11*). This conclusion is not only subjective but has been confirmed also by the IQ index, where the processed LDR schlieren image achieved the highest score overall.

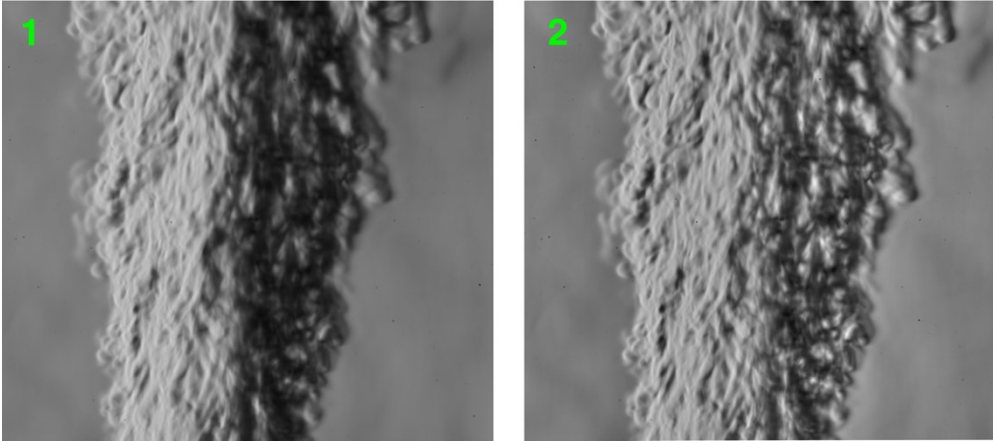


Figure 8.11 – Classic schlieren image taken at 50% cut-off (1) and enhanced with Darktable (2)

8.5. CONCLUSIONS

The Dual ISO technique has successfully allowed to capture high dynamic range images of an unsteady flow. These pictures have been post-processed with two different workflows: shadows lifting and HDR blending. Darktable produced the best shadow lifted image, while Exposure Fusion was the best blending algorithm. Overall, the most detailed Dual ISO picture after processing was the one obtained with Darktable, since it could show more flow features and make them clearly visible with an increased local contrast. Using the many additional image enhancement tools available in a professional editing software could improve the final picture even more. On the other hand, this procedure would be hardly automatable, requiring a manual editing of the pictures thus extending the post-processing time. Exposure Fusion could be used to expedite the procedure when many photos need to be processed, but to generate the synthetic bracketed images the CRF is needed. If this function is unknown it must be estimated, forcing to acquire additional images during the experiment.

The Dual ISO processing workflow is longer since after capturing the image it is necessary to interpolate the ISO lines, an operation that also halves the vertical resolution. The advantages of the Dual ISO pictures (more flexibility during post-processing and limited noise) are not very appreciable, especially with grayscale images. Furthermore, when comparing a Dual ISO image with a classic schlieren photo captured a lower cut-off rates, the latter provides a better representation of the flow after some basic editing with Darktable, and it seems ultimately the best way of acquiring an image of an unsteady flow. Moreover, using lower cut-off rates allow to use

faster shutter speeds that help freeze the dynamic phenomenon and provide a wider and symmetric measurement range to avoid the issues seen in *Chapter 5*. Nevertheless, the Dual ISO technique could still be useful when really high cut-off rates are essential and if the apparatus use older sensors with a limited dynamic range that outputs files normally not very suitable for post-processing.

9. FINAL CONCLUSIONS

The HDR imaging technique has successfully recovered over ranged regions of the pictures and extended their dynamic range at higher cut-off rates, when the schlieren apparatus can generate luminance intensities that push the limits of the camera sensor. Unfortunately, the final tone mapped images are not overall better than classic schlieren images. While some weak details could be improved with a higher sensitivity, the latter disrupts the already strong flow features, that appear as uniform dark regions. This behaviour was caused neither by missing information in the images (the bracketing sequence was spread over the whole luminance range of the scene) nor by the radiance map processing (the same issues would have appeared even if the images had been displayed on an HDR monitor without any tone mapping). Instead, this occurrence is a limitation of the schlieren apparatus, that at high cut-off rates has a strongly asymmetric measurement range, thus these details cannot be recovered with the HDR method (as explained in *Section 6.4*). Ultimately it has not been possible to improve the visualization of both strong and weak flow features in a single image with this technique.

It may be investigated the applicability of the technique in other facilities that use older sensors with limited dynamic range or wind tunnels that operate at atmospheric pressures. These tunnels produce strong density gradients that could over range the system already at 50% cut-off, where the measurement range is symmetric, and could saturate very large regions of the scene at higher sensitivities. In these conditions the HDR technique may yield much more satisfactory results.

Moreover, the contrast enhancement of the weak features obtained by increasing the sensitivity of the system has been fairly low. More knife-edge positions should be tested to identify the one that can produce the strongest contrast. This operation would need a large number of experiments and it is time consuming. Running a wind tunnel many times could also not be economically sustainable. In this case, the study should be carried on by employing the Background-Oriented Schlieren technique, that lets the user create a synthetic knife-edge during the post processing. This way, many positions can be investigated using only one image.

The same conclusions are valid for the Dual ISO technique. Modern camera sensors, even if APS-C format, can already capture the entire dynamic range of the schlieren apparatus. A single image is enough to render the phenomenon completely when the cut-off rate is not extremely

high. If needed, the images can be improved with some basic post-processing in MATLAB or with some professional image editing software without having to resort to HDR images.

A Full Frame camera would not improve the situation and could actually make the technique less effective since these sensors perform better at high ISO and have a slightly wider dynamic range when compared to APS-C sensors with the same resolution and technology.

Dual ISO might still be useful in older facilities with limited dynamic range sensors and when high cut-off rates are needed, keeping in mind the disadvantages resulting from the asymmetric measurement range.

10. FUTURE WORK

The investigation has shown how the HDRI technique could not produce satisfactory results when applied to the University of Manchester schlieren apparatus. The wind tunnel used for the experiments could be blamed as one of the main reasons why such behaviour occurred. The low density at which the tunnel operates made it necessary to use high cut-off rates to be able to saturate the camera sensor, introducing the issues discussed in the previous chapters (particularly in *Section 6.4*). Future investigations could employ the methods developed in this Thesis with tunnels operating at atmospheric densities. Doing so would help verify if the stronger density gradients could over range modern camera sensors at less extreme cut-off rates. Under those circumstances, without diffraction phenomena and with a much wider and symmetric measurement range, the HDRI techniques could become significantly more effective and might produce superior images when compared to traditional schlieren pictures. If the outcome will be positive, the methods proposed in this Thesis could then be improved by automating some steps (for example the middle grey background setting during the experiments or the pixel sampling before the HDR blending) to expedite the process. Developing a tone mapping operator specifically for schlieren images could also be extremely useful. Moreover, HDR techniques for videos could be implemented to be used with unsteady flows. Finally, it could be worth considering researching the use of radiance maps with calibrated schlieren, since they contain actual irradiance values instead of pixel values. These values could be directly translated to density values, making possible to capture a wider range of densities at once and more accurately, especially when 16-bits images are employed.

REFERENCES

- [1] Settles, G. S. (2006). *Schlieren and Shadowgraph Techniques: Visualizing Phenomena in Transparent Media* (2nd Ed.), Springer, Berlin
- [2] Kleine, H.; Grönig, H. (1991). Color Schlieren Methods in Shock Wave Research, *Shock Waves*, Vol. 1, No. 1, 51–63. doi:10.1007/BF01414868
- [3] Mariani, R.; Zang, B.; Lim, H. D.; Vevek, U. S.; New, T. H.; Cui, Y. D. (2019). A Comparative Study on the Use of Calibrated and Rainbow schlieren Techniques in Axisymmetric Supersonic Jets, *Flow Measurement and Instrumentation*, Vol. 66, 218–228. doi:10.1016/j.flowmeasinst.2019.01.007
- [4] Hargather, M.; Settles, G. (2010). *Recent Developments in Schlieren and Shadowgraphy, 27th AIAA Aerodynamic Measurement Technology and Ground Testing Conference 2010*. doi:10.2514/6.2010-4206
- [5] Debevec, P. E.; Malik, J. (1997). Recovering High Dynamic Range Radiance Maps from Photographs, *Proceedings of the 24th Annual Conference on Computer Graphics and Interactive Techniques*, ACM Press/Addison-Wesley Publishing Co., New York, NY, USA, 369–378. doi:10.1145/258734.258884
- [6] Nayar, S. K.; Mitsunaga, T. (2000). High Dynamic Range Imaging: Spatially Varying Pixel Exposures, *Proceedings IEEE Conference on Computer Vision and Pattern Recognition. CVPR 2000 (Cat. No. PR00662)* (Vol. 1), 472–479 vol.1. doi:10.1109/CVPR.2000.855857
- [7] Mann, S.; Picard, R. (1996). On Being “Undigital” With Digital Cameras: Extending Dynamic Range by Combining Differently Exposed Pictures, *Proc. IS & T Annual Meeting*, Vol. 48. doi:10.1.1.21.3141
- [8] Stevenson, R. L.; Robertson, M. A.; Borman, S. (1999). *Dynamic Range Improvement Through Multiple Exposures*. doi:10.1.1.71.859
- [9] Quinn, M. (2016). *Schlieren and Shadowgraph Lectures*, Manchester
- [10] Mazumdar, A. (2013). *Principles and Techniques of Schlieren Imaging Systems*, New York. doi:10.7916/D8TX3PWV
- [11] Mantiuk, R. K.; Myszkowski, K.; Seidel, H.-P. (2015). High Dynamic Range Imaging, *Wiley Encyclopedia of Electrical and Electronics Engineering*, John Wiley & Sons, Inc., Hoboken, NJ, USA, 1–42. doi:10.1002/047134608X.W8265
- [12] Reinhard, E.; Ward, G.; Pattanaik, S.; Debevec, P. (2006). *High Dynamic Range Imaging: Acquisition, Display, and Image-Based Lighting*, Morgan Kaufman

- [13] Paris, S.; Durand, F. (2009). A Fast Approximation of the Bilateral Filter using a Signal Processing Approach, *International Journal of Computer Vision*, Vol. 81, No. 1, 24–52. doi:10.1007/s11263-007-0110-8
- [14] Inanici, M. N. (2006). Evaluation of High Dynamic Range Photography as a Luminance Data Acquisition System, *Lighting Research and Technology*, Vol. 38, No. 2, 123–136. doi:10.1191/1365782806li164oa
- [15] Grossberg, M. D.; Nayar, S. K. (2003). What is the Space of Camera Response Functions?, *IEEE Computer Society Conference on Computer Vision and Pattern Recognition*, IEEE, Madison, WI, USA, II–602. doi:10.1109/CVPR.2003.1211522
- [16] Mertens, T.; Kautz, J.; Reeth, F. v. (2007). Exposure Fusion, *15th Pacific Conference on Computer Graphics and Applications (PG'07)*, 382–390. doi:10.1109/PG.2007.17
- [17] Banterle, F.; Artusi, A.; Debattista, K.; Chalmers, A. (2011). *Advanced High Dynamic Range Imaging: Theory and Practice* (1st ed.), A. K. Peters, Ltd., Natick, MA, USA. doi:10.1201/b11373
- [18] Fisher, T. B.; Quinn, M. K.; Smith, K. L. (2019). An Experimental Sensitivity Comparison of the Schlieren and Background-Oriented Schlieren Techniques Applied to Hypersonic Flow, *Measurement Science and Technology*, Vol. 30, No. 6, 65202. doi:10.1088/1361-6501/ab1582
- [19] Istvan, D. (2014). digiCamControl, from <http://digidcamcontrol.com>, accessed 7-11-2019
- [20] Hudson, T. (2009). Magic Lantern, from <https://magiclantern.fm>, accessed 23-12-2019
- [21] Rueden, C. T.; Schindelin, J.; Hiner, M. C.; DeZonia, B. E.; Walter, A. E.; Arena, E. T.; Eliceiri, K. W. (2017). ImageJ2: ImageJ for the Next Generation of Scientific Image Data, *BMC Bioinformatics*, Vol. 18, No. 1, 529. doi:10.1186/s12859-017-1934-z
- [22] Hanika, J. (2009). Darktable, from <https://www.darktable.org>, accessed 17-1-2020
- [23] Coffin, D. (1997). Decoding Raw Digital Photos in Linux, from <https://www.dechifro.org/dcrow/>, accessed 7-11-2019
- [24] Paris, S.; Hasinoff, S. W.; Kautz, J. (2011). Local Laplacian Filters: Edge-aware Image Processing with a Laplacian Pyramid, *ACM SIGGRAPH 2011 Papers*, ACM, New York, NY, USA, 68:1–68:12. doi:10.1145/1964921.1964963
- [25] Ames Research Staff. (1953). *Equations, Tables, and Charts for Compressible Flow*, Moffett Field. doi:19930091059
- [26] Zuiderveld, K. (1994). Contrast Limited Adaptive Histogram Equalization, P. S. Heckbert (Ed.), *Graphics Gems*, Academic Press, 474–485. doi:10.1016/B978-0-12-336156-1.50061-6

- [27] Farbman, Z.; Fattal, R.; Lischinski, D.; Szeliski, R. (2008). Edge-preserving Decompositions for Multi-scale Tone and Detail Manipulation, *ACM SIGGRAPH 2008 Papers*, ACM, New York, NY, USA, 67:1–67:10. doi:10.1145/1399504.1360666
- [28] Reinhard, E.; Stark, M.; Shirley, P.; Ferwerda, J. (2002). Photographic Tone Reproduction for Digital Images, *Proceedings of the 29th Annual Conference on Computer Graphics and Interactive Techniques*, ACM, New York, NY, USA, 267–276. doi:10.1145/566570.566575
- [29] Kim, M. H.; Kautz, J. (2008). Consistent Tone Reproduction, *Proceedings of the Tenth IASTED International Conference on Computer Graphics and Imaging*, ACTA Press, Anaheim, CA, USA, 152–159
- [30] Drago, F.; Myszkowski, K.; Annen, T.; Chiba, N. (2003). Adaptive Logarithmic Mapping for Displaying High Contrast Scenes, *Computer Graphics Forum*, Vol. 22, No. 3, 419–426. doi:10.1111/1467-8659.00689
- [31] Ashikhmin, M. (2002). A Tone Mapping Algorithm for High Contrast Images, *Proceedings of the 13th Eurographics Workshop on Rendering*, Eurographics Association, Aire-la-Ville, Switzerland, Switzerland, 145–156. doi:0.2312/EGWR/EGWR02/145-156
- [32] Durand, F.; Dorsey, J. (2002). Fast Bilateral Filtering for the Display of High Dynamic Range Images, *Proceedings of the 29th Annual Conference on Computer Graphics and Interactive Techniques*, ACM, New York, NY, USA, 257–266. doi:10.1145/566570.566574
- [33] Mantiuk, R.; Kim, K. J.; Rempel, A. G.; Heidrich, W. (2011). HDR-VDP-2: A Calibrated Visual Metric for Visibility and Quality Predictions in All Luminance Conditions, *ACM SIGGRAPH 2011 Papers*, ACM, New York, 40:1-40:14. doi:10.1145/1964921.1964935
- [34] Aydın, T. O.; Mantiuk, R.; Seidel, H.-P. (2008). Extending Quality Metrics to Full Luminance Range Images, B. E. Rogowitz; T. N. Pappas (Eds.), *Human Vision and Electronic Imaging XIII (Vol. 6806)*, SPIE, 109 – 118. doi:10.1117/12.765095
- [35] Venkatanath, N.; Praneeth, D.; Bh, M. C.; Channappayya, S. S.; Medasani, S. S. (2015). Blind Image Quality Evaluation Using Perception Based Features, *2015 Twenty First National Conference on Communications (NCC)*, 1–6. doi:10.1109/NCC.2015.7084843
- [36] Yeganeh, H.; Wang, Z. (2013). Objective Quality Assessment of Tone-Mapped Images, *IEEE Transactions on Image Processing*, Vol. 22, No. 2, 657–667. doi:10.1109/TIP.2012.2221725
- [37] Lim, J. S. (1990). *Two-Dimensional Signal and Image Processing*, Prentice-Hall, Inc., USA
- [38] *Dynamic Range Improvement for some Canon DSLRs by Alternating ISO During Sensor Readout.* (2013)

A. APPENDIX - SCRIPTS

A.1 SHUTTER SPEEDS ESTIMATION

This script estimates the shutter speeds to set on the camera to obtain the desired cut-offs with a middle grey background, as described in *Section 4.2*.

```
refDeltaT = 1/3200; %Shutter speed when there is no cut-off and back-
ground is middle gray (127)
refE = log2(1/refDeltaT); %f-stops value = 1
%Real 1/shutter speed available in the camera settings
realT = [4000,3200,2500,2000,1600,1250,1000,800,640,500,...
         400,320,250,200,160,125,100,80,60,50,30];

%Calculating stops between no cut-off and the wanted cut-off values
f = @(x) log2(-1.*x + 1);
cutoffs = [0.5,0.75,0.85,0.9,0.95]; %Cut-off values wanted
stops = feval(f,cutoffs);

%Exposure values for each cut-off value
Exposures = ones(1,length(cutoffs)).*refE + stops;
g = @(x) 1./(2.^x);
%Computed shutter speeds
deltaT = 1./feval(g,Exposures);
%Finding the closest available shutter speed
closestT = zeros(1,length(deltaT));
for i = 1:length(cutoffs)
    [val,idx] = min(abs(realT - deltaT(i)));
    closestT(i) = realT(idx);
    fprintf("Cut-Off %.0f%%: \t Computed Exposure Time: 1/%.0f \t
Closest Real Shutter Speed: 1/%.0f \n",...
           cutoffs(i)*100,deltaT(i),closestT(i));
end

%Computing actual exposure values with the just found shutter speeds
f = @(t) log2(1./t);
realExposures = feval(f,1./closestT);
dE = realExposures - refE.*ones(1,length(realExposures));
%Calculating actual cut-off value achievable with these shutter speed
%settings
g = @(x) (2.^x - 1)./(-1);
realCutoffs = feval(g,dE);
for i = 1:length(cutoffs)
    fprintf("Initial Cut-Off: %.0f%% \t Actual Cut-Off: %.0f%% \n",...
           cutoffs(i)*100,realCutoffs(i)*100);
end
```

A.2 HDR BLENDING

These functions implement the Debevec algorithm to recover the camera response function and blend the bracketed images into an HDR radiance map.

main.m

```
clc; clear all;
tic;
%Add the tools folder to MatLab path
addpath 'path_to_tools_folder'
%Add the tonemapping folder to MatLab path
addpath 'path_to_tonemapping_functions'

fprintf('--- STARTING --- \n\n');

%% FLAGS

flag_montage = false; %Display the original images
flag_crf = true; %Display the recovered CRF
flag_render = true; %Display the final tonemapped image
flag_save = false; %Save the HDR radiance map
flag_weights = 1; %Type of weighting function (1 = Hat, 2 = Gaussian,
Default = 1);
flag_tonemap = 5; %Type of tonemapping (1 = global, 2 = local, 3 =
farbman, 4 = reinhard, 5 = linear, 6 = bilateral, Default = 1);

%% PARAMETERS

defaultT = [1/250,1/1000,1/60]; %Exposure Times

%% PICTURES LOADING

fprintf('Loading Images... \n');
folder = "img";
format = "jpg";
[images,B] = loadStack(folder,format,defaultT);
P = max(size(images)); %Number of pictures
[height, width, nChannel] = size(images{1}); %width, height and number
of channel of the images
if(flag_montage)
    figure(1);
    montage(images);
end

%% HDR BLENDING

%Check the bit depth of the images
if(isa(images{1}, 'uint8'))
    bitDepth = 8;
    [g,imgHDR] = enfuse8bit(images,B,1,flag_weights,flag_save);
elseif(isa(images{1}, 'uint16'))
    bitDepth = 16;
```



```

    [g,imgHDR] = enfuse16bit(images,B,l,flag_weights,flag_save);
else
    error('Images are neither 8 bits nor 16 bits');
end
range = 0:1:(2^bitDepth-1);

%% CAMERA RESPONSE FUNCTION PLOTS

if(flag_crf)
    figure(3); hold on;
    if(nChannel == 1) %Grayscale images
        plot(g,range,'--k','LineWidth',2);
    elseif(nChannel == 3) %RGB images
        vetLineStyle = ["--r","-.g",":b"];
        for i = 1:1:nChannel
            plot(g(:,i),range,vetLineStyle(i),'LineWidth',2);
        end
        legend('R','G','B','Location','southeast');
    end
    xlabel('Log-Exposure');
    ylabel('Image Intensity');
    title('Camera Response Function');
    grid on;
    axis('tight');
    hold off;
end

%% DYNAMIC RANGE EVALUATION

fprintf('Calculating Dynamic Range... \n');

original = images{1}; %single LDR image with correct exposure
if(nChannel == 1)
    %Original Dynamic Range
    ypeak = exp(g(max(max(original))+1)-B(1));
    ynoise = exp(g(min(min(original))+1)-B(1));
    %HDR Image Dynamic Range
    ynoiseHDR = min(min(min(imgHDR(imgHDR>0))));
    ypeakHDR = max(max(max(imgHDR)));
else
    %Original Dynamic Range
    lum = grayscale(original);
    ypeak = double(max(max(lum))+1);
    ynoise = double(min(min(lum))+1);
    %HDR Image Dynamic Range
    lumHDR =
0.2126.*imgHDR(:, :, 1)+0.7152.*imgHDR(:, :, 2)+0.0722.*imgHDR(:, :, 3);
    %sRGB to HSV luminance map
    ynoiseHDR = min(min(lumHDR(lumHDR>0)));
    ypeakHDR = max(max(lumHDR));
end
%Original Dynamic Range
stopsLDR = log2(ypeak) - log2(ynoise);
dbLDR = 20*log10(ypeak/ynoise);
fprintf('Original Image: DR Stops = %.1f EVs \t DR = %.1f dB
\n',stopsLDR,dbLDR);
%HDR Image Dynamic Range
stopsHDR = log2(ypeakHDR) - log2(ynoiseHDR);

```

```

dbHDR = 20*log10(ypeakHDR/ynoiseHDR);
fprintf('      HDR Image: DR Stops = %.1f EVs \t DR = %.1f dB
\n',stopsHDR,dbHDR);

%% RENDERING

if(flag_render)

    fprintf('Rendering HDR Image... \n');

    switch flag_tonemap
        case 1
            fprintf('Tonemapping with global operator... \n');
            rgb = tonemap(imgHDR);
        case 2
            fprintf('Tonemapping with local operator... \n');
            rgb = localtonemap(imgHDR);
        case 3
            fprintf('Tonemapping with Farbman multi-scale decomposi-
tion... \n');
            rgb = tonemapfarbman(imgHDR);
        case 4
            fprintf('Tonemapping with Reinhard operator (applied only
to luminance channel)... \n');
            rgb = reinhardLum(imgHDR);
            rgb = imadjust(rgb,[],[],1/2.2);
        case 5
            fprintf('Tonemapping with linear operator... \n');
            rgb = lineartonemap(imgHDR);
            rgb = imadjust(rgb,[],[],1/2.2);
        case 6
            fprintf('Tonemapping with bilateral filter... \n');
            rgb = bilateralfiltertonemap(imgHDR,8,1/2.2);
        otherwise
            warning('Invalid tonemap flag value: Tonemapping with
global operator (fastest)');
            rgb = tonemap(imgHDR);
    end
    figure(4);
    imshow(rgb);
end
fprintf('\n--- DONE --- \n\n');
toc;

function [g,imgHDR] = enfuse8bit(images,B,l,flag_weights,flag_save)

    %{
        Devebec algorithm for to recover the camera response function
and blend
        the exposure to get a radiance map. Works with both grayscale
and color
        8-bits images.
    %}

    %% VAR CHECKS AND FLAGS

    if(~exist('images','var'))

```

```

        error("The stack of photos not found");
    end
    if(~exist('B','var'))
        error("Exposures times not found");
    end

    if(~exist('l','var'))
        l = 40; %smoothing factor
    end

    if(~exist('flag_weights','var'))
        flag_weights = 1; %Type of weighting function (1 = Hat, 2 =
Gaussian, Default = 1);
    end

    if(~exist('flag_save','var'))
        flag_save = 0;
    end

    [height, width, nChannel] = size(images{1});
    P = max(size(images));

    %% MINIMUM PIXELS NUMBER

    Zmax = 2^8-1; %Maximum pixel value
    Zmin = 0; %Minimum pixel value
    Zmid = floor(0.5*(Zmax - Zmin)); %Middle grey value
    minN = ceil((Zmax - Zmin)/(P - 1)); %N(P-1) > Zmax - Zmin
    fprintf('Min. pixels number: %d \n',minN);

    %% PIXELS SELECTION and SAMPLING

    fprintf('Selecting Pixels... \n');
    answer = questdlg('Do you want to load the last saved ROI?');
    if(strcmp(answer,'Yes'))
        try
            load('roi.mat');
        catch
            error('No RoiPoly found in this folder');
        end
    elseif(strcmp(answer,'No'))
        %Select the area of the image from where the pixels will be
sampled
        fig = figure(1);
        if(nChannel == 3)
            hsv = rgb2hsv(images{1});
            imagesc(hsv(:,:,3));
        else
            imagesc(images{1});
        end
        mask = roipoly;
        save 'roi.mat' mask
        close(fig);
    else
        clc;
        fprintf('The process has been arrested \n');
        return;
    end
end

```

```

end

%Sampling pixels
selPixels = sum(mask(:) == 1);
roiPix = zeros(selPixels,P);
step = floor(selPixels/(minN));
if(nChannel == 1) %Grayscale images
    for i = 1:1:P
        im = images{i};
        roiPix(:,i) = im(mask);
    end
    Z(:, :) = roiPix(1:step:end,:);
    fprintf('Actual pixels number: %d \n', length(Z));
elseif(nChannel == 3) %RGB images
    Zrgb = cell(nChannel,1);
    for c = 1:1:nChannel
        for i = 1:1:P
            im = images{i};
            channel = im(:,:,c);
            roiPix(:,i) = channel(mask);
        end
        Z(:, :) = roiPix(1:step:end,:);
        Zrgb{c} = Z;
    end
    fprintf('Actual pixels number: %d \n', length(Z));
end

%% WEIGHTS

w = createWeights(flag_weights);

%% CAMERA RESPONSE FUNCTION

fprintf('Finding the Camera Response Function... \n');
if(nChannel == 1) %Grayscale images
    %Recover the crf with devebec algorithm
    [g,~] = gsolve(Z,B,l,w);
elseif(nChannel == 3) %RGB images
    %Recover the crf of each channel with devebec algorithm
    vet_g = zeros(Zmax+1,3);
    for i = 1:1:nChannel
        [g,~] = gsolve(Zrgb{i},B,l,w);
        vet_g(:,i) = g;
    end
end

%% BLENDING

fprintf('Creating HDR image... \n');
if(nChannel == 1) %Grayscale iamges
    imgHDR = hdrBlend(images, g, B, w);
elseif(nChannel == 3) %RGB images
    channel = cell(P,1);
    channelHDR = cell(nChannel,1);
    for i = 1:1:nChannel
        for j = 1:1:P
            channel{j} = images{j}(:,:,i);

```

```

        end
        g = vet_g(:,i);
        channelHDR{i} = hdrBlend(channel, g, B, w);
    end
    imgHDR = cat(3, channelHDR{1}, channelHDR{2}, channelHDR{3});
end
%% STORAGE

if(flag_save)
    fprintf('Saving HDR image... \n');
    if(nChannel == 1)
        %This is needed because hdrwrite always wants 3 channels
        temp = zeros(size(imgHDR,1),size(imgHDR,2),3);
        temp(:,:,1) = imgHDR;
        temp(:,:,2) = imgHDR;
        temp(:,:,3) = imgHDR;
        imgHDR = temp;
    end
    hdrwrite(imgHDR, 'result.hdr');
end
end

function [g,lE] = gsolve(Z,B,l,w)

%{
From Debevec '97 "Recovering High Dynamic Range Radiance Maps from
Photographs"
Z = Sample pixels
B = natural log of the exposure times
l = smoothing factor
w = weight function
%}

n = 2^8;
A = zeros(size(Z,1)*size(Z,2)+n-1,n+size(Z,1));
b = zeros(size(A,1),1);
k = 1;
%k from 1 to N*P

for i = 1:size(Z,1)
    for j=1:size(Z,2)
        wij = w(Z(i,j)+1);
        A(k,Z(i,j)+1) = wij;
        A(k,n+i) = -wij;
        b(k,1) = wij * B(j);
        k = k +1;
    end
end

A(k,n/2) = 1;
k = k + 1;

for i = 1:(n-2)
    %g'' = (g(z-1)-2g(z)+g(z+1))
    %l*sum(g'') from 1 to 254
    A(k,i) = l*w(i+1);
    A(k,i+1) = -2*l*w(i+1);
end

```

```

        A(k,i+2) = l*w(i+1);
        k = k +1;
    end

    x = A\b;
    g = x(1:n);
    lE = x((n+1):size(x,1));
end

function [imgHDR] = hdrBlend(images, g, B, w)

%{
From Debevec '97 "Recovering High Dynamic Range Radiance Maps from
Photographs" equation (6)
images = cell array that contains all the bracketed pictures
g = camera response function
B = natural log of the exposure times
w = weight function
%}

imgHDR = zeros(size(images{1}));
for i = 1:1:size(imgHDR,1)
    for j = 1:1:size(imgHDR,2)
        val = 0; sum_w = 0;
        for k = 1:1:max(size(images))
            img = images{k};
            pixel_value = img(i,j);
            wij = w(pixel_value +1);
            Xij = g(pixel_value +1);
            val = val + wij*(Xij - B(k));
            sum_w = wij + sum_w;
        end
        lnE = val/sum_w;
        imgHDR(i,j) = exp(lnE);
    end
end
% remove NAN or INF
index = isnan(imgHDR) | isinf(imgHDR);
imgHDR(index) = 0;
imgHDR = single(imgHDR); %single is needed for local tonemapping
end

function [w] = createWeights(type,bitDepth)

%{
Creates the weighting functions needed for the Debevec algorithm.
type = shape of weighting function (1 = Hat, 2 = Gaussian)
bitDepth = bit rate of the pictures
%}

if(~exist('bitDepth','var'))
    bitDepth = 8;
end

Zmax = 2^bitDepth-1; %Maximum pixel value
Zmin = 0; %Minimum pixel value

```

```

Zmid = floor(0.5*(Zmax - Zmin));
if(type == 2)
    %Gaussian-like Function
    w = zeros(Zmax+1,1);
    for z = 0:1:Zmax
        w(z+1) = exp(-4*(z - Zmax/2)^2/(Zmax/2)^2);
    end
else
    %Hat Function
    w = zeros(Zmax+1,1);
    k = 1;
    for z = 0:1:Zmax
        if(z <= Zmid)
            w(k) = z - Zmin;
        else
            w(k) = Zmax - z;
        end
        k = k + 1;
    end
end
end

function [images,B] = loadStack(folder,format,defaultT)

%{
Loads a stack of bracketed pictures and retrieve the shutter
speeds
folder = name of the folder were images are located
format = format of the images (jpeg, jpg, png, tiff, tif)
defaultT = array of exposure times to be used if no metadata is
present
images = cell array containing the bracketed images
B = ln(Exposure Times)
%}

S = dir(fullfile(cd,folder, strcat('*. ',format)));
images = cell(numel(S),1);
deltaT = zeros(length(images),1);

if(~exist('defaultT','var'))
    defaultT = zeros(numel(S),1);
end

for k = 1:numel(S)
    filename = S(k).name;
    F = fullfile(cd,folder,filename);
    [~,~,ext] = fileparts(filename);
    if(ext == ".tiff" || ext == ".tif")
        images{k} = loadTiff(F);
    else
        images{k} = imread(F);
    end
    %Trying to find metadata in the images
    try
        meta = imfinfo(F);
        deltaT(k) = meta.DigitalCamera.ExposureTime;
    catch

```

```
        %If no metadata is present, the supplied one will be used
        warning(strcat('No metadata available for im-
age:',S(k).name));
        deltaT = defaultT;
    end
end
end
B = log(deltaT); %ln(Exposure Times)
end
```


A.3 TMO OPTIMIZATION

This script iterates over some pre-selected TMO parameters and find the combination that leads to highest IQ score, as seen in *Section 6.1*. Either TMQI or *Equation (6.1)* can be used for the IQ evaluation.

```
% Parameters to be tested
param1 = [50,100,200,300];
param2 = [true,false];
M = zeros(length(param1)*length(param2),3);
i = 1;

for p1 = param1
    for p2 = param2
        % Tonemapping with the operator
        tmo = AshikhminTMO(imgHDR, p1,p2);
        tmo = uint8(255.*tmo);
        % Evaluating the IQ
        iq = TMQI(imgHDR, tmo);
        M(i,1) = p1;
        M(i,2) = p2;
        M(i,3) = iq;
        i = i+1;
    end
end

% Finding the highest score
scores = M(:,end);
[max_iq,max_idx] = max(scores);
% Parameters values that give the highest score
best_param1 = M(max_idx,1);
best_param2 = M(max_idx,2);
% Showing the optimal tone mapped image
tmo = AshikhminTMO(imgHDR, best_param1,best_param2);
tmo = uint8(255.*tmo);
imshow(tmo);
```

A.4 TMO IQ ASSESSMENT

This function outputs the visual quality score of an HDR tone mapped image compared to the original single exposure picture (*Section 6.2*). The score is based on the number of noisy pixels, over ranged pixels, artefacts and dynamic range. A higher score is better.

```
function [score] = IQ_noref(img,weights)

%{
No reference IQ quality assessment for 8-bits and 16-bits images.
Takes into account noise and artefacts presence, dynamic range and
number of over ranged pixels. Minimum score is 0, maximum score is
100. The higher the better.
%}

% Check if the image is 8-bits or 16-bits
if(isa(img, 'uint8'))
    bit = 8;
elseif(isa(img, 'uint16'))
    bit = 16;
else
    error('Images are neither 8 bits nor 16 bits');
end

% Computing non-noisy pixels percent
[~,noiseScore] = evalNoise(img);
noiseScore = 100 - noiseScore;
% Computing non-artefacts pixels percent
[~,artScore] = evalArtifacts(img);
artScore = 100 - artScore;
% Computing number of over ranged pixels
[~,orScore] = evalOverRange(img);
orScore = 100 - orScore;
dr = calcDR(img);

% Computing score
score = (orScore*weights(1) + noiseScore*weights(2) +
artScore*weights(3) + (100/bit)*dr*weights(4))/sum(weights);
end

function [artPixels,artifactScore] = evalArtifacts(img)

[height, width, ~] = size(img);
totPixels = height*width;
[~,~,noticeableArtifactsMask,~] = piqe(img);
artPixels = sum(noticeableArtifactsMask,'all');
% Lower is better
artifactScore = artPixels/totPixels*100;
end

function [noisyPixels,noiseScore] = evalNoise(img)
```

```

[height, width, ~] = size(img);
totPixels = height*width;
[~,~,~,noiseMask] = piqe(img);
noisyPixels = sum(noiseMask,'all');
% Lower is better
noiseScore = noisyPixels/totPixels*100;
end

function [orPixels,orScore] = evalOverRange(img)

if(isa(img, 'uint16'))
    maxVal = 2^16-1;
    minVal = 0;
elseif(isa(img, 'uint8'))
    maxVal = 2^8-1;
    minVal = 0;
else
    maxVal = max(max(max(img)));
    minVal = min(min(min(img)));
end

[height, width, ~] = size(img);
totPixels = height*width;
black = sum(img(:,:,) == minVal,'all');
white = sum(img(:,:,) == maxVal,'all');
orPixels = black + white;
% Lower is better
orScore = orPixels/totPixels*100;
end

```

A.5 TONE MAPPING OPERATORS

These functions implement the custom tone mapping operators seen in *Section 6.1*. The others TMOs are either found in MATLAB or HDR Toolbox [17].

```
function rgb = lineartoneimap(hdr,outputBitRate)

% Linearly tone map the radiance values of and HDR image in the
limited dynamic range of 8-bits and 16-bits images.

if(~exist('outputBitRate','var'))
    outputBitRate = 8;
end

Emin = min(min(min(hdr))); % Minimum radiance value
Emax = max(max(max(hdr))); % Maximum radiance value
Zmax = 2^outputBitRate-1; % Maximum pixel value

% Linear mapping function
m = (Zmax)/(Emax-Emin);
q = -m*Emin;
f = @(x) m.*x + q;

% Tone mapping
rgb = feval(f,hdr);
rgb = round(rgb,0);

if(outputBitRate == 16)
    rgb = uint16(rgb);
else
    rgb = uint8(rgb);
end
end
```

```
function rgb = reinhardLum(hdr, a )

% Tone maps an HDR image using the Reinhard Operator from "Photo-
graphic tone reproduction for digital images"

if(~exist('a','var'))
    a = 0.36;
end

[height, width, nChannel] = size(hdr);
N = height*width; %number of pixels
delta = 0.001; %delta to avoid singularities
deltaM = delta*ones(height,width);

if(nChannel == 3)
    Y = double(grayscale(hdr));
    l_wbar = exp(sum(sum(log(deltaM + Y)))/N);
    L = (a/l_wbar).*Y; %scaled luminance
    l_white = max(max(L)); %maximum pixel value
```

```

L_d = L .* (1 + (L./l_white^2)) ./ (1 + L);
scale = L_d ./ Y;
r = hdr(:,:,1); g = hdr(:,:,2); b = hdr(:,:,3);
r = r .* scale;
g = g .* scale;
b = b .* scale;
rgb = cat(3,r,g,b);
else
Y = hdr;
l_wbar = exp(sum(sum(log(deltaM + Y)))/N);
L = (a/l_wbar).*Y; %scaled luminance
l_white = max(max(L)); %maximum pixel value
L_d = L .* (1 + (L./l_white^2)) ./ (1 + L);
rgb = L_d;
end
end

```

A.6 POST-PROCESSING

This script applies the post-processing techniques described in *Chapter 7* to a Schlieren picture. This can be a classic low dynamic range image or a tone mapped HDR picture.

```
% Loading image
img = grayscale(imread(path));
[height, width, nChannel] = size(img);

% Linear Contrast Stretch
img_lcs = imadjust(img,stretchlim(img),[]);

% Histogram Equalization
img_eq = histeq(img);

% Unsharp Masking without Contrast Stretch
img_sharp_nocont = imsharpen(img);

% Unsharp Masking with Contrast Stretch
img_sharp = imsharpen(img_lcs);

% Unsharp Masking with Contrast Stretch and Denoise
img_denoised = wiener2(img_sharp,[5 5]);
```

A.7 TONE CURVE PROCESSING

This script transforms the tone curve of an image to an s-tone curve that brightens the shadows while slightly reducing the highlights, as described in *Chapter 8*. The anchor points in the curve can be modified and more points can be added for a more accurate editing.

```
%% PARAMS

cutoff = "95";
iso = "1600";
name = "img";
format = "tiff";

flag_tone_curve = 1; %Show the tone curve graph
flag_montage = 0; %Show comparison between original and processed image

%% CONTROLS

% Sliders Values (strength of the editing) [-100,100]
black_slider = 0;
white_slider = 0;
shadows_slider = 60;
highlights_slider = -25;
midtone_sliders = 0;

% Actual Pixel value increase/decrease
blacks_strength = black_slider/100*0.25;
whites_strength = white_slider/100*0.25;
shadows_strength = shadows_slider/100*0.25;
highlights_strength = highlights_slider/100*0.25;
midtone_strength = midtone_sliders/100*0.25;

%Anchor points in the tone curve for shadows and highlights. More
points
%can be added for a more accurate editing of the tone curve
shadows_anchor = 0.25;
highlights_anchor = 0.85;

%% LOADING IMAGE

F = strcat("img/Tiffs.nosync/",cutoff,"/",iso,"/",name,".",format);
img = grayscale(loadTiff(F));

[height, width, nChannel] = size(img);
totPixels = height*width*nChannel;
bit = bitDepth(img);

%Converting to [0,1] floating point pixel values
L = double(img)./(2^bit-1);
```

```

%% TONE CURVE
min_val = 0; max_val = 1;
middle_val = 0.5;
graylevel_in = linspace(min_val,max_val,2^bit);

% Anchor points in the tone curve and their new values
x = [min_val,shadows_anchor,middle_val,highlights_anchor,max_val];
y = [min_val+blacks_strength,shadows_anchor+shadows_strength,mid-
dle_val+midtone_strength,highlights_anchor+high-
lights_strength,max_val+whites_strength];

% New tone curve made with a spline passing through the new anchor
points
pp = spline(x,y);
yy = ppval(pp,graylevel_in);

if(flag_tone_curve)
    fig = figure;
    set(fig,'defaultAxesColorOrder',[0.85 0.33 0.1]; [0 0.45 0.74]);
    hold on;
    % Image Histogram
    yyaxis right;
    h = imhist(img);
    imhist(img);
    scale_factor = max(h);
    ylim([0 scale_factor]);
    % Original and modified tone curves
    yyaxis left;
    ylim([0 2^bit-1]);
    plot(graylevel_in.*255,graylevel_in.*255,'--','LineWidth',1.5);
    plot(graylevel_in.*255,yy.*255,'-','LineWidth',1.5);
    % Anchor points
    plot(x.*255,x.*255,'o','HandleVisibility','off');
    plot(x.*255,y.*255,'o','HandleVisibility','off');
    axis('tight');
    legend("Linear Tone Curve","S Tone Curve","Histogram","Loca-
tion",'east',"FontSize",13);
    grid on;
    title("Tone Curve & Histogram","FontSize",15);
    hold off;
end

%% IMAGE PROCESSING

% Evaluating the new pixel values with the modified tone curve
L = ppval(pp,L);
figure;
imshow(L);

% Saving the image with 8-bits encoding
img_new = im2uint8(L);
imwrite(img_new,"res.png");

if(flag_montage)
    figure();
    montage({img,img_new});
end

```


A.8 HDR BLENDING WITH VIRTUAL BRACKETING

This script creates virtual bracketed images by increasing and decreasing the exposure of a Dual ISO picture as described in *Chapter 8*, then proceed to blend them with the Debevec algorithm. The CRF recovery and image blending process is the same seen in *Chapter 4* and *5*, and *Appendix A.2*, so only the virtual images creation will be reported here.

```
%% PARAMETERS

shutter_speeds =
1./[4000,3200,2500,2000,1600,1250,1000,800,640,500,...
400,320,250,200,160,125,100,80,60,50,30,25,20,15,13,10,8,6,5,4,...
3,2.5,2,0.6,0.3,1]; % all the camera real shutter speed from
1/4000 to 1"
defaultT = 1/250;
path = "img/dualiso.tiff"; % Path to the Dual ISO image
path_ref = "img/ref.tiff"; % Path to the reference LDR image
exposures = [-2,-1,1,2]; % virtual bracketing stops [EVs], only multi-
ples of 1/3
l = 40; % Lambda (Smoothing factor)

%% PICTURES LOADING

fprintf('Loading Image... \n');

original = grayscale(imread(path));
[height, width, nChannel] = size(original);
try
    meta = iminfo(path);
    deltaT = meta.DigitalCamera.ExposureTime;
catch
    deltaT = defaultT;
end

%% CREATING VIRTUAL IMAGES

fprintf('Creating Virtual Images... \n');

% Loading CRF
g = load("crf.mat");

% Converting image to an irradiance map
Emap = im2ev(original,g,log(deltaT));

% All the bracketed images included the original one
images = cell(length(exposures)+1,1);
B = zeros(length(exposures)+1,1);
images{1} = original;
B(1) = log(deltaT);
original_idx = find(shutter_speeds == deltaT);
```

```

for i = 1:length(exposures)
    img = original;
    % Finding the shutter speed related to the new exposure
    try
        new_deltaT = shutter_speeds(original_idx + 3*exposures(i));
    catch
        error("The exposure increment is too high or too low. No real
shutter speeds available.");
    end
    % Creating the virtual image by converting the irradiance map to an
image using the new shutter speed
    new_img = ev2im(Emap,g,log(new_deltaT));
    images{i+1} = new_img;
    B(i+1) = log(new_deltaT);
end

```

```

function [Emap] = im2ev(img,g,B)

    %{
        Recover an irradiances map of the scene from an image, using its
original shutter speed and the camera response function
    %}

    max_val = length(g)-1;
    range = 0:1:max_val;
    img = double(img);

    pp = spline(range,g);
    Xmap = ppval(pp,img);

    Emap = exp(Xmap-B);
end

```

```

function [img] = ev2im(Emap,g,B)

    %{
        Uses the irradiances map to create a virtual image of the scene
taken at a chosen shutter speed
    %}

    [h,w] = size(Emap);
    img = zeros(h,w);
    Xmap = log(Emap)+B;

    for i = 1:length(g)
        mask = Xmap > g(i);
        img = img + mask;
    end
    img = uint8(img);
end

```

A.9 TOOLS

In this section the various support functions used in all the previous scripts will be reported, in no particular order.

```
function [bit] = bitDepth(img)

    % Recover the bit depth of the images

    if(isa(img, 'uint8'))
        bit = 8;
    elseif(isa(img, 'uint16'))
        upper_limit = max(max(max(img)));
        if(upper_limit >= 2^14-1)
            bit = 16;
        elseif(upper_limit >= 2^12-1)
            bit = 14;
        elseif(upper_limit >= 2^10-1)
            bit = 12;
        elseif(upper_limit >= 2^8-1)
            bit = 10;
        else
            error('Image is encoded as 16-bits but pixels values are
8-bits or lower');
        end
    else
        error('Image is neither encoded as 8-bits nor 16-bits');
    end

end

function [tiff] = loadTiff(filename)

    tiff = imread(filename);
    if(size(tiff,3) > 3)
        %Eliminate alpha channel
        tiff = tiff(:,:,1:3);
    end

end

function [RMSE] = crfError(vetg,hdr,B,original,flag_montage)

    %{
    Estimate the error of the recovered camera response function by
    creating a virtual image from the HDR radiance map using the same shutter
    speed as the original image. The error is computed as the
    RMSE of the difference between the two images.
    The process can be really slow for large images.
    %}

    if(~exist('flag_montage','var'))
        flag_montage = 0;
    end

end
```

```

fprintf("Estimating CRF Error... \n");

[h, w, c] = size(original);

if(not(h == size(hdr,1) && w == size(hdr,2) && c == size(hdr,3)))
    error("\n Images must have the same dimensions\n");
end

virtual = zeros(h,w,c);
Xmap = log(hdr)+B;

for k = 1:c
    g = vetg(:,k);
    for i = 1:length(g)
        mask = Xmap(:,:,k) > g(i);
        virtual(:,:,k) = virtual(:,:,k) + mask;
    end
end

if(bitDepth(original) == 8)
    virtual = uint8(virtual);
else
    virtual = uint16(virtual);
end

% Calculating Error
E = double(original-virtual);
SQE = E.^2;
MSE = mean(SQE(:));
RMSE = sqrt(MSE);

fprintf("\nDone \n");

% Show the comparison
if(flag_montage)
    figure();
    montage({original,virtual});
    figure();
    diff = abs(original-virtual);
    diff = imadjust(diff,stretchlim(diff),[]);
    imshow(diff); title("Differences");
end
end

function img = grayscale(rgb)

[~, ~, nChannel] = size(rgb);
if(nChannel == 3)
    % RGB Image
    redChannel = rgb(:, :, 1);
    greenChannel = rgb(:, :, 2);
    blueChannel = rgb(:, :, 3);
    % RGB to Luminance Conversion (PAL)
    img = .2126*double(redChannel) + ...
          .7152*double(greenChannel) + ...
          .0722*double(blueChannel);
end

```

```
    if(isa(rgb, 'uint8'))
        img = uint8(img);
    else
        img = uint16(img);
    end
else
    % Greyscale Image
    img = rgb;
    warning("The image is already gray scale. No processing
needed");
end
end
```